Electronic Supplementary Material (ESI) for Chemical Science.
This journal is © The Royal Society of Chemistry 2019

Single electron transfer events and dynamical heterogeneity in the small protein azurin from *Pseudomonas aeruginosa*

Supporting Information

Biswajit Pradhan, Christopher Engelhard, Sebastiaan Van Mulken, Xueyan Miao, Gerard W. Canters*, Michel Orrit*

Table of Contents

1. Results and Discussion

1.1. An overview of *P. aeruginosa* Azurin

Bacterial azurin (Az) functions *in vivo* as an electron shuttle and appears to be involved in stress response[1] (see[2] for further details). Az fulfills this physiological role by acting as a temporary storage for electrons, through reversible interconversion between the (oxidized) Cu(II) and the (reduced) Cu(I) form.

Structure and mobility. Az has a β-sandwich structure in which the Cu atom is eccentrically placed at a distance of 7 Å from the surface. A conspicuous feature is the occurrence of a low- and a high-pH form of the protein, the 3D structures of which differ in the area around His35, located in the hydrophobic interior of the protein.[3] With His35 in the deprotonated form (low pH), its ND1 and NE2 ring nitrogen atoms form H-bridges with the backbone carbonyl groups of Pro36 and Met44, respectively. At high pH, His35 is mono-protonated and exhibits a different H-bond pattern: Its ND1 atom now makes a H-bond with the backbone NH group of Gly37, while the H-bond between NE2 and C0 (Met44) is maintained, and, concomitantly, the Pro36/Gly37 peptide bond has flipped by 180°.[3]

Due to the compact and stable structure of Az, its internal mobility appears to be limited. NMR studies have evidenced backbone mobility on the pico- to nanosecond time scale.[4-6] Motions on the (sub-)millisecond to second time scale occur in three regions: the 'southern' end of the protein, close to the structure's (only) S-S bridge, and two small, contiguous 'northern' regions termed here A and B, located in the vicinity of His35 and Cu, respectively.[5,6] The motions are diagnostic of an exchange between two forms, which, for region A, have been connected with the protonated/deprotonated states of His35. The connection is more tenuous for region B.[3-5] For the deprotonation rate of His35, values ranging from 45 s^{-1} to 0.53 s^{-1} have been reported.[4,7,8]

Midpoint potential and electron transfer reactions. The pH behavior of His35 has been studied extensively by electrochemistry and NMR.[4,7-11] Oxidation of Cu is associated with a change of the pK_a of His35 of ΔpK_a = 0.85 (from 7.34 for the Cu(I) to 6.49 in the Cu(II) form[7-11]). Conversely, a change in the protonation state of His35 is connected with a change in midpoint potential of Cu. A ΔpK_a = 0.85 is calculated to correspond to a change in midpoint potential of ΔE^0 = 50 mV.[10-12] Other protonatable residues may affect the midpoint potential, though to a lesser extent. The strongest influence after His35 was reported for His83, with ΔpK_a = 0.22 and ΔE^0 = 13 mV.[10,11] The combined effects of His35 and His83 amount to ΔE^0 = 63 mV, indicating that the observed total shift of 62 mV[11] is adequately explained by the influence of these two residues. The midpoint potential of Az at pH 7 amounts to 80 mV vs. SCE.[11,12]

1.2. Michaelis-Menten equilibrium for Azurin

Copper-Az (Cu-azurin, Cu-Az) is in equilibrium with the electron mediators $Fe(CN)_6^{3-}$ (Fe(III) , concentration [Fe(III)]) and $Fe(CN)_6^{4-}$ (Fe(II), concentration[Fe(II)]). The concentration ratio of these two species is fixed by the electrochemical potential in the potentiostat.

Introducing bound complexes of the protein with the mediators (B is the complex of the oxidized protein with (Fe(II) and C the complex of the reduced protein with (Fe(III)), we obtain the following kinetic scheme:

$$\mathrm{Fe(II)} + A \leftrightharpoons B \leftrightharpoons C \leftrightharpoons D + \mathrm{Fe(III)},$$

where A and B are oxidized, dark forms of fluorescently labeled Cu-Az, while C and D are reduced, fluorescent forms of fluorescently labeled Cu-Az. This equilibrium is described by the following kinetic system:

$$\dot{[A]} = -k_1[\mathrm{Fe(II)}][A] + k_{-1}[B]$$

$$\dot{[B]} = k_1[\mathrm{Fe(II)}][A] - k_{-1}[B] + k_{-3}[C] - k_3[B]$$

$$\dot{[C]} = k_2[\mathrm{Fe(III)}][D] - k_{-2}[C] - k_{-3}[C] + k_3[B]$$

$$\dot{[D]} = -k_2[\mathrm{Fe(III)}][D] + k_{-2}[C]$$

Steady-state solutions

In steady state, all time derivatives are nil and the following relations hold:

$$[A] = \frac{k_{-1}}{k_1[\mathrm{Fe(II)}]}[B], \qquad [B] = \frac{k_{-3}}{k_3}[C], \qquad [D] = \frac{k_{-2}}{k_2[\mathrm{Fe(III)}]}[C].$$

As we are interested in the probabilities or concentrations of the oxidized form $[Ox] = [A] + [B]$ and reduced form $[Red\} = [C] + [D]$, we find the ratio of these two probabilities as:

$$\frac{[Ox]}{[Red]} = \frac{\frac{k_{-3}}{k_3}\left(1+\frac{k_{-1}}{k_1[\mathrm{Fe(II)}]}\right)}{1+\frac{k_{-2}}{k_2[\mathrm{Fe(III)}]}}. \qquad (1)$$

Bright and dark times for fast complex formation

Here, we assume that complex formation and decomposition rates are much faster than the electron transfer. We may thus assume the forms A and B to be in equilibrium at all times. To find the distribution of dark times, we suppose the molecule is in a bright state (necessarily C) immediately before the dark time starts at $t = 0$, when the molecule enters state B. We look for the *first* reduction event, or $B \to C$ transition, to signal the end of the dark time. The probability of finding Az in the oxidized form obeys:

$$\dot{[Ox]} = k_{-3}[C] - k_3[B],$$

Because $[C] = 0$ during the entire dark time period, and using the kinetic equations for species A and B, we find:

$$\dot{[Ox]} = -\frac{k_3}{1+\left(\frac{k_{-1}}{k_1[\mathrm{Fe(II)}]}\right)}[Ox].$$

Thus, the probability of finding oxidized Az decays exponentially with the average dark time:

$$\langle\tau\rangle_d = k_3^{-1}\left(1 + \frac{\mathrm{k_{-1}}}{\mathrm{k_1[Fe(II)]}}\right). \qquad (2)$$

A similar reasoning for the bright times gives a single exponential with average bright time:

$$\langle\tau\rangle_b = k_{-3}^{-1}\left(1 + \frac{\mathrm{k_{-2}}}{\mathrm{k_2[Fe(III)]}}\right). \qquad (3)$$

We obviously recover the above ratio of the oxidized to reduced forms from the ratio of times, but a direct measurement of dark and bright times by single-molecule spectroscopy yields much more information about the system, and enables the extraction of more parameters than their ratio alone.

Bright and dark times in the general case

For the dark times, we again have the following chain of reactions:

$$\mathrm{Fe(II)} + A \leftrightharpoons B \to C,$$

where the production of C signals the end of the dark time. With the notations $[A] = a, [B] = b, [\mathrm{Fe(II)}] = f_2, [\mathrm{Fe(III)}] = f_3$ we obtain the following kinetic equations:

$$\dot{b} = -k_3 b - k_{-1} b + k_1 f_2 a$$

$$\dot{a} = k_{-1}\dot{b} - k_1 f_2 a.$$

By elimination of a and after simple algebraic manipulation, we get the following second-order equation for b:

$$\ddot{b} + (k_3 + k_{-1} + k_1 f_2)\dot{b} + k_3 k_1 f_2 b = 0$$

The general solutions are exponential decays with rates given by the roots of the characteristic second-degree equation,

$$\lambda = \frac{1}{2}\left[-(k_3 + k_{-1} + k_1 f_2) \pm \sqrt{(k_3 + k_{-1} + k_1 f_2)^2 - 4k_3 k_1 f_2}\right]$$

For realistic values of the rates, one of the roots will be much larger than the other one. The larger rate will be approximately:

$$\lambda \approx k_{-1} + k_1 f_2$$

and the smaller rate approximately:

$$\mu \approx k_3/(1 + \frac{k_{-1}}{k_1 f_2}).$$

We look for the kinetics of the total probability of the oxidized form $[Ox] = a + b$, with $\left[\dot{Ox}\right] = -k_3 b$, whose general solution is $[Ox](t) = \alpha e^{-\lambda t} + \beta e^{-\mu t}$, with the initial conditions $[Ox](t = 0) = 1$ and $[Ox\dot{]}(t = 0) = -k_3$. Indeed, when the dark time begins, the B form has just been created from the C form. Thus $\alpha + \beta = 1$ and $\lambda\alpha + \mu\beta = k_3$. Because we assume $\mu \ll \lambda$, the contribution from α is small and approximately equal to:

$$\alpha \approx \frac{k_3 k_{-1}}{(k_{-1} + k_1 f_2)^2}. \qquad (4)$$

Thus, the oxidized form has a small transient decay with a high rate λ, followed by a slower decay with rate μ, close to the previous value in the approximation of fast binding.

The distribution of dark times $p_d(t) = -\left[(\dot{Ox})\right](t) = \alpha\lambda e^{-\lambda t} + \beta\mu e^{-\mu t}$ is given by the time-derivative of the oxidized state population. This distribution is thus bi-exponential, with two decaying components. Note that the small contribution α due to the fast binding kinetics is always positive. Therefore, it cannot be mistaken for a possible artefact of the change point algorithm due to low photon counts, as this artefact appears as a buildup of the time distribution. Similar results can be obtained for the distribution of dark times.

1.3. Labeling and switching in bulk experiments

1.3.1. Structure and position of dye

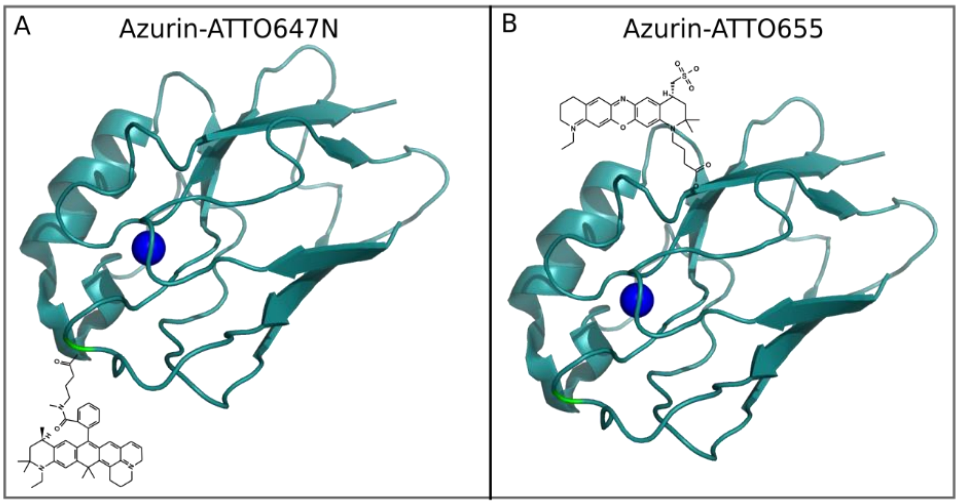

Figure S1: Ribbon structure of Az.[13] The dye ATTO647N is attached to Cys42 (A), the dye ATTO655 is attached to Lys122 (B).

Fluorescence measurements in a bulk Az-ATTO647N sample (Fig. S2A) were carried out to determine the FRET switching ratio. The measurements were carried out in a Cary Eclipse Spectrometer (Varian Inc. Agilent Technology, USA). A 50 nM sample was excited with 665 nm laser and the intensity was monitored above 675 nm. Sodium ascorbate (reductant) and potassium ferricyanide (oxidant) were added in an alternating fashion. The fluorescence intensity of Cu-Az-ATTO647N shows a switching ratio of 90 % (Fig. S2B), whereas Zn-Az-ATTO647N shows little or no change in intensity, as expected.

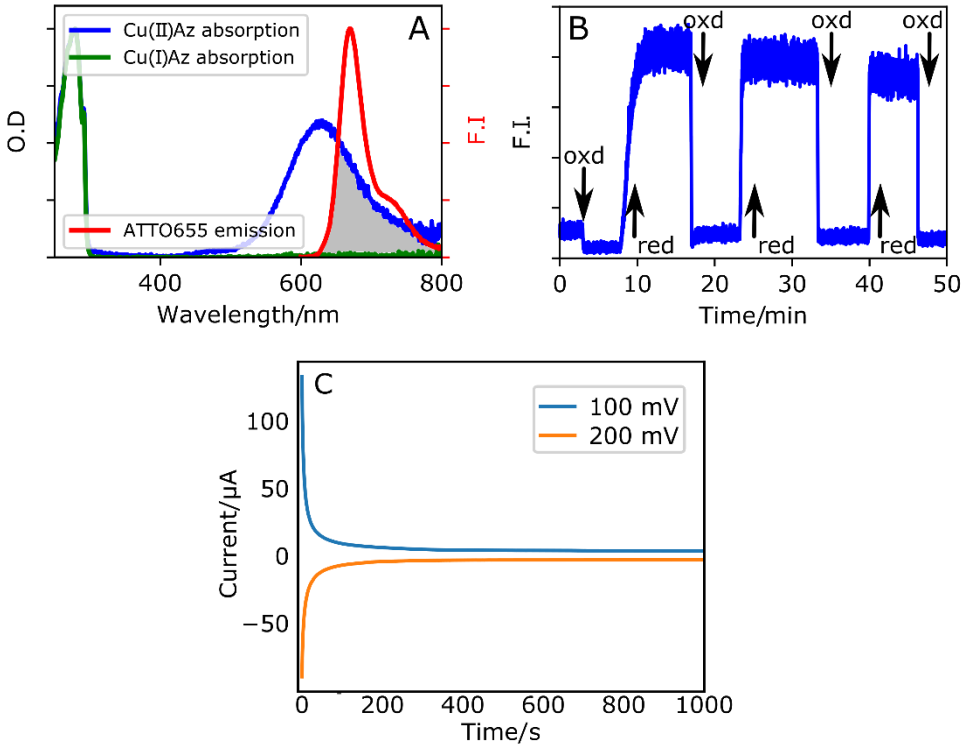

Figure S2: Spectral overlap and Bulk switching. (A) Absorption spectrum of Cu(I)-Az (green), Cu(II)-Az (blue). The emission spectrum of ATTO647N (red) has a good enough overlap with the absorption of Cu(II)-Az to show high FRET. (B) Fluorescence intensity of 50 nM Cu-Az-ATTO647N shows high intensity in the presence of reductant and low intensity with oxidant. The switching ratio is 90 %, high enough to try single-molecule FRET. (C) Current at the working electrode after the application of a constant potential of 100 mV (blue) and 200 mV (orange). The steady state potential is reached in about 100 s.

1.4. Fluorescence lifetimes

Fluorescence lifetimes can be obtained from the arrival time of photons with respect to the laser pulse. The fluorescence lifetime of ATTO647N in Zn-Az is 4.1 ns (Fig. S3, green). To calculate the fluorescence lifetime of ATTO647N in the two redox forms of Cu-Az, photon delay histograms were recorded at low intensity, corresponding to the Cu(II) form, and at high intensity, corresponding to the Cu(I) form. The lifetimes are 0.6 ns (Fig. S3, red) and 3.8 ns (Fig. S3, blue) for the Cu(II) and Cu(I) forms, respectively . The reduction in the lifetime reconfirms the FRET process as the responsible mechanism for the blinking in Cu-Az. The instrument response function is shown in black (Fig. S3) and has a width of 0.3 ns.

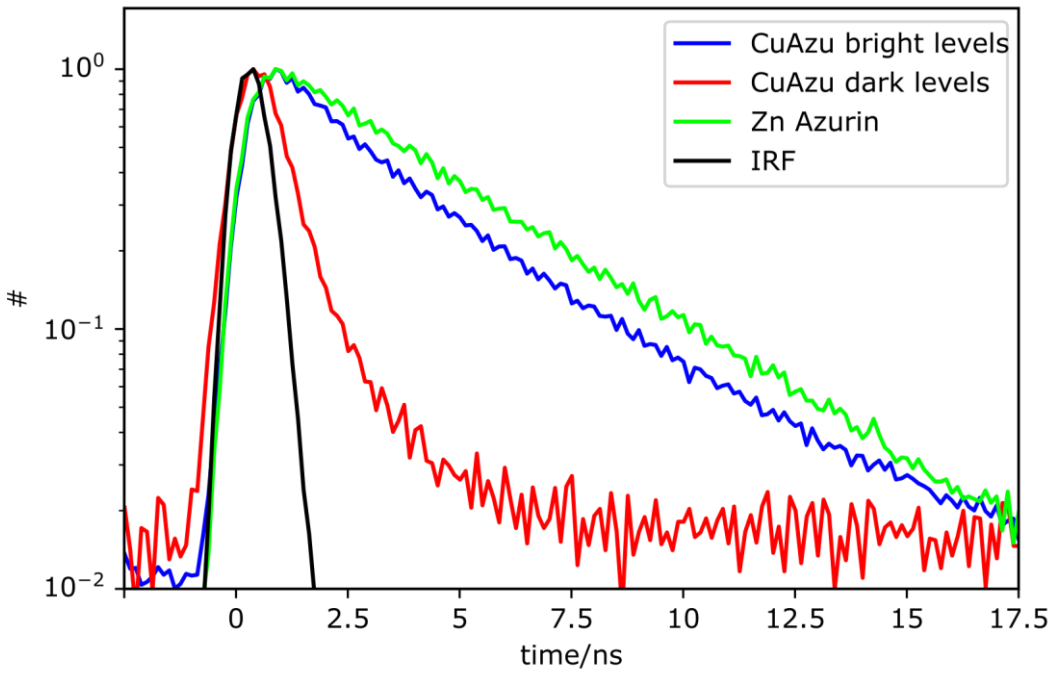

Figure S3: Fluorescence lifetime histograms of labeled Az. The lifetime histogram corresponding to bright state (blue), oxidized state (red) and instrument response function (black). The lifetime of the oxidized state is much shorter than that of the reduced state due to FRET quenching. The lifetime histogram of Zn-Az ATTO647N is shown in green.

1.5. Midpoint potentials from bright and dark times

Calculating the ratio of bright and dark times for various total concentrations of hexacyanoferrate enables us to estimate the error introduced in our calculations due to assuming the ratio to depend linearly on the applied potential (Fig. S4A). Data with linear fits of these ratios for different molecules, shown exemplarily for 3 molecules in Fig. S4B, and the same molecule at different times (Fig. S4C) yields the histograms shown in the main text Fig. 3. Panel S4D shows the noise-limited histogram of midpoint potentials as extracted from simulated data comparable to the experimental ones.

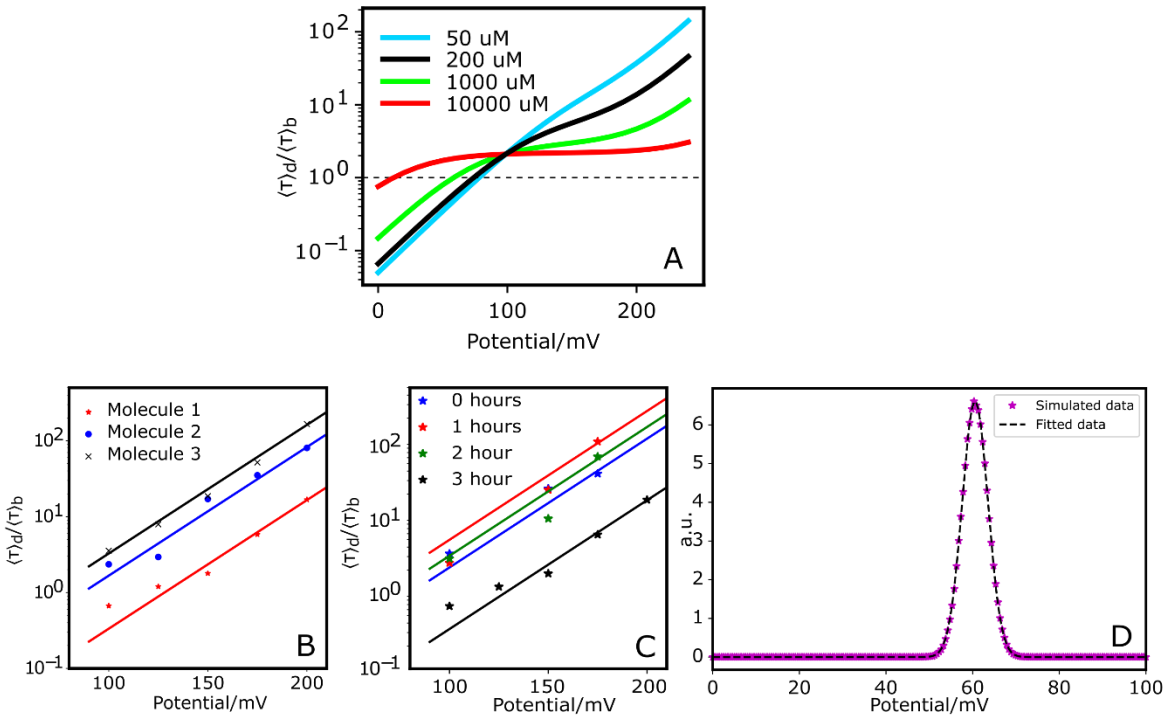

Figure S4: A) Calculated ratio of dark and bright times at different total concentrations of $Fe(CN)_6$. The curve deviates from linearity at higher concentrations (> 50 µM) of electron mediator. Calculations are based on the observed values (See main text): k_3 = (10 ± 4) s^{-1}, k_{-3} = (21 ± 3) s^{-1}, K_1 = (2.8 ± 1.4) x 10^3 M^{-1}, K_2 = (5.9 ± 1.1) x 10^4 M^{-1}, $E_{0,Fe(CN)_6}$ = 180 mV vs. SCE, total haxacyanoferrate concentation 200 µM. The isosbestic point corresponds to the potential at which K_1 [Fe(II)] = K_2[Fe(III)], yielding a constant $\langle\tau\rangle_d/\langle\tau\rangle_b = k_{-3}/k_3 = 1/K_3$. The following experiments were performed at 200 mV (black curve). B) Ratio of dark and bright times as a function of applied potential for different Az molecules. Each color represents a single Az molecule and the solid line is a linear fit by Nernst's equation). C) Plot of the ratio of average dark to bright times for Molecule 1 at four different times separated by 1 hour. Each color represents a particular measurement, which lasted 120 s. D) Noise-limited width of the distribution of potentials, derived from simulated, non-fluctuating time traces, the FWHM is 9 mV.

1.6. Control for transient binding of azurin to the surface

By removing NeutrAvidin, we can exclude specific binding of Az to the surface. Transient binding can be investigated by comparing the fluorescence with the laser focused onto the surface or in the solution. Transient sticking of the protein to the surface would manifest itself in multi-component diffusion times with longer decay times when the laser is focused on to the surface.

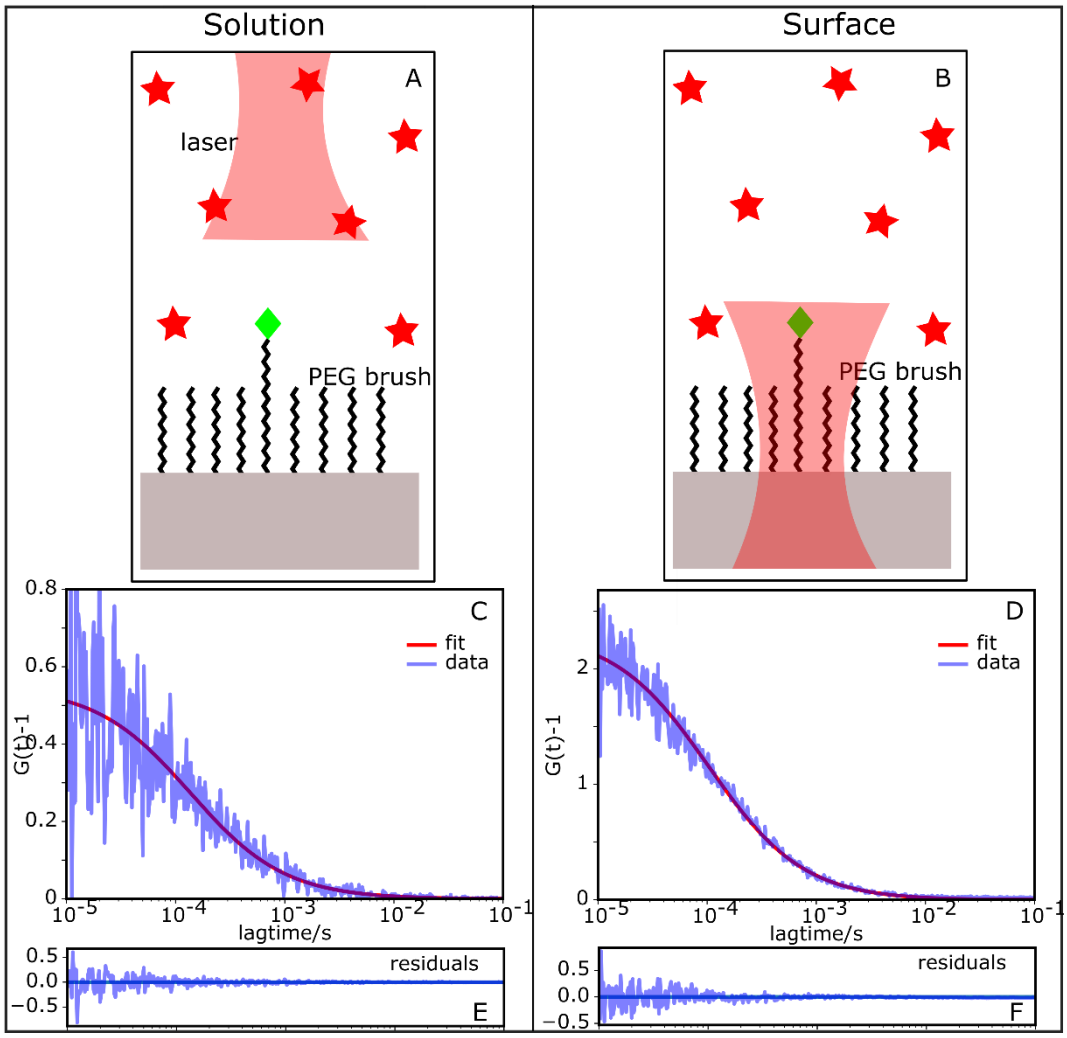

Figure S5: FCS on surface and solution. Scheme of the experiment showing the PEG-functionalized glass surface and 10 nM Zn-Az ATTO647N (red stars) in the solution. Because there is no NeutrAvidin on the surface, we expect no specific binding of Az to the surface. The laser waist (red, shaded) was parked in the bulk of the solution A) or on the surface (B) and time traces recorded for 1000 s. (C) The FCS curve in the solution was fitted with a single diffusion component. The residuals are shown in E. (D) FCS curve measured on the surface. It is also well fitted with a single diffusion component. The residuals are shown in F. The absence of decay at longer times (milliseconds to seconds) confirms the absence of sticking of the protein to the surface.

1.7. Controls for Dynamic Heterogeneity & Alternative Evaluation Method

1.7.1. Segmental analysis

As described in the main text, the analysis of our data was performed on the basis of the change point algorithm. Change point analysis, however, is subject to artefacts at short times due to insufficient numbers of photons. As shown by Terentyeva *et al.*,[14] such artefacts can undermine the evaluation of dynamic heterogeneity, notably by biasing non-exponential time distributions towards more exponential ones.

To verify that this effect was not present in our data, we analyzed the time traces of our single Az molecules through methods that minimize free parameters as much as possible. We performed the following analysis of the time traces (See section 1.9 and 1.10, an example is presented in Fig. S6): The trace is plotted in Fig. S6A with a bin time of 5 ms. We divided the whole time trace into 100 s segments. Each color in the trace in Fig. S6A represents such a segment, with detailed views of the first and last segment of the trace shown in Figs. S6B and C. To evaluate changes between the different segments quantitatively, we calculated for each segment intensity autocorrelation functions according to $G(t_{lag}) = \langle I(t)I(t+t_{lag})\rangle / \langle I(t)\rangle^2$, with t_{lag} the lag time. This provides a parameter-free way of

tracking temporal fluctuations of the intensity $I(t)$. By comparing this autocorrelation function between different segments, changes in the temporal behavior of the molecule can be identified, with the length of the segment as the only free parameter.

The autocorrelation functions in Fig. S6D can be fitted with an exponential function $G(t) = G_0 \exp\left(-\frac{t}{\tau}\right) + 1$ where τ is the characteristic correlation time and G_0 is the correlation contrast. From these, the average bright times $\langle\tau\rangle_b$ and dark times $\langle\tau\rangle_d$ in each segment can be estimated.

Finally, time-correlated single-photon counting, in which the arrival times of fluorescent photons relative to the excitation laser pulse are measured, can be used to extract the fluorescence lifetimes of the label in the dark and bright states from each segment. We plot a histogram of the arrival times for each segment of the time trace (Fig. S6E).

1.7.2. Control experiments for dynamic heterogeneity

We recorded time traces of Zn-Az-ATTO647N at different potentials to determine if the dye itself responds to the applied potentials or to the electron mediators in the solution. Figure S7 shows time traces of Zn-Az-ATTO647N at 0 mV, 100 mV and 200 mV. No blinking of intensity is observed within the potentials of interest (0 to 200 mV). This result therefore excludes any effect of redox mediators on the fluorescence of the dye. In contrast to ATTO647N, the ATTO655 dye shows blinking at low potentials (< 50 mV) as can be seen in Fig. S8. Segmental analysis was performed for the blinking in Zn-Az-ATTO655 at -50 mV (Fig. S8). The autocorrelations and fluorescence lifetime histograms were identical for different parts of the trace. Similarly, segmental analysis of Zn-Az-ATTO647N shows no variation in the correlation functions (Fig. S6D) and fluorescence lifetimes (Fig. S6E). The correlation does not show any decay, indicating that blinking is negligible. Figure S8F shows a 2D scatter plot of these average bright and dark times extracted from the autocorrelation function (colored triangles), with the distribution of times extracted by the same method from simulated data shown as shaded black dots, yielding a similar representation of variation between segments as the 2D scatter plots in the main text (Fig. 4). Finally, a simulated trace with similar blinking as the Cu-Az was analyzed identically to experimental data (Fig S9,10). As expected, we find identical FCS curves and lifetime histograms. All these controls confirm that the dynamic heterogeneity observed in Cu-Az-ATTO647N does not arise from experimental instability, blinking, or analysis artefacts.

In all cases, the properties of the simulated trace meet expectations for a purely uncorrelated process: weak fluctuations of averaged times around their mean value, Gaussian-like histograms of values, constant correlation and lifetime histograms along the trace, absence of correlation of successive times, and absence of feature in the correlation function of bright and dark times.

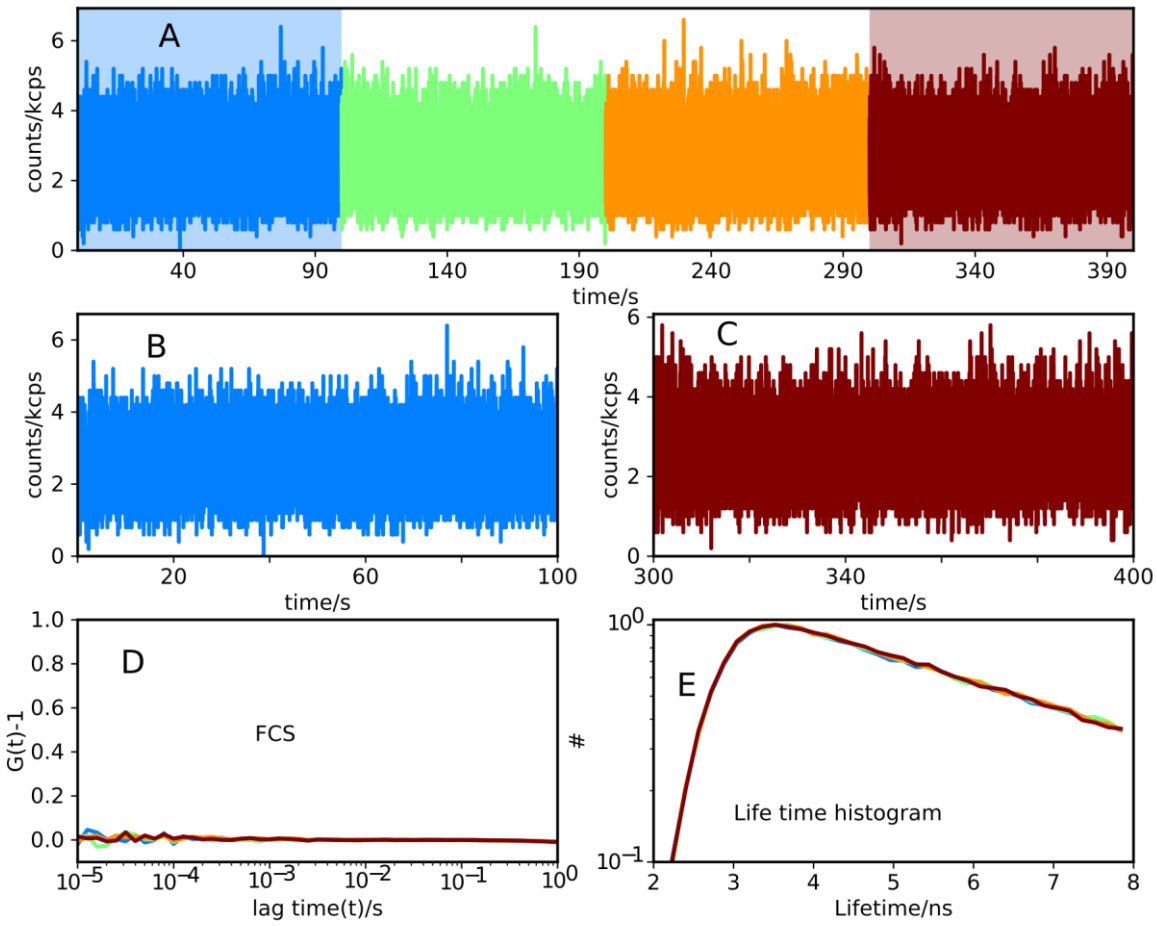

Figure S6: Segmental analysis of Zn-Az-ATTO647N. (A) A long time trace of Zn-Az-ATTO647N with a length of 400 s. The time trace is divided into four parts, each 100 s long. Magnified first and last part of the trace are shown in blue (B) and brown (C). The FCS curves of each part of the trace show flat and identical correlations (D) indicating no fluctuation of intensity. The lifetime histogram of different parts of the trace are also identical (E).

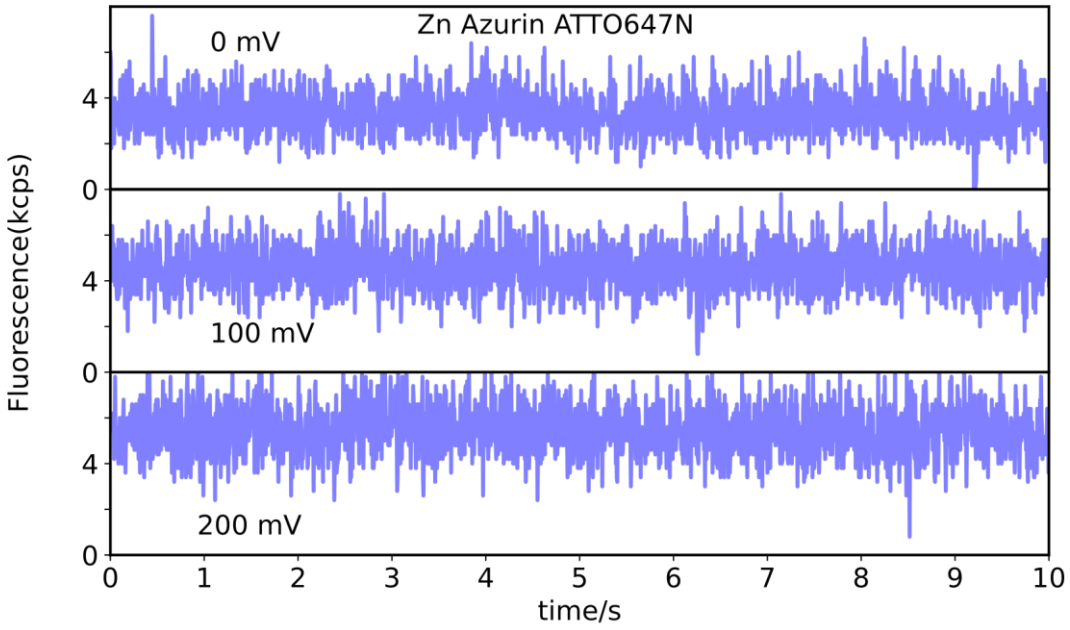

Figure S7: Zn-Az-ATTO647N vs Potential. Time traces of Zn-Az-ATTO647N at 0 mV, 100 mV and 200 mV. No blinking or variation in intensity is observed at different potentials indicating minimal effect of redox chemicals on the dye.

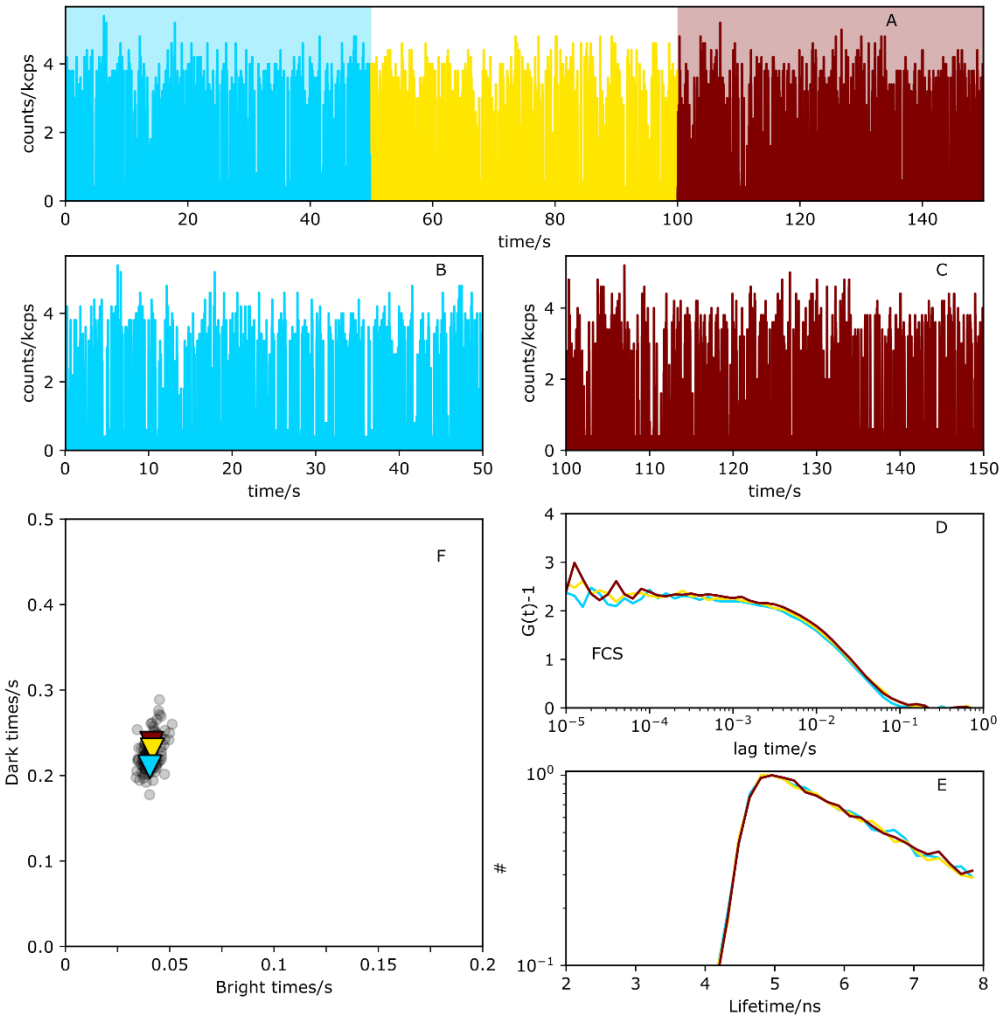

Figure S8: Segmental analysis of Zn-Az-ATTO655 blinking. (A) A trace of Zn-Az-ATTO655 at potential -50 mV with a length of 150 s. These traces show blinking, which we assign to photoexcited electron transfer of ATTO655 in the presence of reductant in the solution. The time trace is divided into three parts each 50 s long. The enlarged first and last parts of the trace are shown in blue (B) and brown (C). The FCS curves of each part of the trace show similar correlations (D) indicating similar fluctuations of intensity. The lifetime histograms of different parts of the trace are also identical (E), and the distribution of per-segment dark vs bright times (F, triangles) matches that of a simulated, non-fluctuating trace (F, black dots).

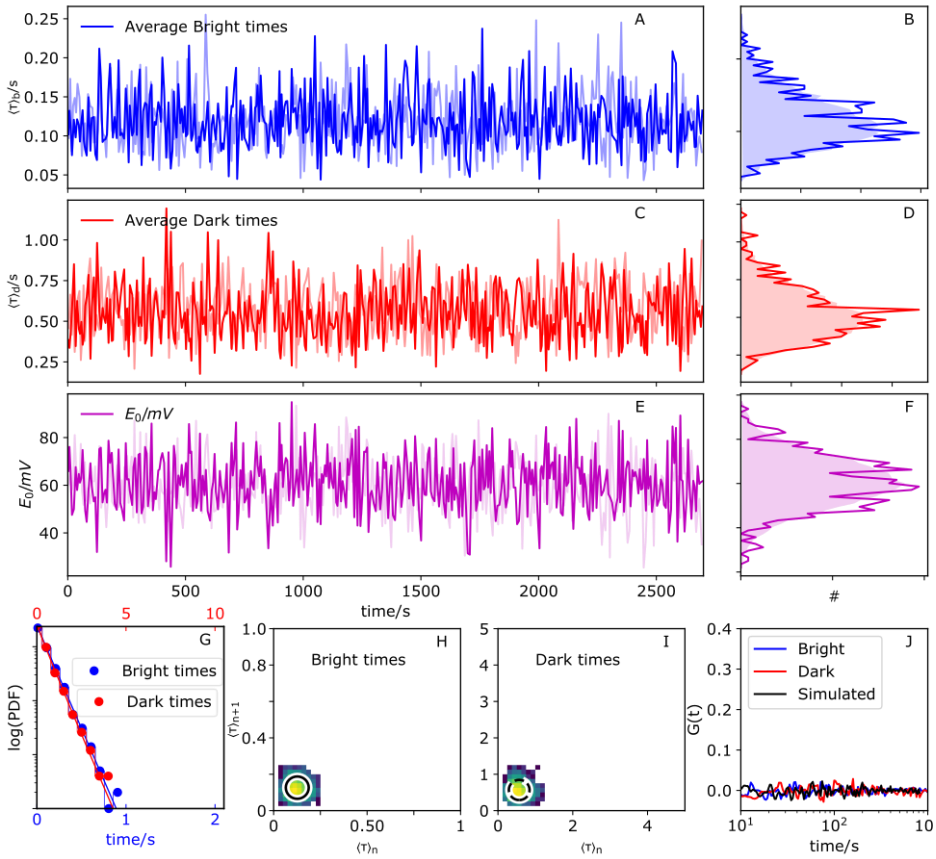

Figure S9: Simulated trace: change point analysis. A, C) Average bright and dark times of a simulated time trace exhibiting times matching those of a single Az, but without any dynamic heterogeneity, plotted as functions of time. Each point is obtained through binning and averaging 10 successive redox events. B, D) Histograms of average bright and dark times found in traces A and B. The shaded areas are histograms of Poisson processes with the same average time. E) Time trace of midpoint potentials obtained from the bright and dark times using Nernst's equation F) Histogram of midpoint potentials with a Gaussian fit. G) Histogram of unaveraged bright (blue) and dark (red) times. H, I) 2D correlation plots of average bright and dark times. J) Autocorrelation of average bright and dark times. The autocorrelation of average bright or dark times of the simulated trace is shown in black.

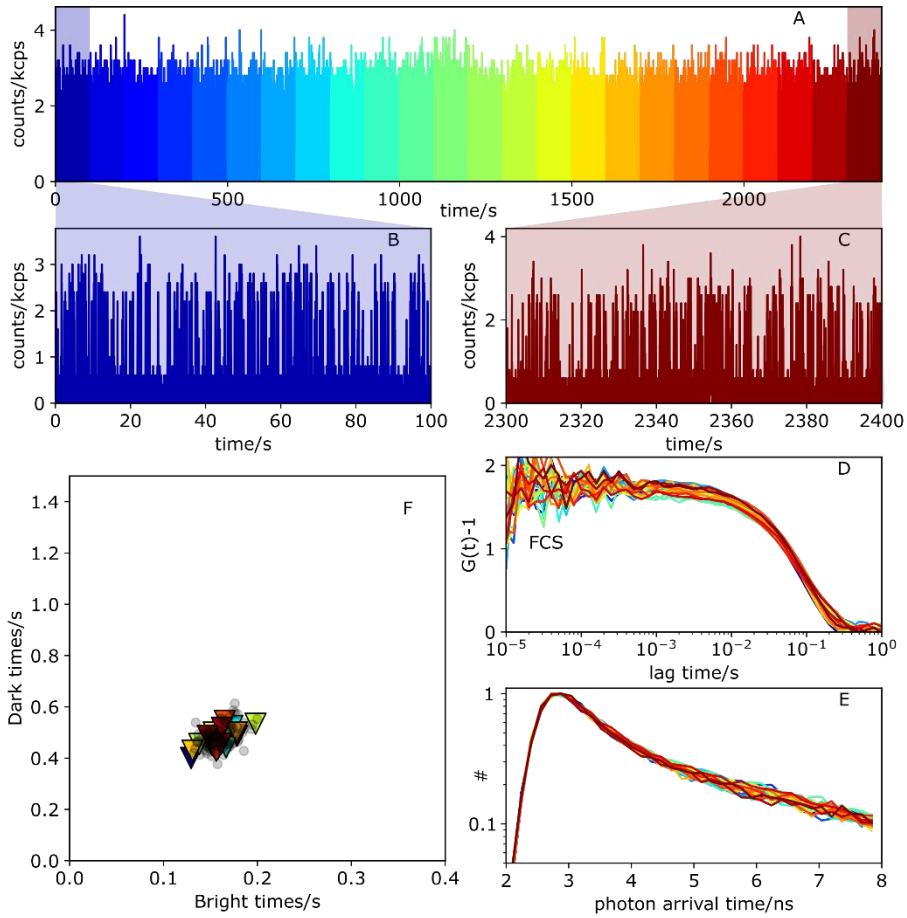

Figure S10: Simulated trace, segmental analysis. (A) A simulated time trace of 2600 s length that has similar blinking times as the Cu-Az but with no heterogeneity in the rates. The distribution of bright and dark times are single-exponential. The time trace is divided into small parts each 100 s long. Magnified first and last segments of the trace are shown in blue (B) and brown (C). The FCS curves of each part of the trace show similar correlations (D) indicating similar fluctuation of intensity. The lifetime histogram of different parts of the trace are also identical (E), and no correlation between the bright and dark times deduced from correlation functions appears (F).

1.8. Verifying the change-point analysis with simulated data.

The validity of the change point analysis can be verified by processing a simulated data set, and testing whether the analysis does indeed recover the bright and dark times, known *a priori* (Fig S11). The good agreement between the obtained bright and dark times and the known ones proves that the change-point algorithm is working reliably within the range of parameters used in this work.

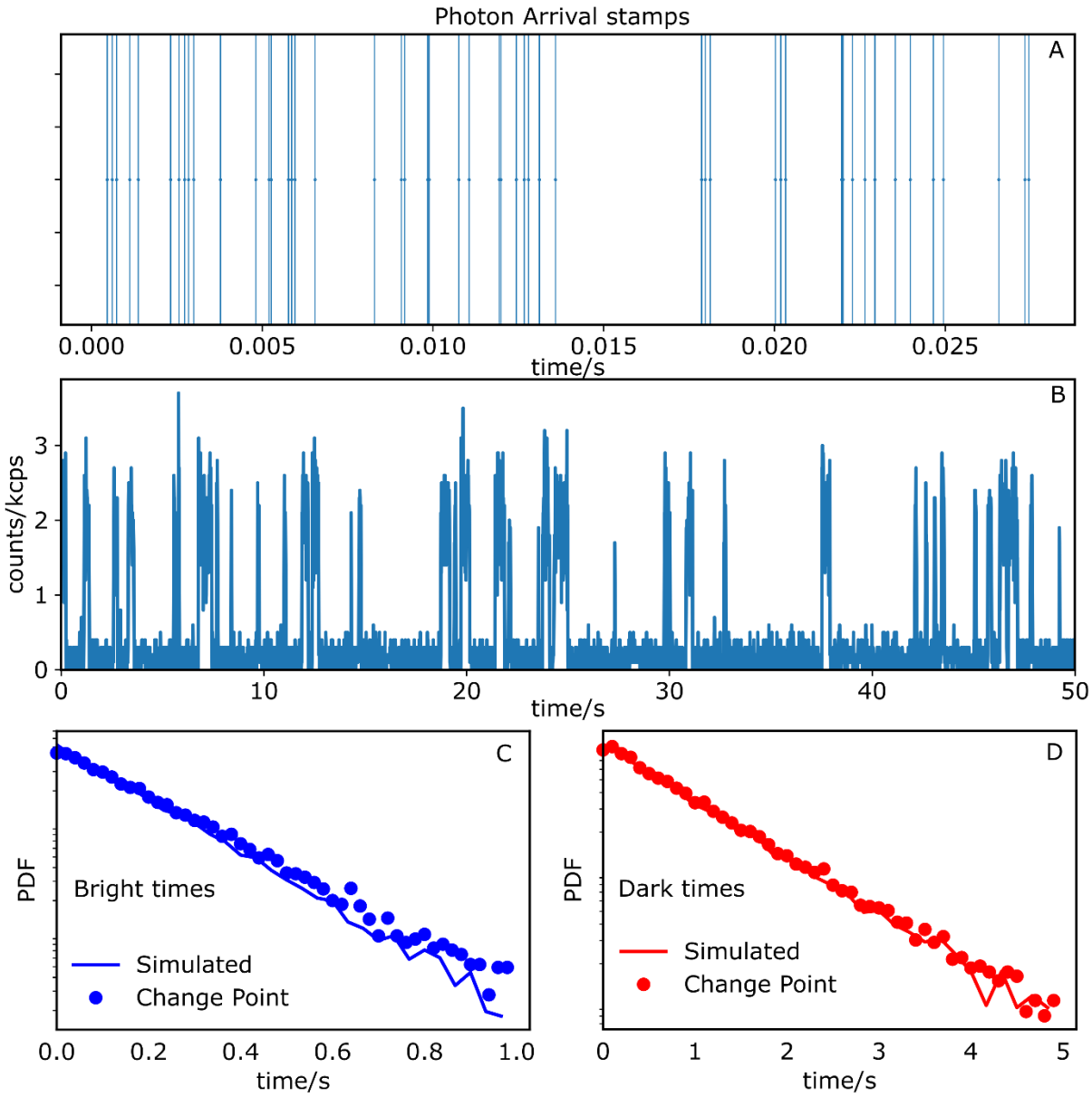

Figure S11: Simulated trace and change point. (A) Simulated arrival times of photons. (B) Binned time trace of the simulated photons with a binning time of 5 ms. The time traces were analyzed using a change point algorithm. (C) Histogram of bright times from change point analysis (blue solid line), compared with the simulated (blue solid circles) bright times. (D) Histogram of dark times obtained from change point analysis (red solid line), compared with the simulated (red solid circles) dark times.

1.9. Dynamic Heterogeneity in Cu-azurin-ATTO647N

This section (Figs. S12-S37) shows the results of change-point and segmental analysis of all Cu-Az-ATTO647N molecules for which long enough time traces could be measured (the molecules are arbitrarily numbered 1-13, molecule 1 being the one shown in the main text). For each molecule, the first figure is the equivalent of Fig. 4 in the main text, the second figure shows the corresponding segmental analysis (see section 1.7.1).

Different molecules present more or less strong evidence for dynamical heterogeneity, which may appear more or less clearly from the change point analysis or from the segmental analysis. Although the number of molecules is too small to extract statistically significant percentages of the observed behaviors, we show and discuss the ensemble of our data qualitatively to demonstrate the large variety and extent of the dynamical heterogeneity of Az. We stress that the data hereafter pertain to *all* single Cu-Az molecules we studied. *We did not select data for or against dynamical heterogeneity*.

Section 1.10 (Figs. S38-S67) is devoted to similar observations done on single Cu-Az molecules labeled with ATTO655. As they show the same qualitative behavior, we conclude that the nature of the dye label, in particular the hydrophobicity of ATTO647N, has no strong influence on the conformational dynamics of Az.

Summarizing the results shown below and in Section 1.10, the quantitative examination of these traces shows a large variety of behaviors, where changes in bright and dark times can be uncorrelated, correlated, or anti-correlated. The correlated changes can give rise to increases, decreases, or negligible changes of the mid-point potential. Therefore, these observations point to a large complexity of the system, with many possible conformations, and many possible pathways with various timescales between them.

The conventional way of characterizing the spread of correlation times in an ensemble is to fit the ensemble correlation function with a stretched exponential. For reference, Panels E in the even-numbered Figs. S12-S66 show the distribution of un-averaged bright and dark times of the single molecule under study together with stretched exponential fits.

1.9.1. Molecule 1

The change point analysis of molecule 1 has been discussed in the main text (Fig. 4) and is repeated here for reference.

In the segmental analysis, molecule 1 shows significantly higher intensity in later segments of the trace when compared to the earlier ones (Fig S13A). Accordingly, the dark and bright times show significantly larger variations than would be expected for a simulated/non-fluctuating trace (Fig. S13F). This matches what can been observed in change point analysis.

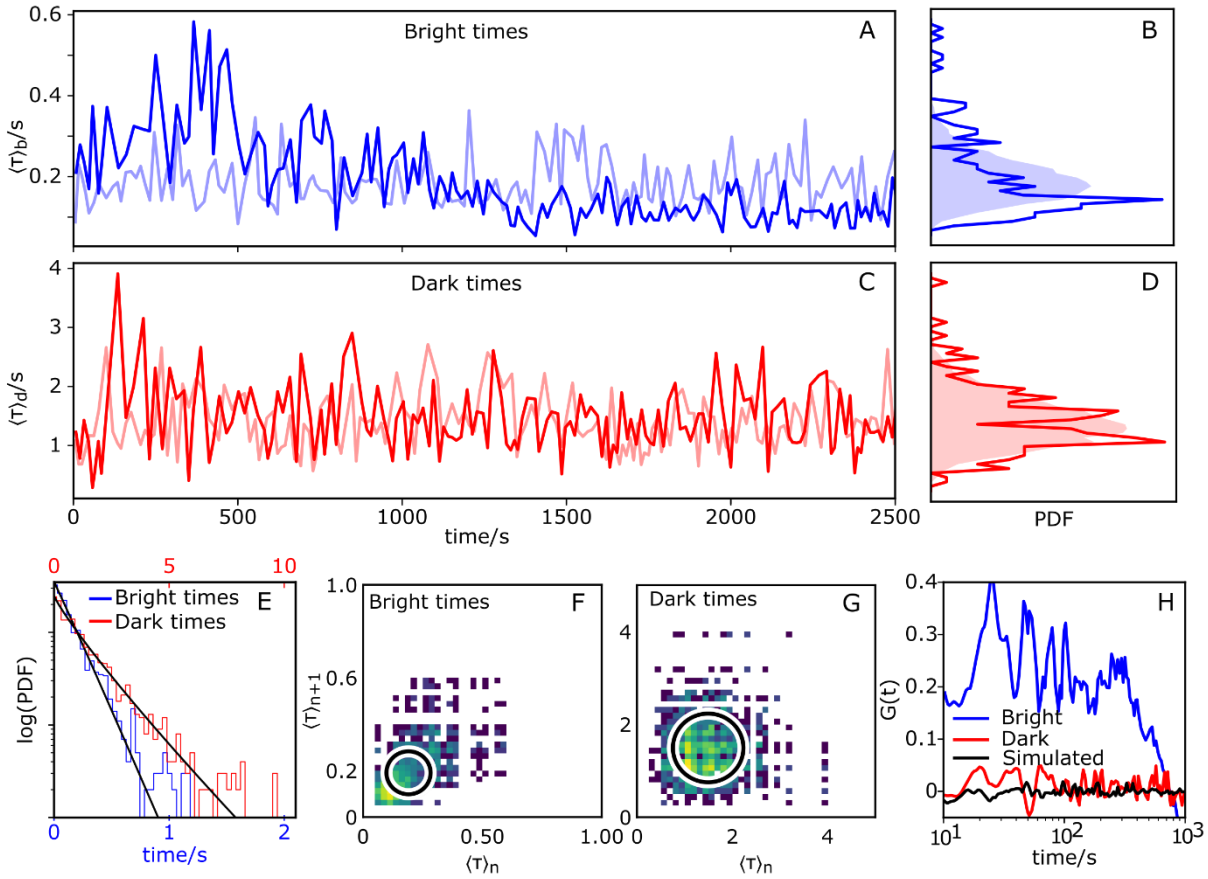

Figure S12: Dynamic heterogeneity obtained from a change point analysis. A, C) Average bright and dark times of a single Az plotted as functions of time. Each point is obtained through binned averaging of 10 successive redox events. B, D) Histograms of average bright and dark times in A, B. The shaded areas are histograms of Poisson processes with constant rates and same average times over a long simulation time. E) Histogram of un-averaged bright (blue) and dark (red) times. The time axis for bright times is shown in blue in the lower axis while the axis for dark times is shown in red in the upper axis. The black lines are stretched exponential fits of the data, with β = 0.85±0.04, τ = (0.14±0.02) s (bright) and β = 0.87±0.04, τ = (1.13±0.08) s (dark). F, G) 2D correlation plots of average bright and dark times $\langle\tau\rangle_{n+1}$ vs $\langle\tau\rangle_n$, where n = 0, 1, 2, … is the index of the data points in panels A,C. The circles indicate the 95th percentile of the simulated traces. H) Autocorrelation of average bright (blue) and dark (red) times. The corresponding autocorrelation of a simulated trace is shown in black.

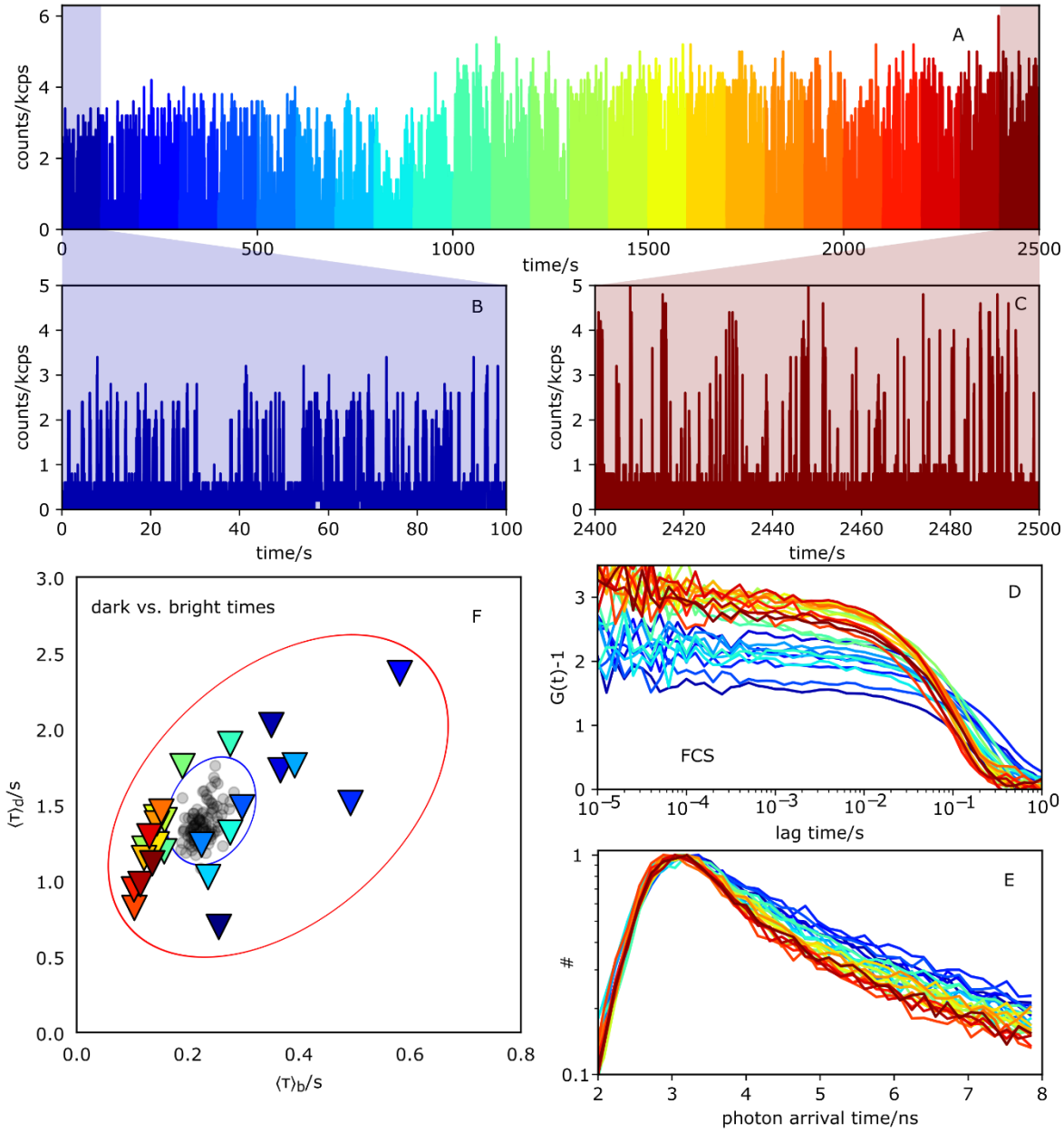

Figure S13: Change-point-free segmental analysis. A) The long time trace of Fig. 4 with binning time of 5 ms. The time trace is divided into small segments which are shown in different colors. B, C) Two segments of the trace: the first and last part. D) Fluorescence correlation of each segment of the trace. E) Photon arrival times of each segment. The colors of the FCS and lifetime curves correspond to the colors in the trace in A. F) Scatter plot between dark and bright times deduced from the correlation functions of (D). Triangles correspond to experimental data from Cu-Az while dots correspond to simulated data. The corresponding E^0 values vary between 41 mV and 75 mV, with about half of the values falling in the 40-45 mV range.

1.9.2. Molecule 2

Molecule 2 has a comparatively short trace and rather long switching times, so that its statistics are rather poor. Any deviations, if statistically significant, are best seen in the scatter plot of dark times (Fig. S14I) and in the changes of the segmental correlation function (Fig. S15D).

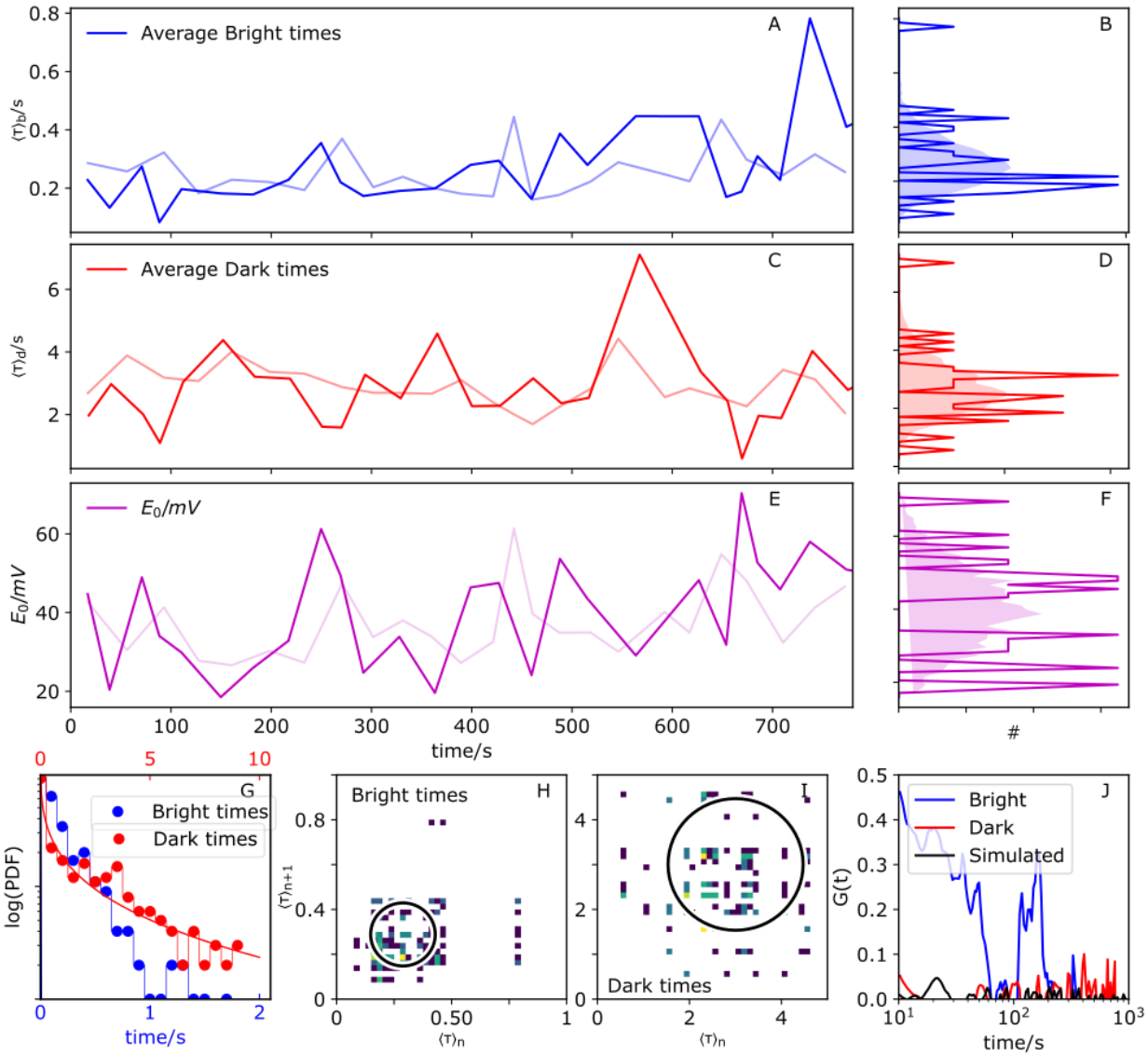

Figure S14: Dynamic heterogeneity from a change point analysis. See Fig. S12 for details.

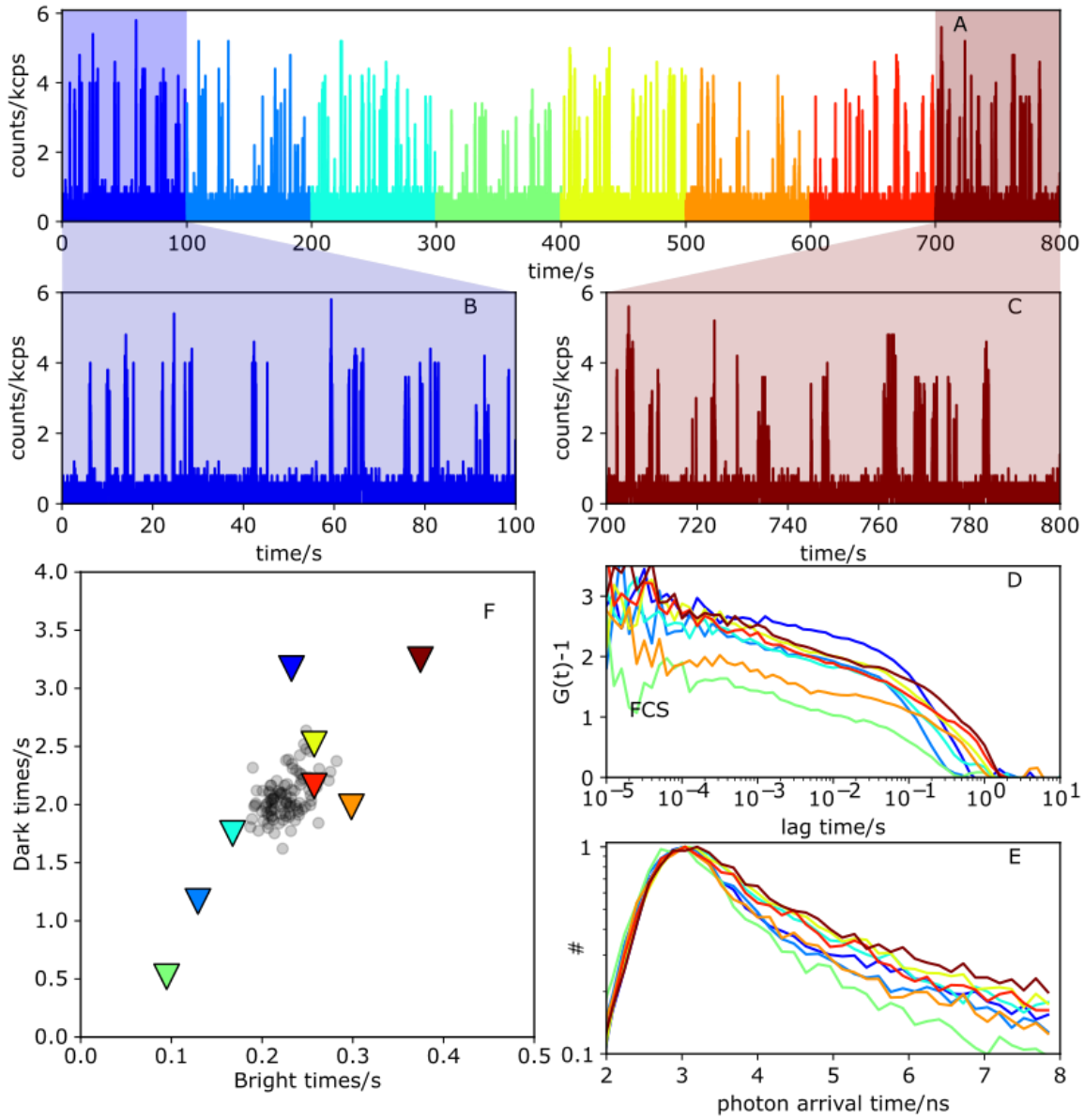

Figure S15: Dynamic heterogeneity from a change point-free segmental analysis. See Fig. S13 for details.

1.9.3. Molecule 3

Molecule 3 presents only weak dynamical heterogeneity, mostly visible for dark times around 300 s in Fig. S16B, and in the deviation from the circle in the correlation plot of Fig. S16H, I. Changes in the correlation function are also clear in Fig. S17D and in the lifetime histogram of Fig. S17E.

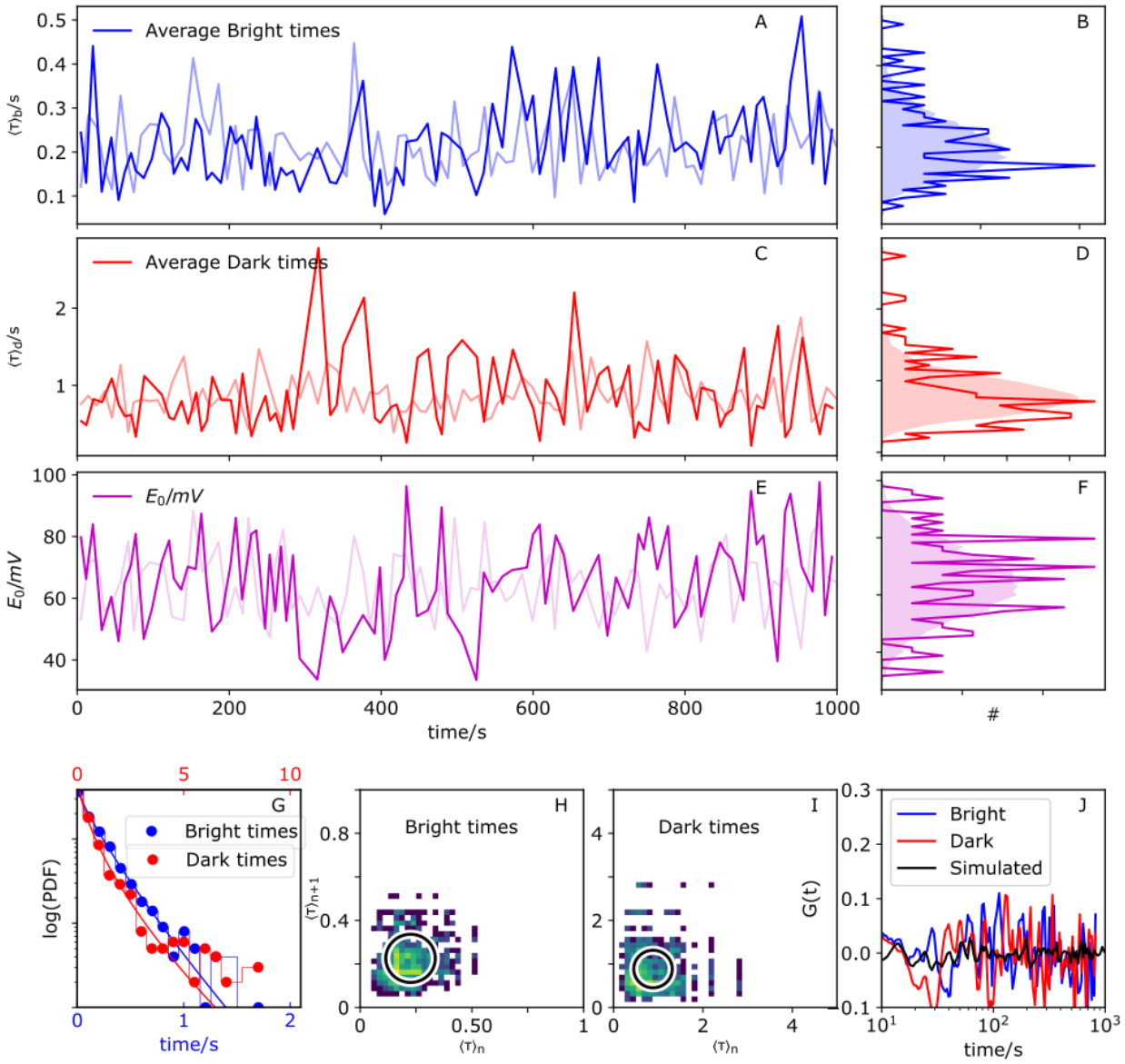

Figure S16: Dynamic heterogeneity from a change point analysis. See Fig. S12 for details.

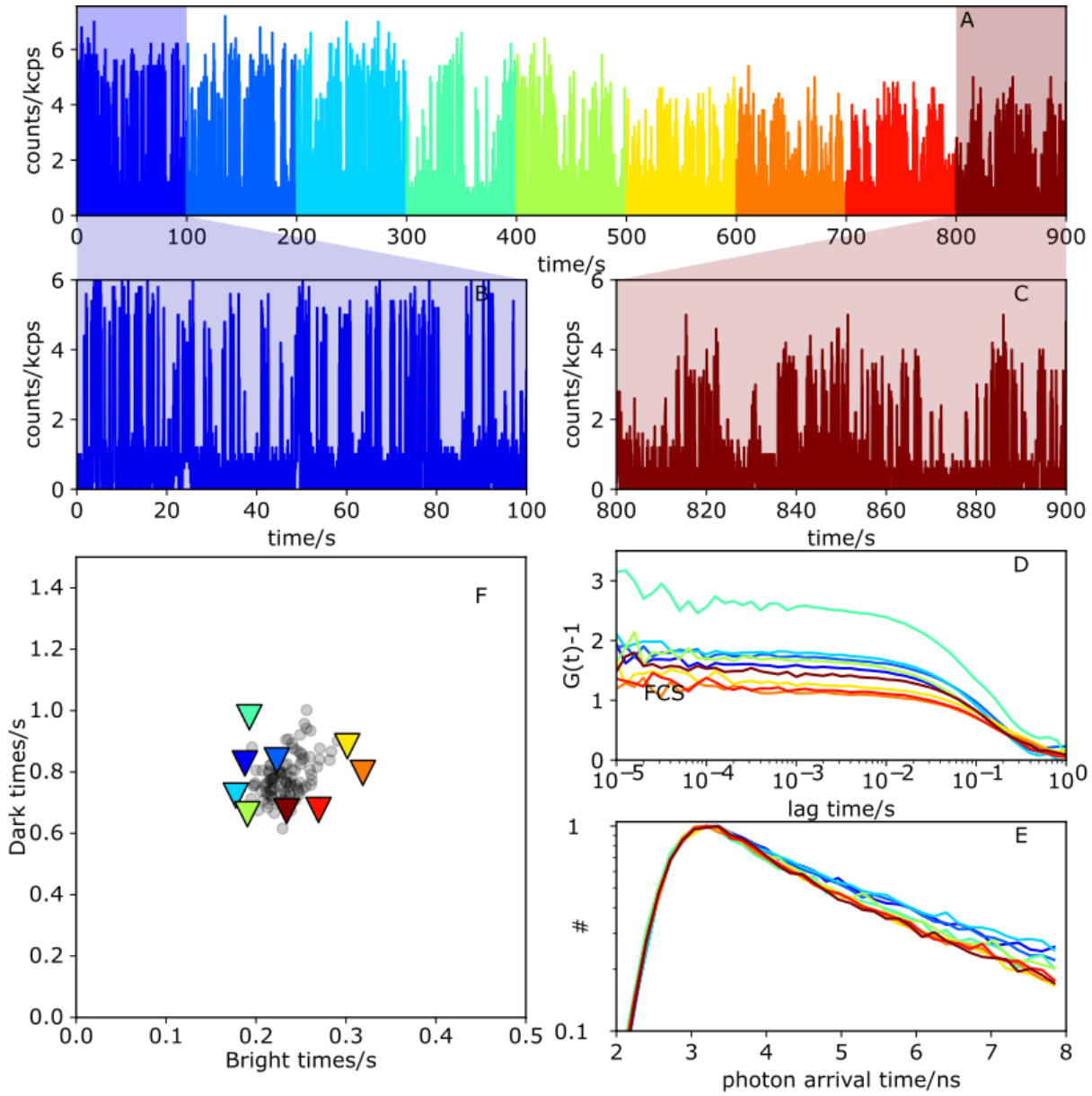

Figure S17: Dynamic heterogeneity from a change point-free segmental analysis. See Fig. S13 for details.

1.9.4. Molecule 4

Molecule 4 presents a spectacular variation of dark times (and to a lesser extent of bright times) between 200 and 720 s. We find variations from very short times (less than 1 s) between 0 and 200 s and between 720 and 750 s, to long dark times (up to 10 s) between 200 and 750 s. Note the spacing of averaged measured points in this region due to the lengthening of the dark times. The bright times also appear to lengthen during this interval, although the effect is weaker. Variations in bright and dark times appear to be correlated in this case. This extreme event leaves traces in all analysis modes: histograms of Figs. S18B, D, F, stretching histograms of Fig. S18G, correlation plots of S18H, I, and correlation function of dark times in S18J. These variations are also conspicuous in all panels of the segmental analysis of Fig. S19.

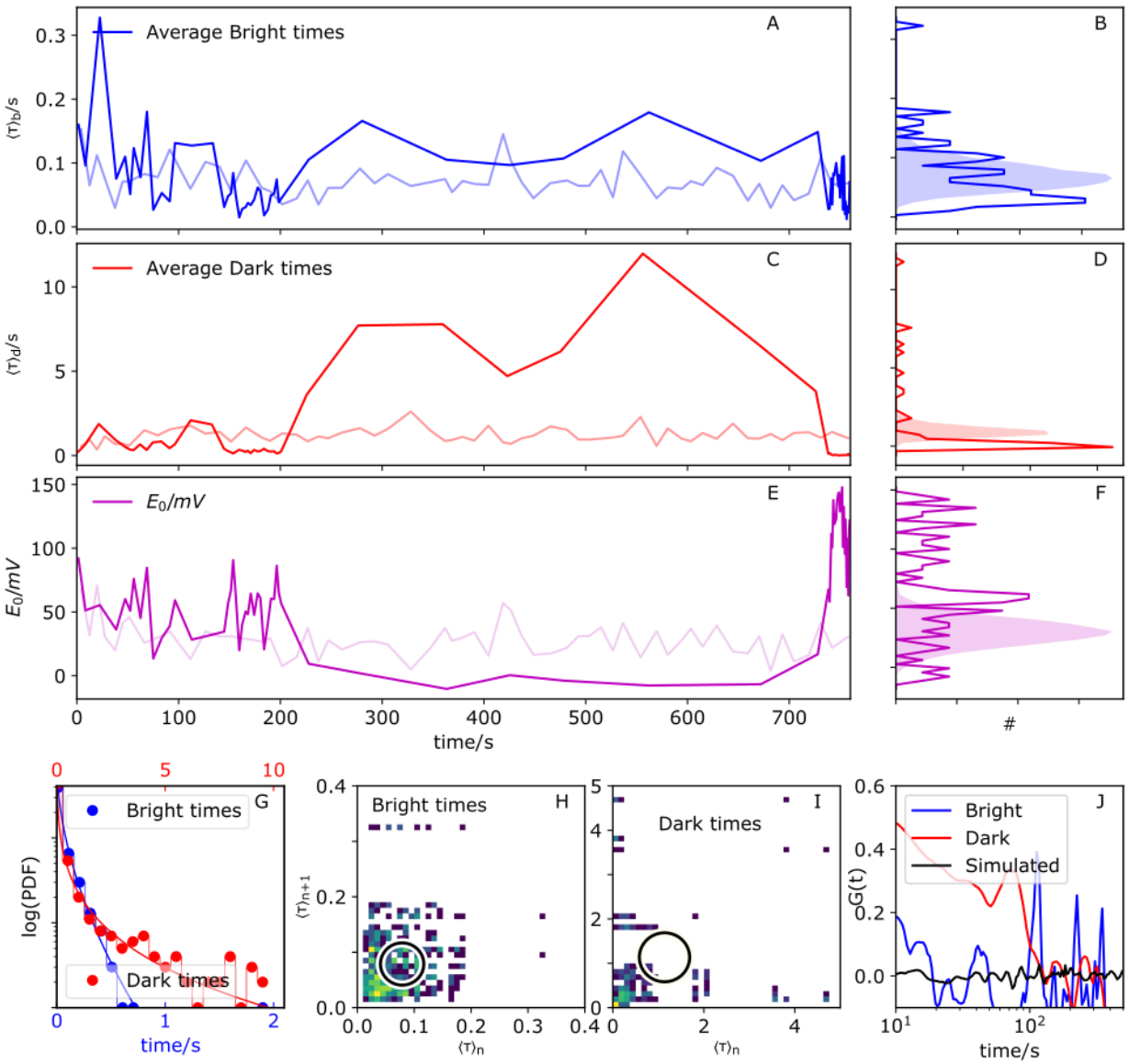

Figure S18: Dynamic heterogeneity from a change point analysis. See Fig. S12 for details.

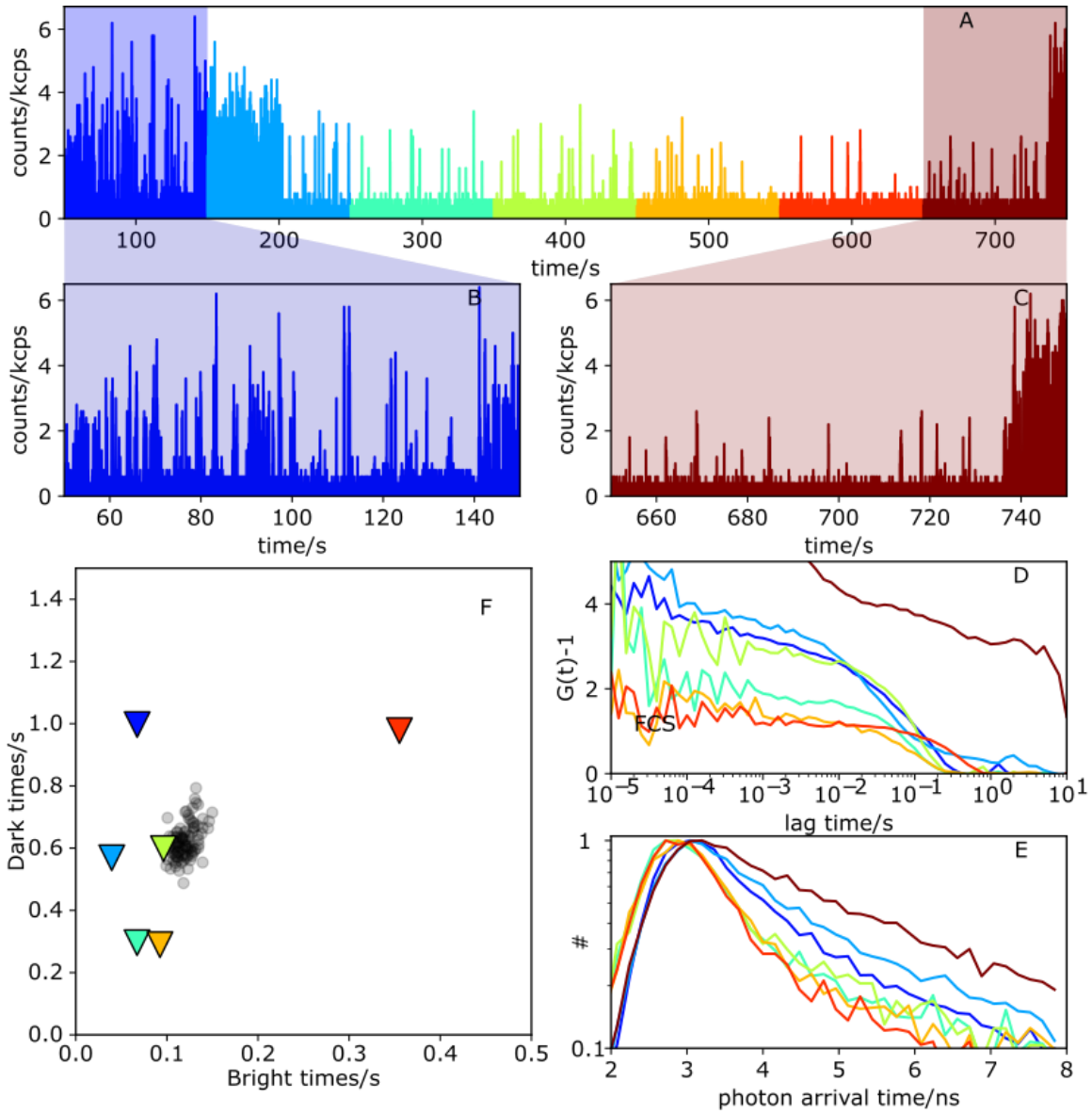

Figure S19: Dynamic heterogeneity from a change point-free segmental analysis. See Fig. S13 for details.

1.9.5. Molecule 5

Molecule 5 presents one large deviation of bright and dark times from average in the first 100 s of the time trace, followed by a deviation of dark times between 300 and 500 s. These deviations are very apparent in the histograms Fig.S20B, D and the correlation plots Fig. S20H, I. The segmental analysis confirms these deviations.

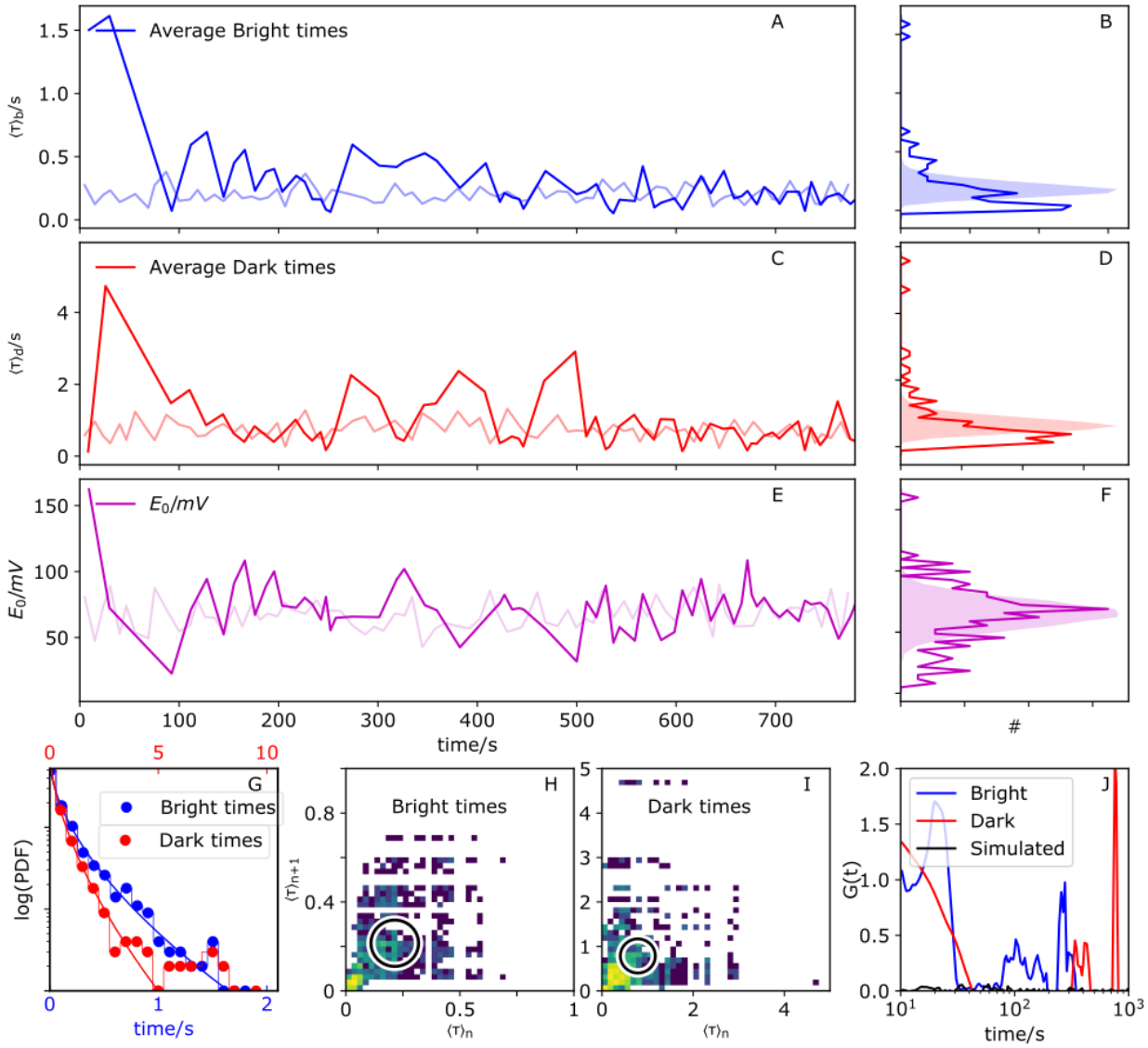

Figure S20: Dynamic heterogeneity from a change point analysis. See Fig. S12 for details.

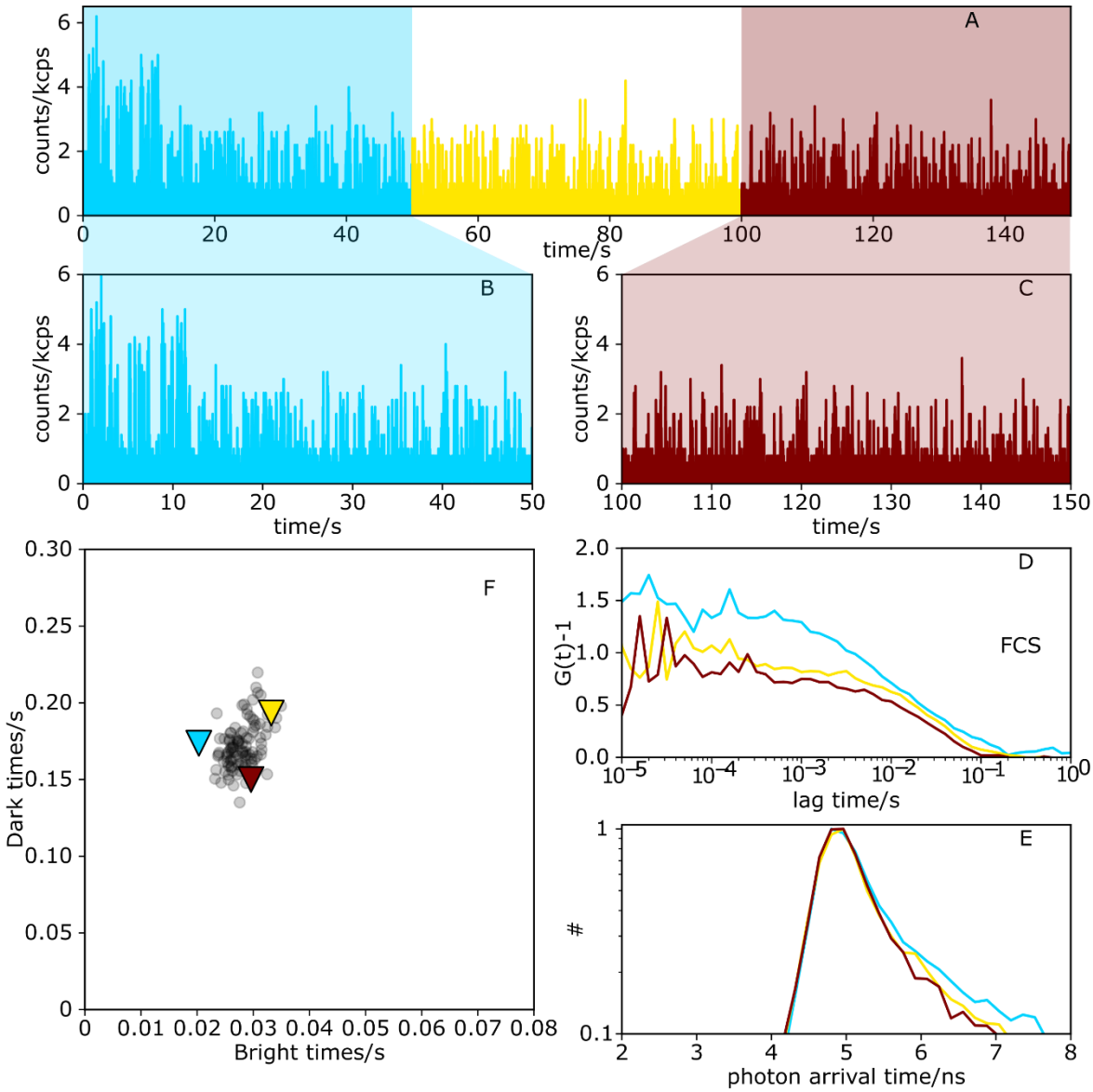

Figure S21: Dynamic heterogeneity from a change point-free segmental analysis. See Fig. S13 for details.

1.9.6. Molecule 6

The dark times of Molecule 6 agree very well with a purely Poissonian distribution of times, without heterogeneity (see Fig. S22D, I). The bright times, however, present a significant deviation from random, mostly visible in Fig. S22H, but also visible in the histogram of Fig. S22B. Again, the segmental analysis of Fig. 23 confirms the presence of significant heterogeneity, although it cannot be obviously assigned to bright times from the correlation analysis (scatter plot of Fig. 23F). The different heterogeneity of bright and dark times is very clear in Figs. 22H, I.

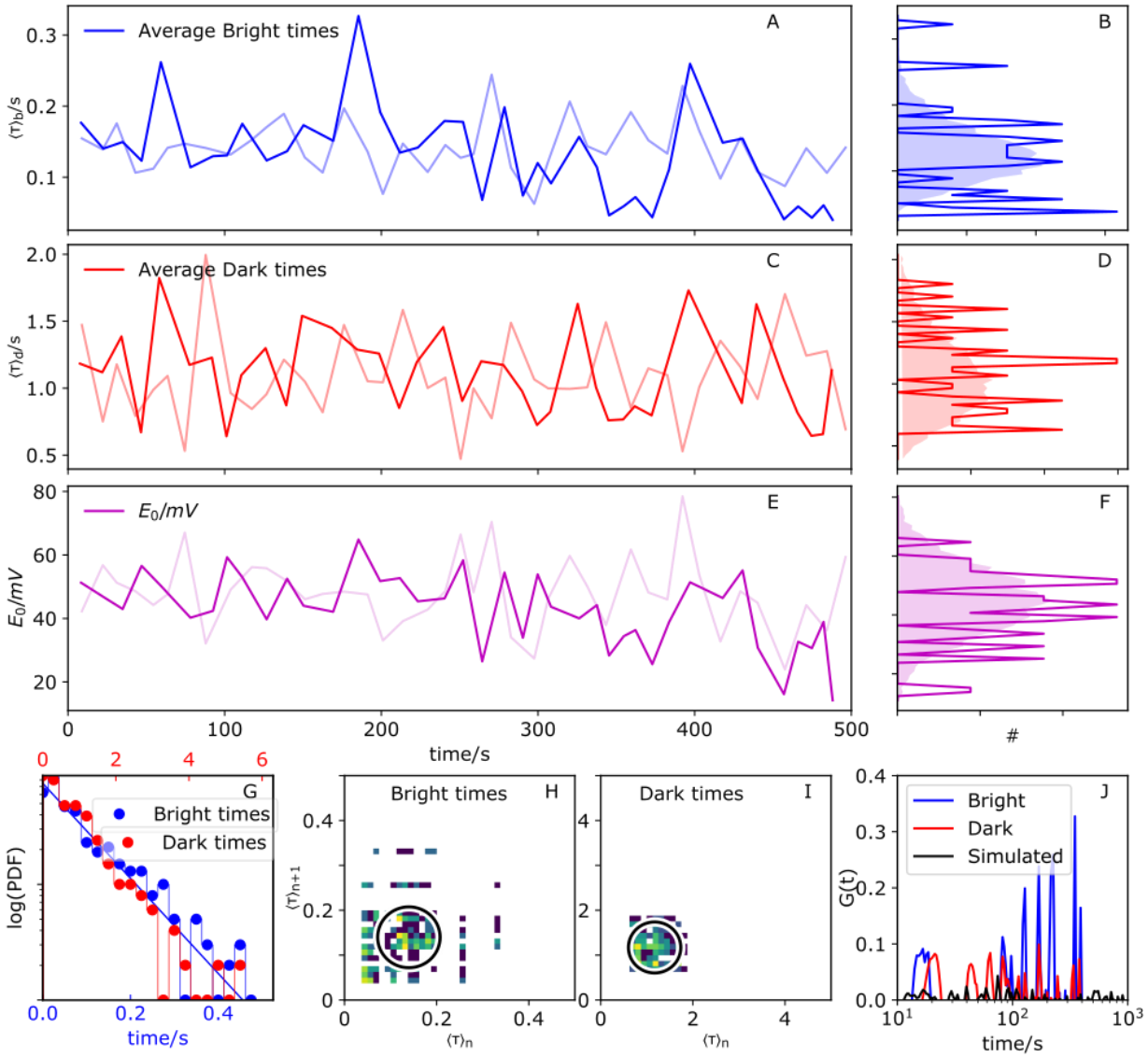

Figure S22: Dynamic heterogeneity from a change point analysis. See Fig. S12 for details.

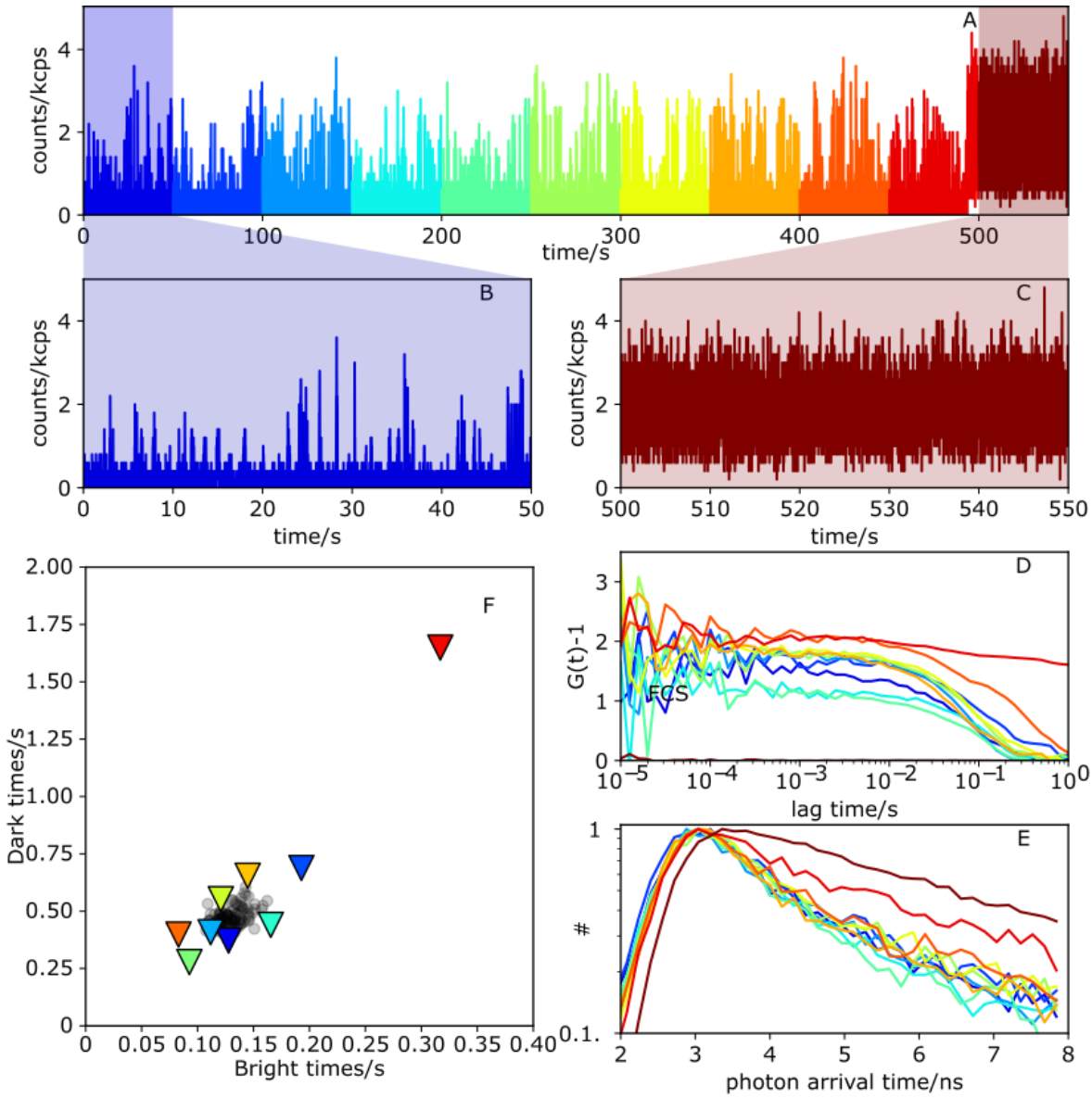

Figure S23: Dynamic heterogeneity from a change point-free segmental analysis. See Fig. S13 for details.

1.9.7. Molecule 7

The dark times of Molecule 7 change significantly between the first 50 s of the trace and the rest. This event leads to a double peak in the histogram of Fig. S24D and to a double spot in Fig. S24I. Bright times appear much more compatible with a random distribution. The change of dark times also leads to changes of the correlation function in the segmental analysis of Fig. S25D.

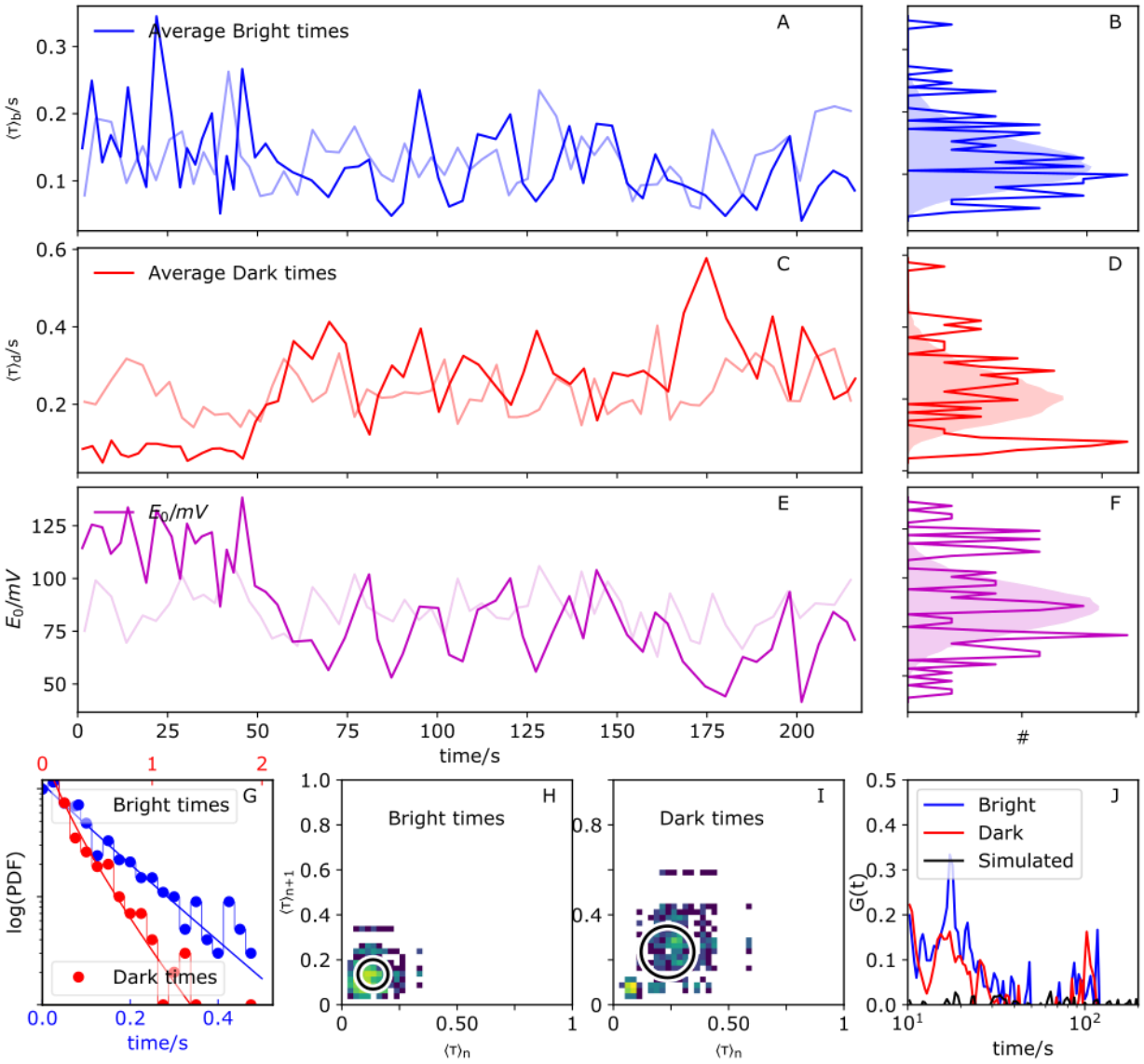

Figure S24: Dynamic heterogeneity from a change point analysis. See Fig. S12 for details.

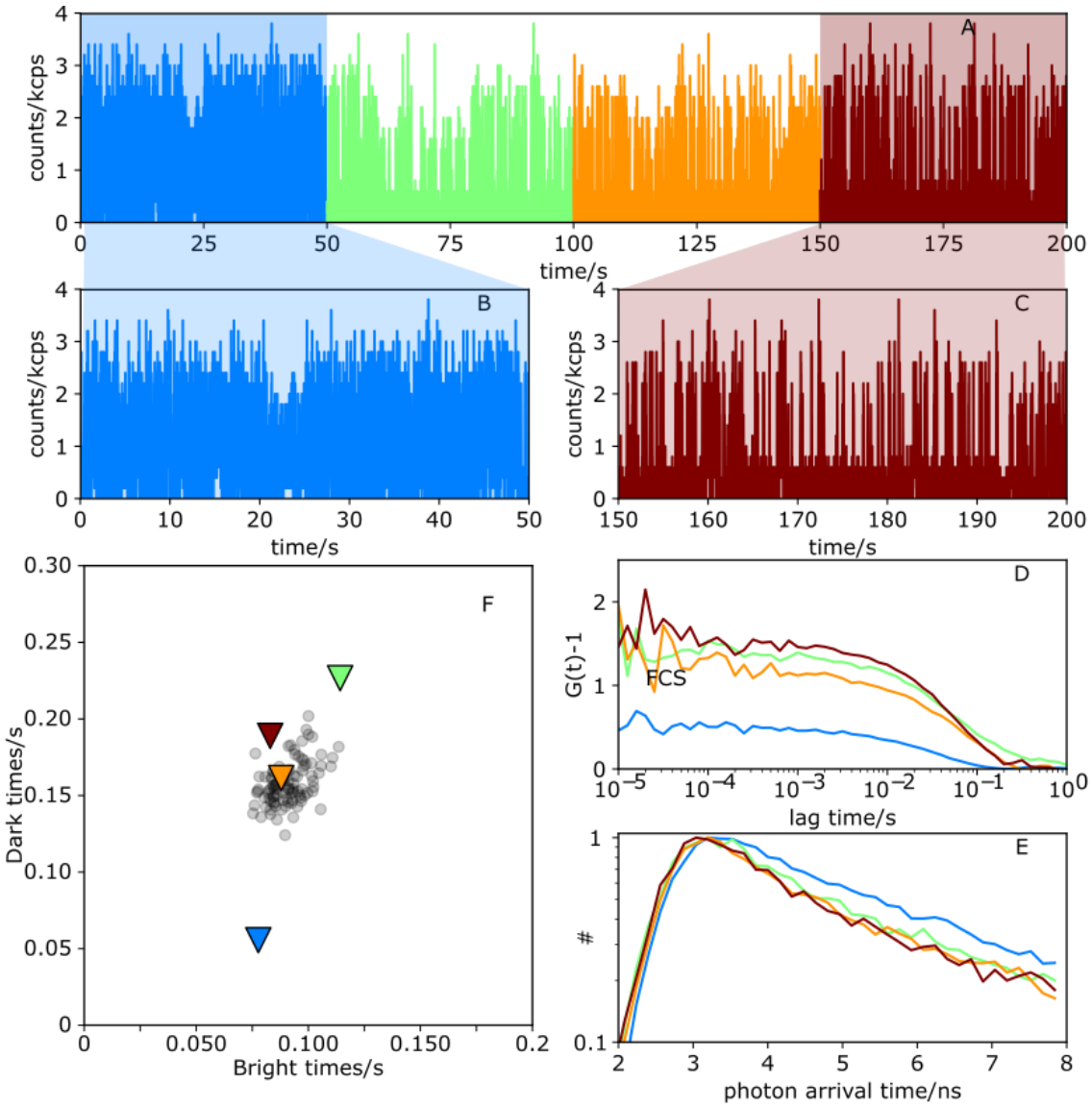

Figure S25: Dynamic heterogeneity from a change point-free segmental analysis. See Fig. S13 for details.

1.9.8. Molecule 8

Molecule 8 presents weak deviations from random jumps, mostly visible in Fig. S26C, at the beginning of the trace, to a lesser extent in the histogram of Fig. S26D and by the excess of correlation points outside the 95 % circle in Fig. S26H,I. Changes in the correlation function are also clear in Fig. S27D.

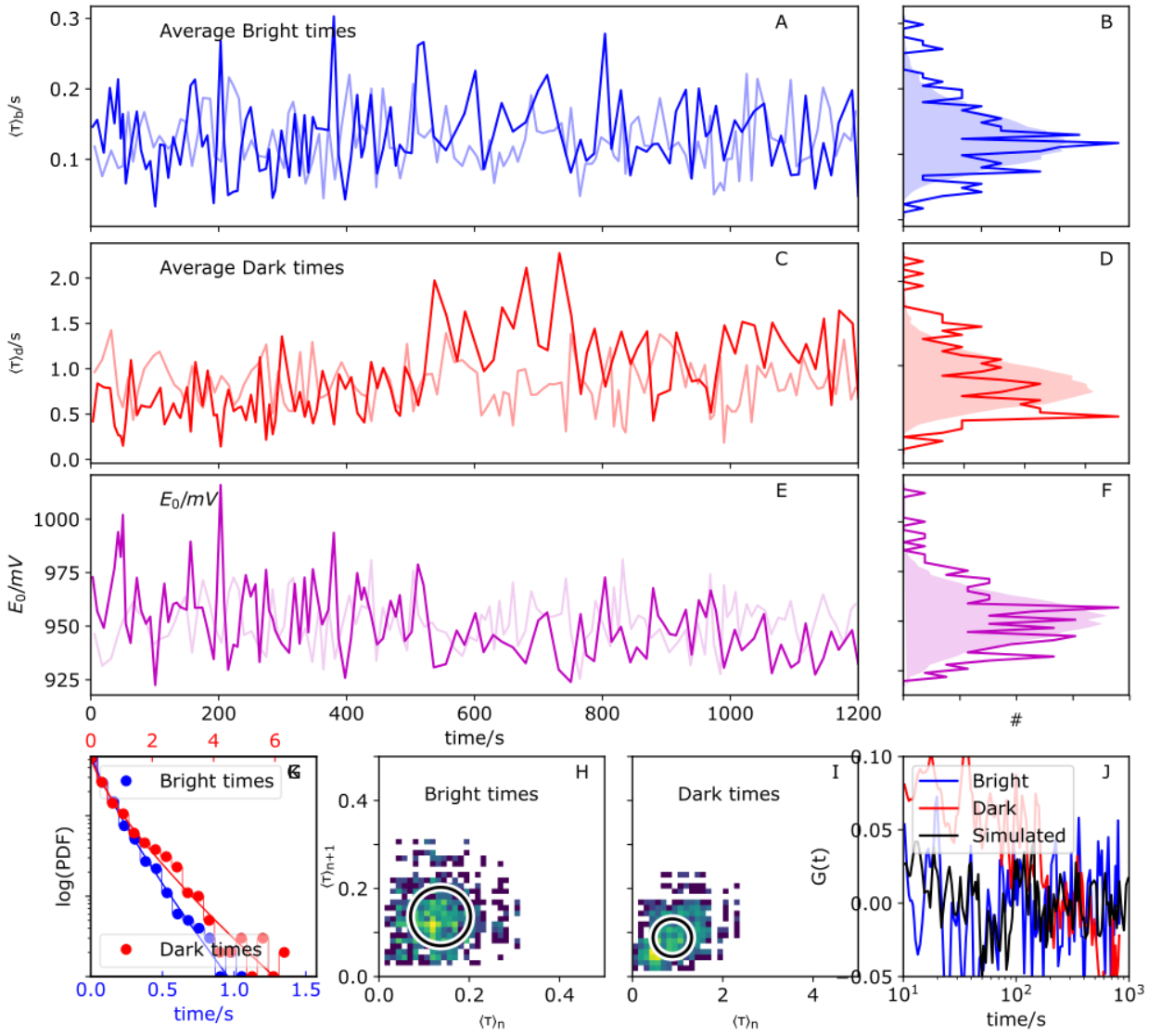

Figure S26: Dynamic heterogeneity from a change point analysis. See Fig. S12 for details.

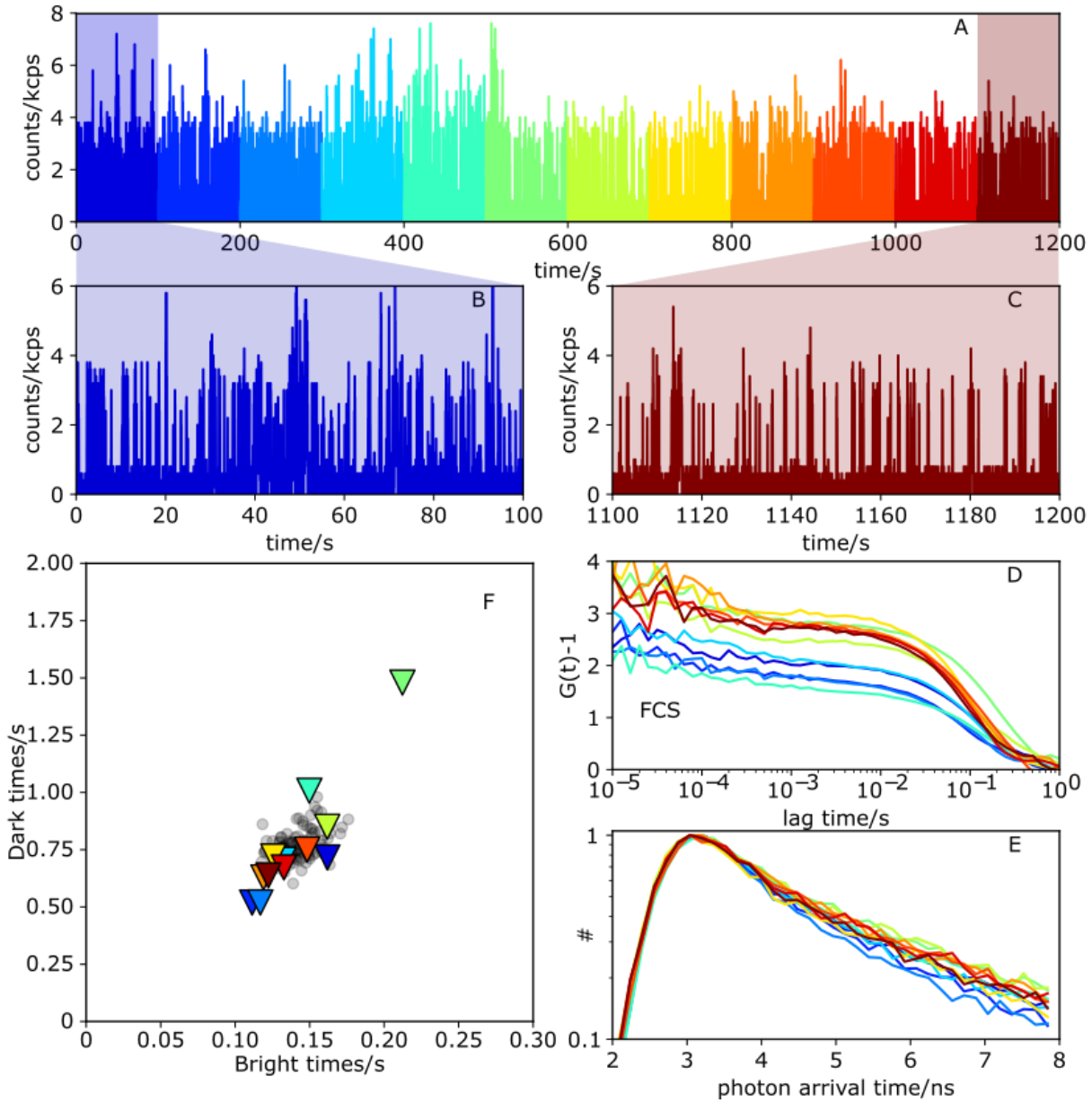

Figure S27: Dynamic heterogeneity from a change point-free segmental analysis. See Fig. S13 for details.

1.9.9. Molecule 9

Molecule 9 is a case where no obvious sign of heterogeneity appears in the time traces. All bright and dark times appear compatible with Poisson distributions, as confirmed by all histograms, and correlation plots. The segmental analysis also confirms that this molecule doesn't seem to undergo much conformational rearrangement during the measurement.

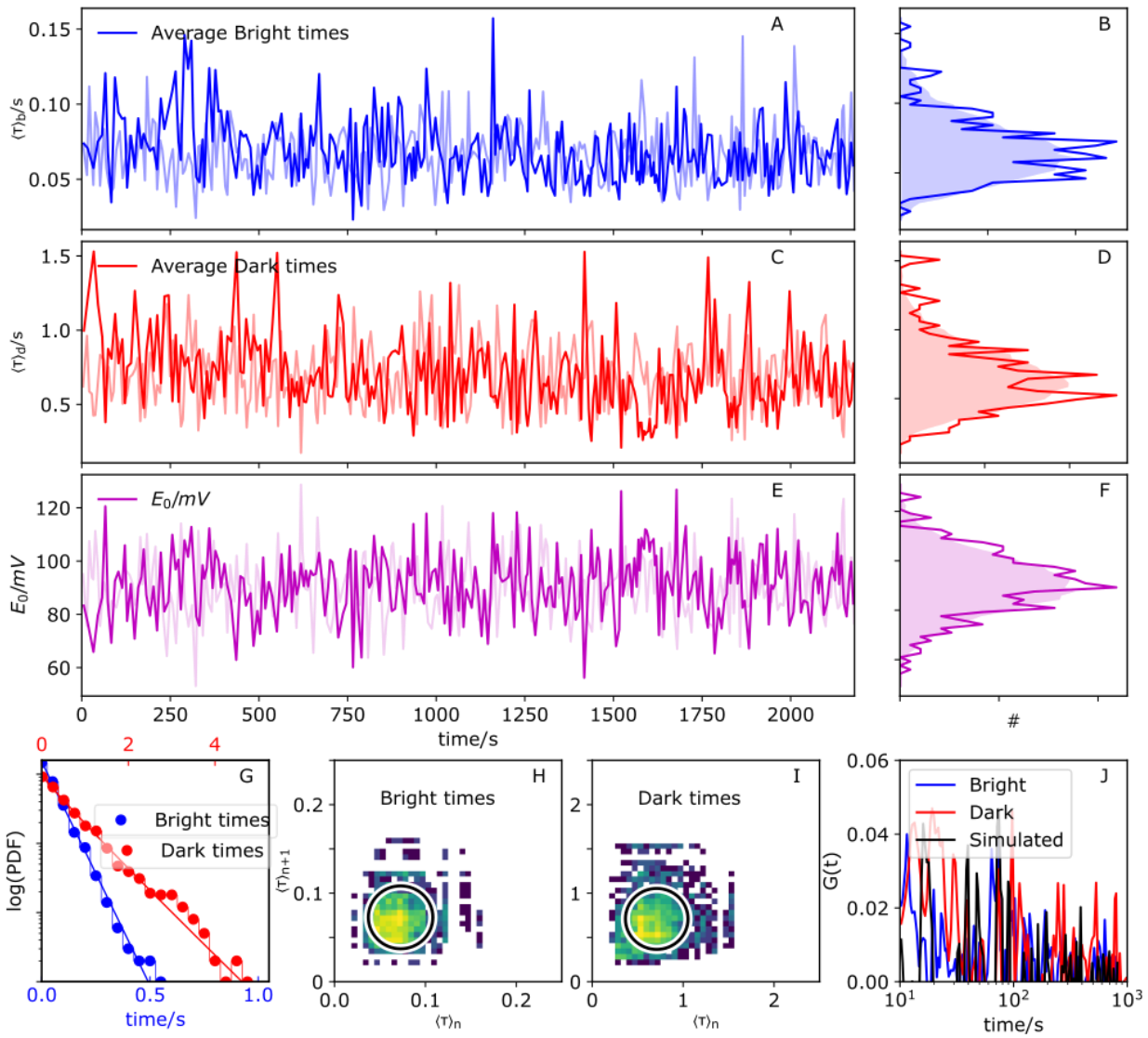

Figure S28: Dynamic heterogeneity from a change point analysis. See Fig. S12 for details.

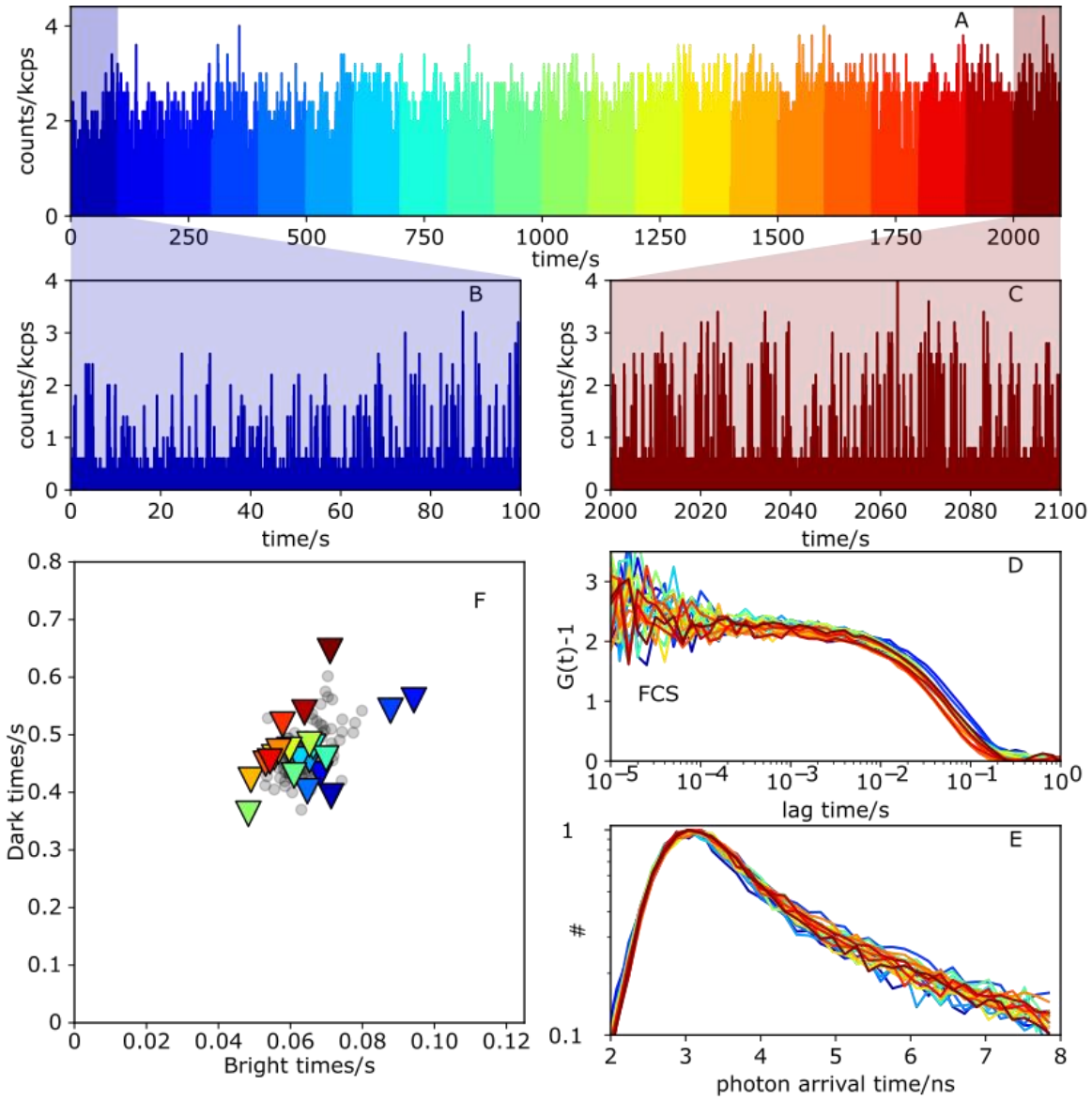

Figure S29: Dynamic heterogeneity from a change point-free segmental analysis. See Fig. S13 for details.

1.9.10. Molecule 10

Molecule 10 is another case of a quiet molecule with little or no evidence for dynamical heterogeneity. Deviation from the circle in the bright times scatter plot (Fig. S30H) is the only possible indication of small rearrangements, too subtle to be visible on the time trace or the histograms. The correlation functions in the segmental analysis (Fig. S31D) confirm the occurrence of a small change after 600 s.

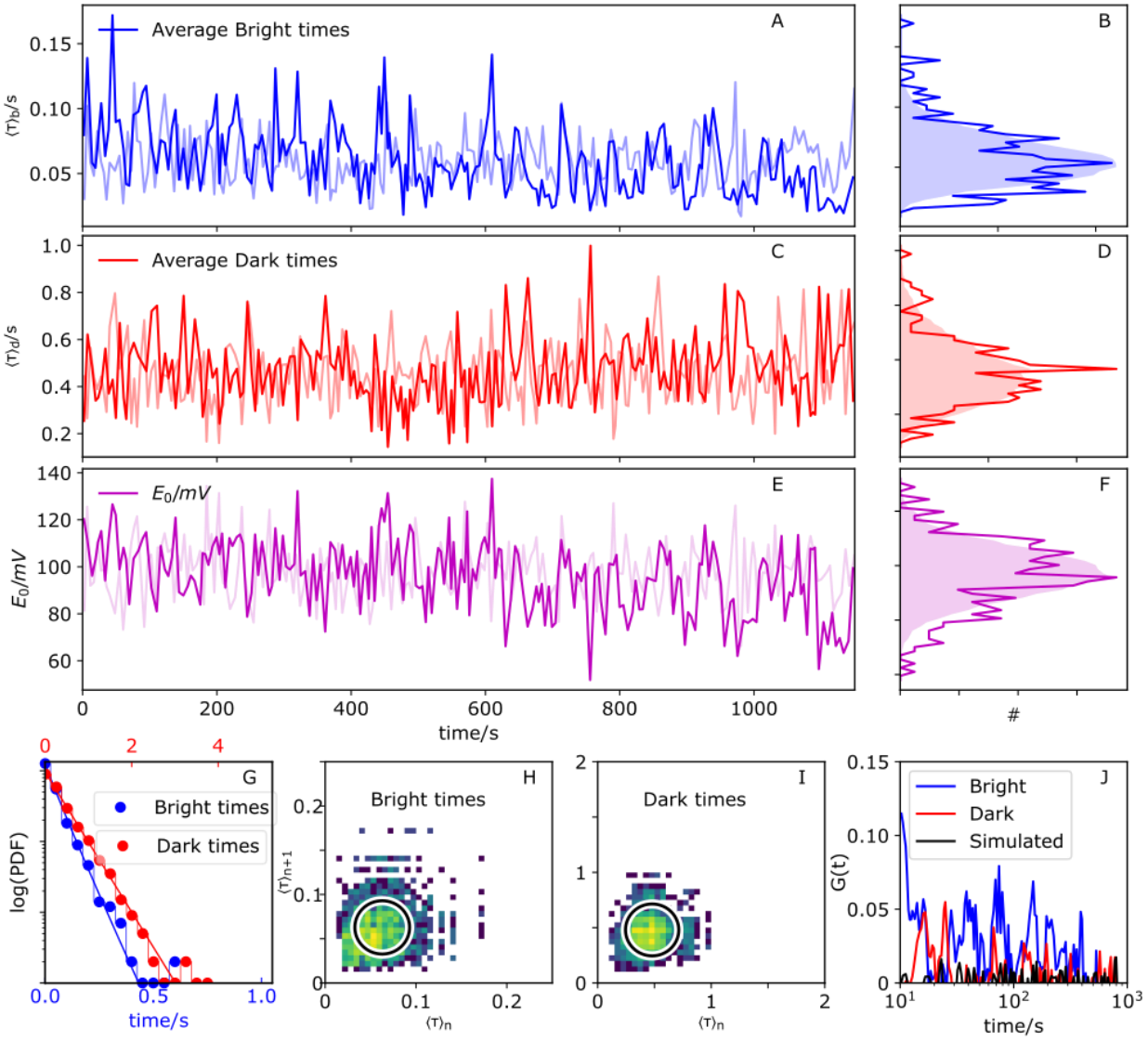

Figure S30: Dynamic heterogeneity from a change point analysis. See Fig. S12 for details.

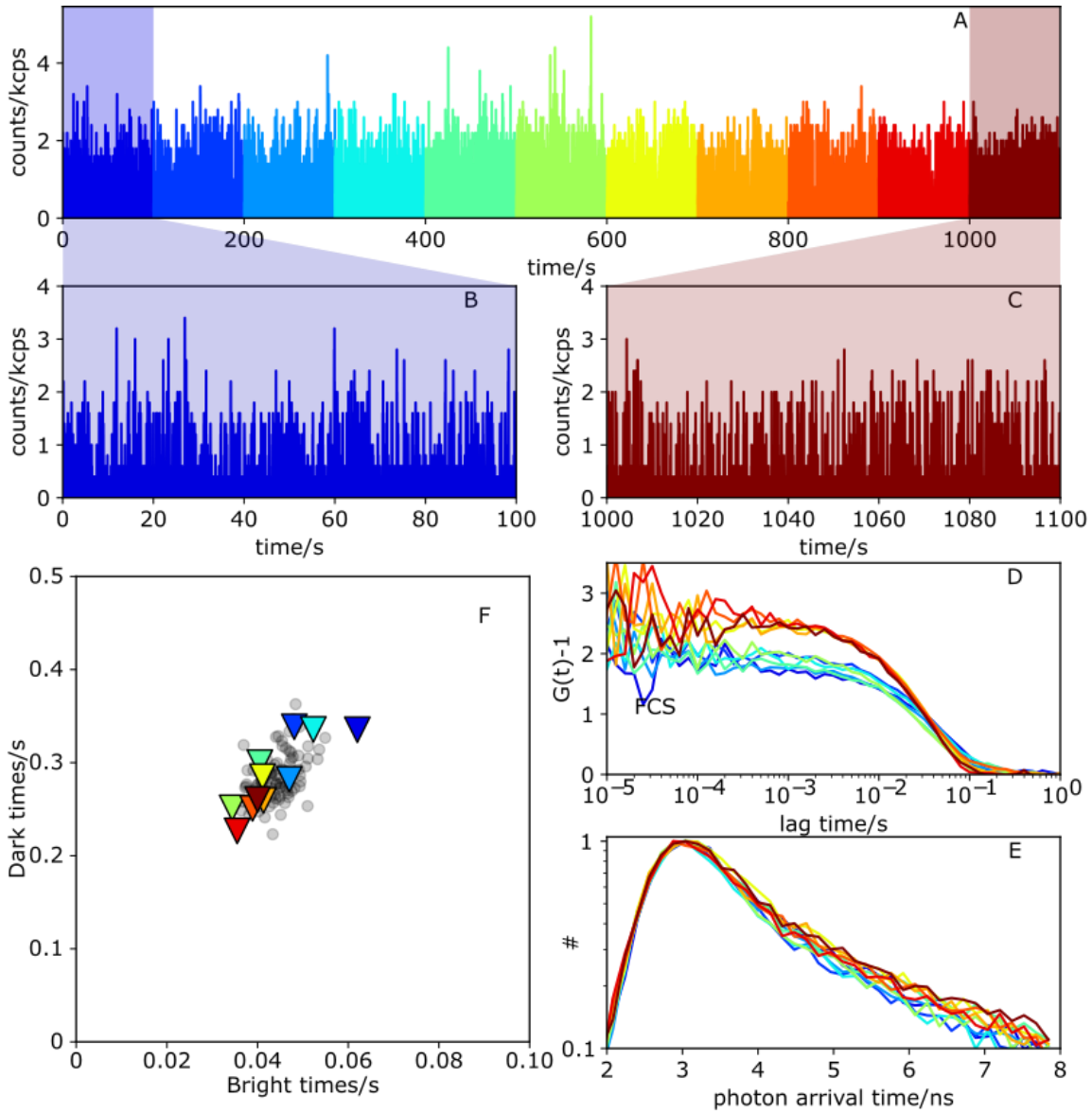

Figure S31: Dynamic heterogeneity from a change point-free segmental analysis. See Fig. S13 for details.

1.9.11. Molecule 11

Molecule 11 has a short trace with comparatively few events, showing longer dark times in the first 150 s. This deviation is best seen in the histogram of Fig. S32I. The segmental analysis doesn't indicate any strong conformational rearrangement.

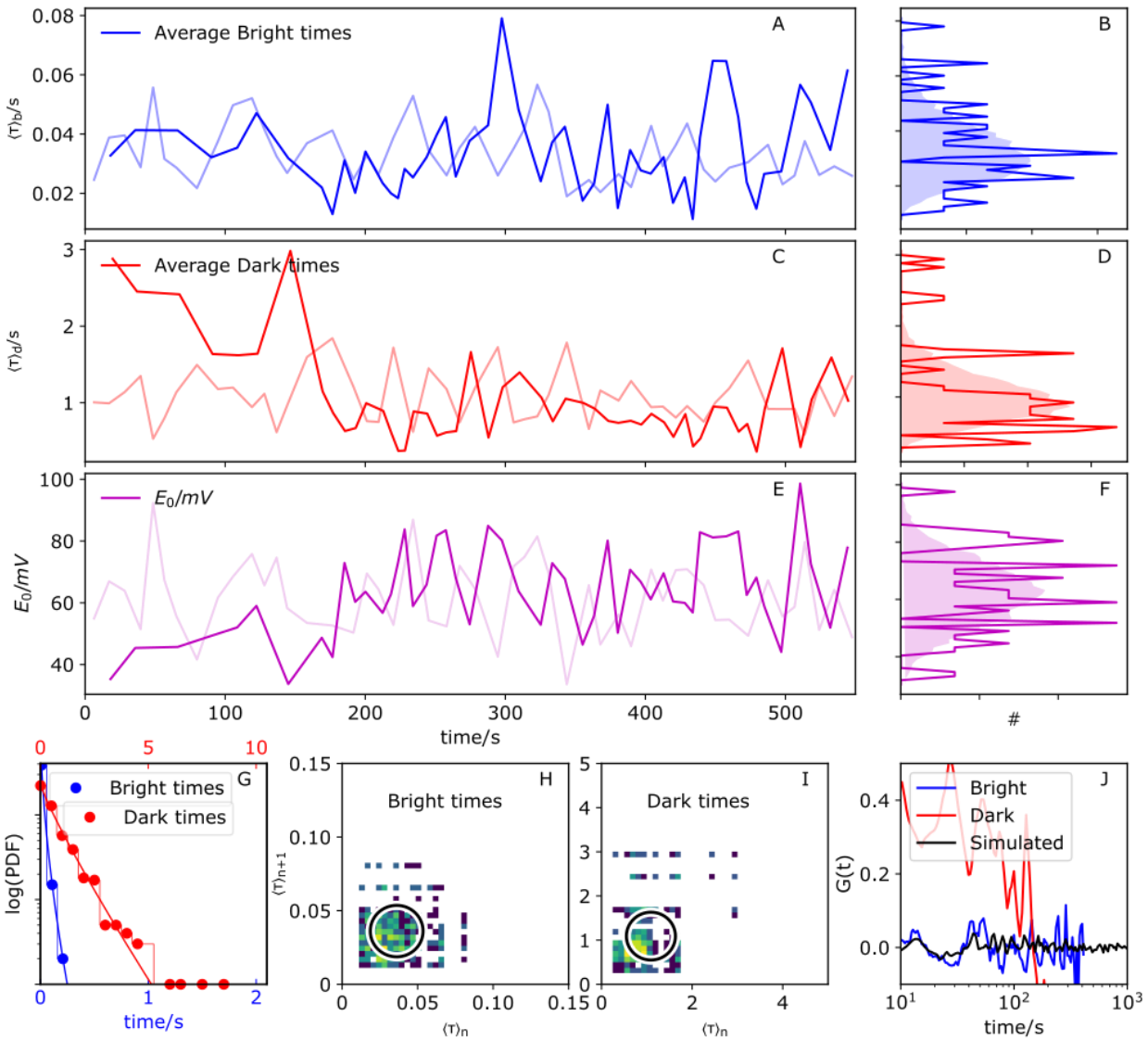

Figure S32: Dynamic heterogeneity from a change point analysis. See Fig. S12 for details.

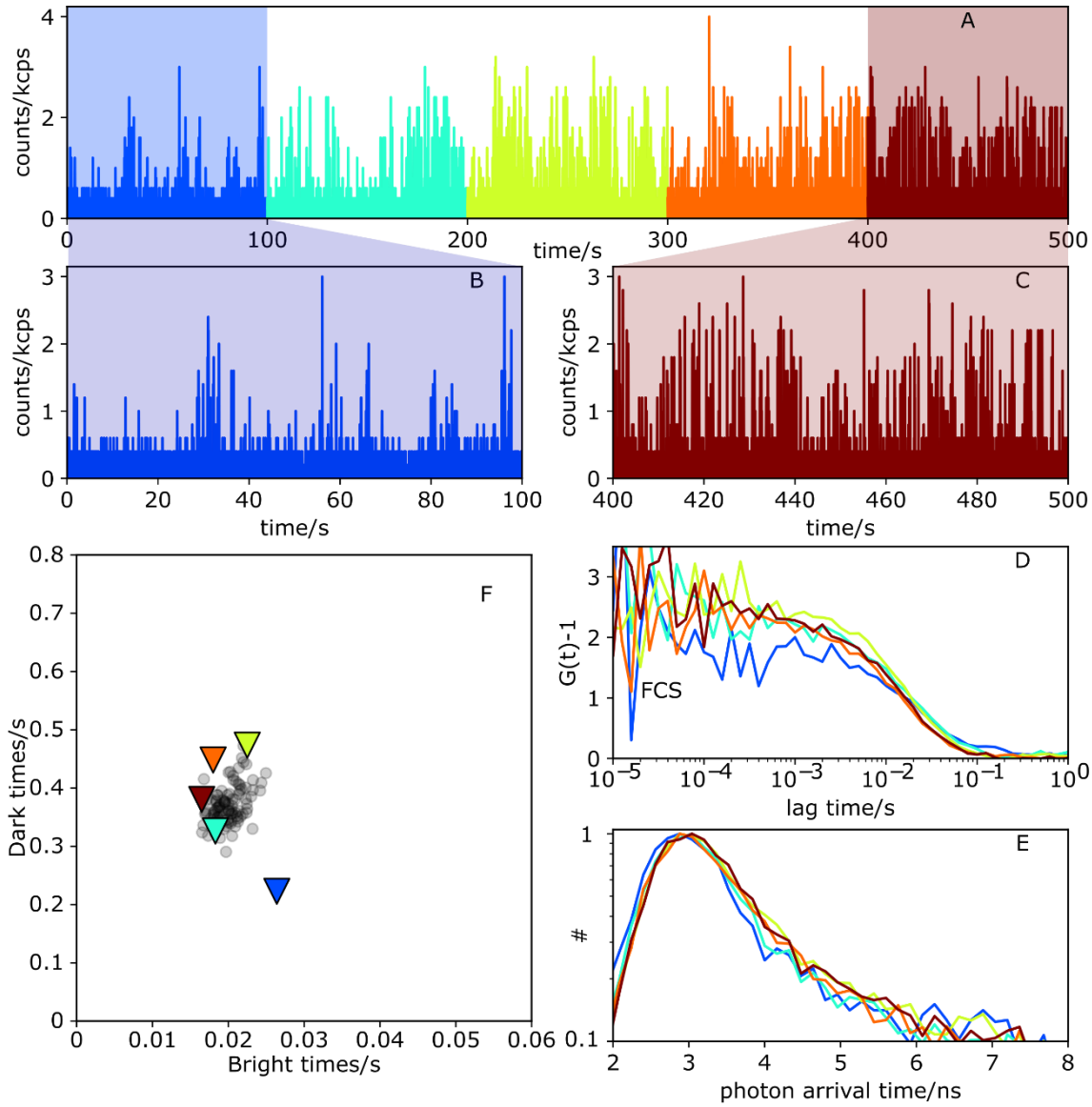

Figure S33: Dynamic heterogeneity from a change point-free segmental analysis. See Fig. S13 for details.

1.9.12. Molecule 12

The statistics are too poor in the case of Molecule 12 for any strong statement about heterogeneity from the time trace. The segmental analysis of Fig. S35D, E, however, clearly shows changes in the correlation function.

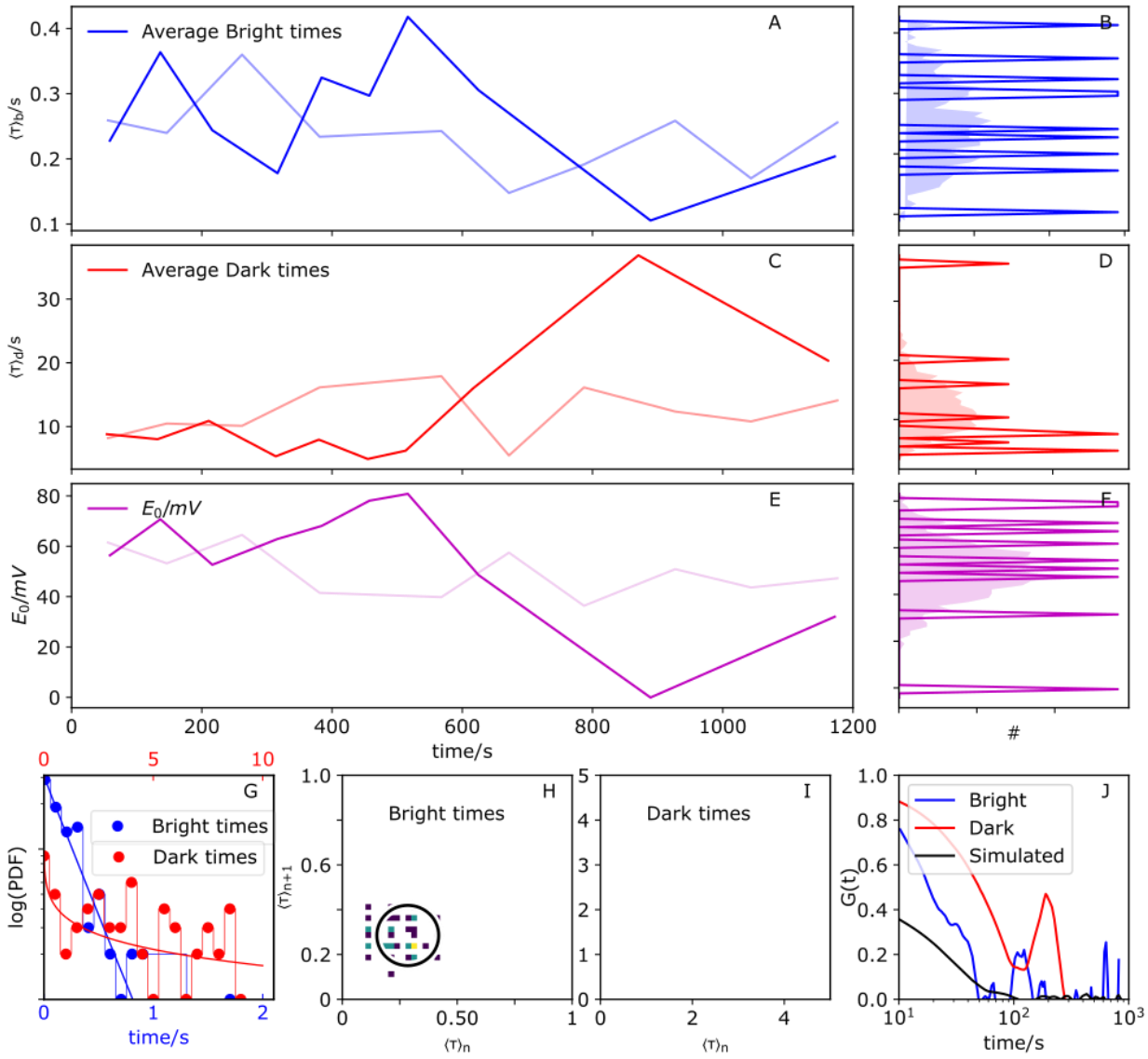

Figure S34: Dynamic heterogeneity from a change point analysis. See Fig. S12 for details.

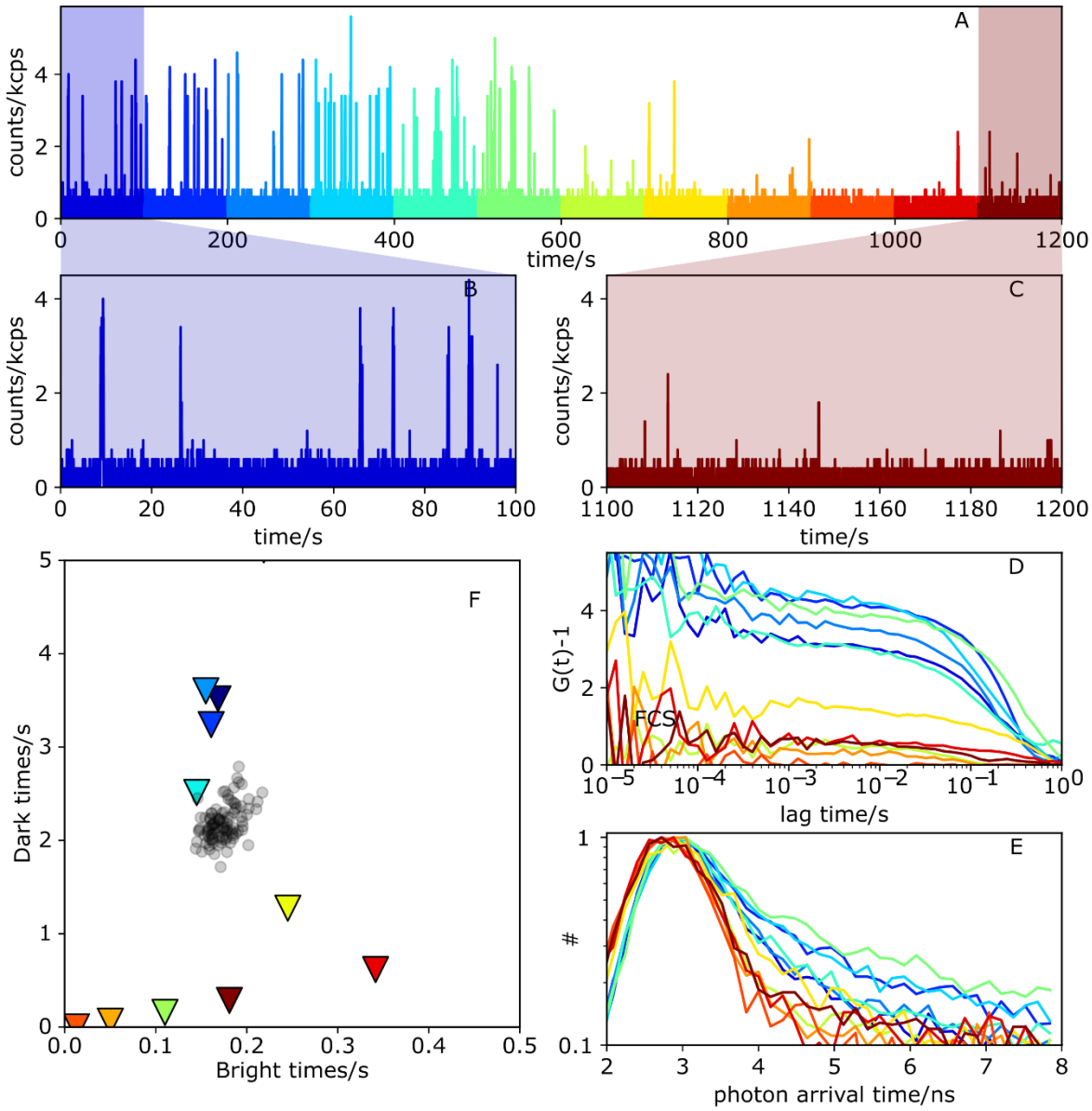

Figure S35: Dynamic heterogeneity from a change point-free segmental analysis. See Fig. S13 for details.

1.9.13. Molecule 13

Molecule 13 shows a significant shortening of the dark times across the time trace, from 6 s at the beginning, to about 1 s towards the end of the trace. The dark times then rise again to about 3 s. The bright times, show a similar, if much less pronounced, behaviour. This is confirmed by the scatter plots of Fig. S36H, I and by the correlation function of bright times in Fig. S36J. The segmental analysis also confirms the gradual change in correlation function along the trajectory (Fig. S37D).

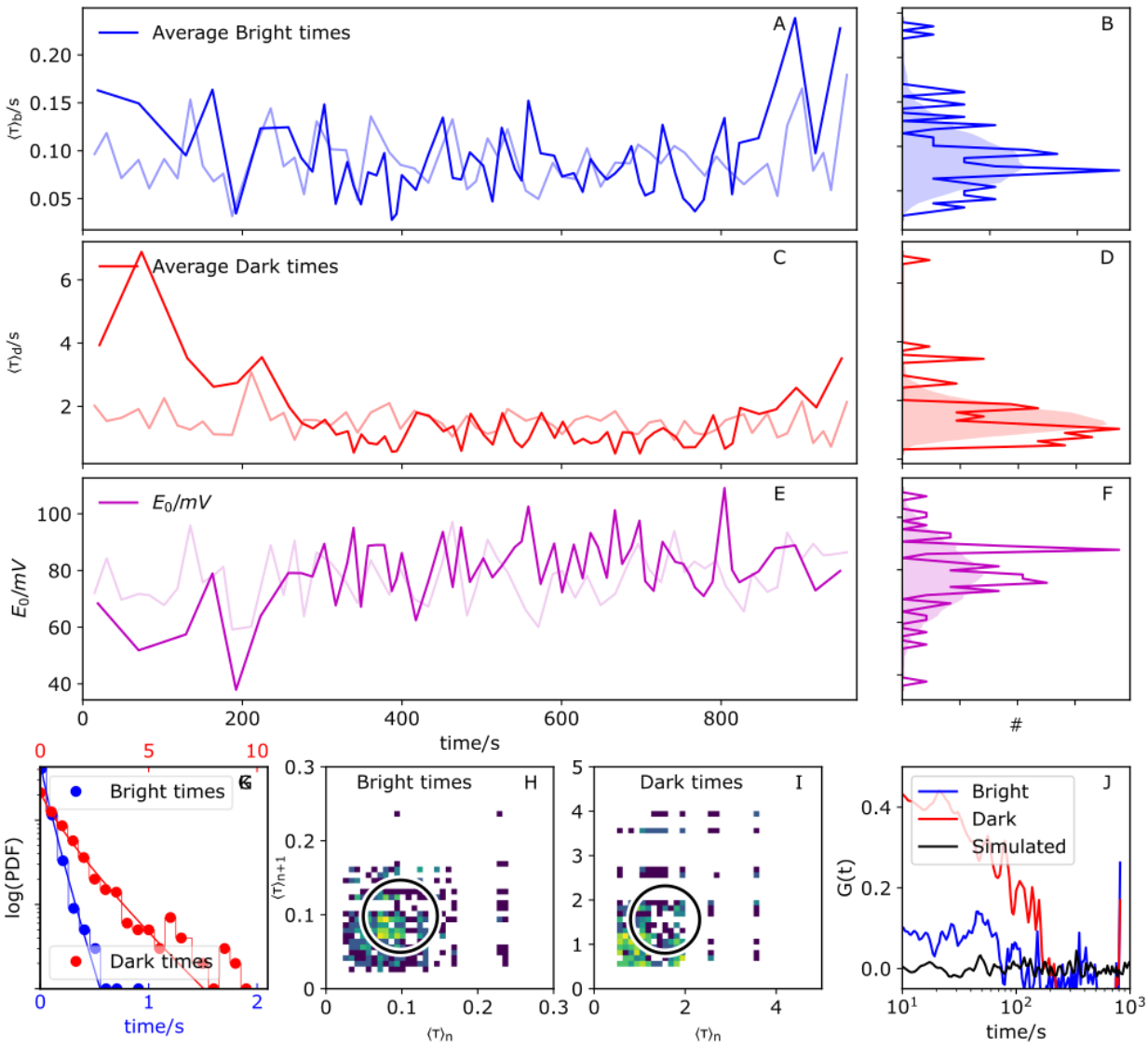

Figure S36: Dynamic heterogeneity from a change point analysis. See Fig. S12 for details.

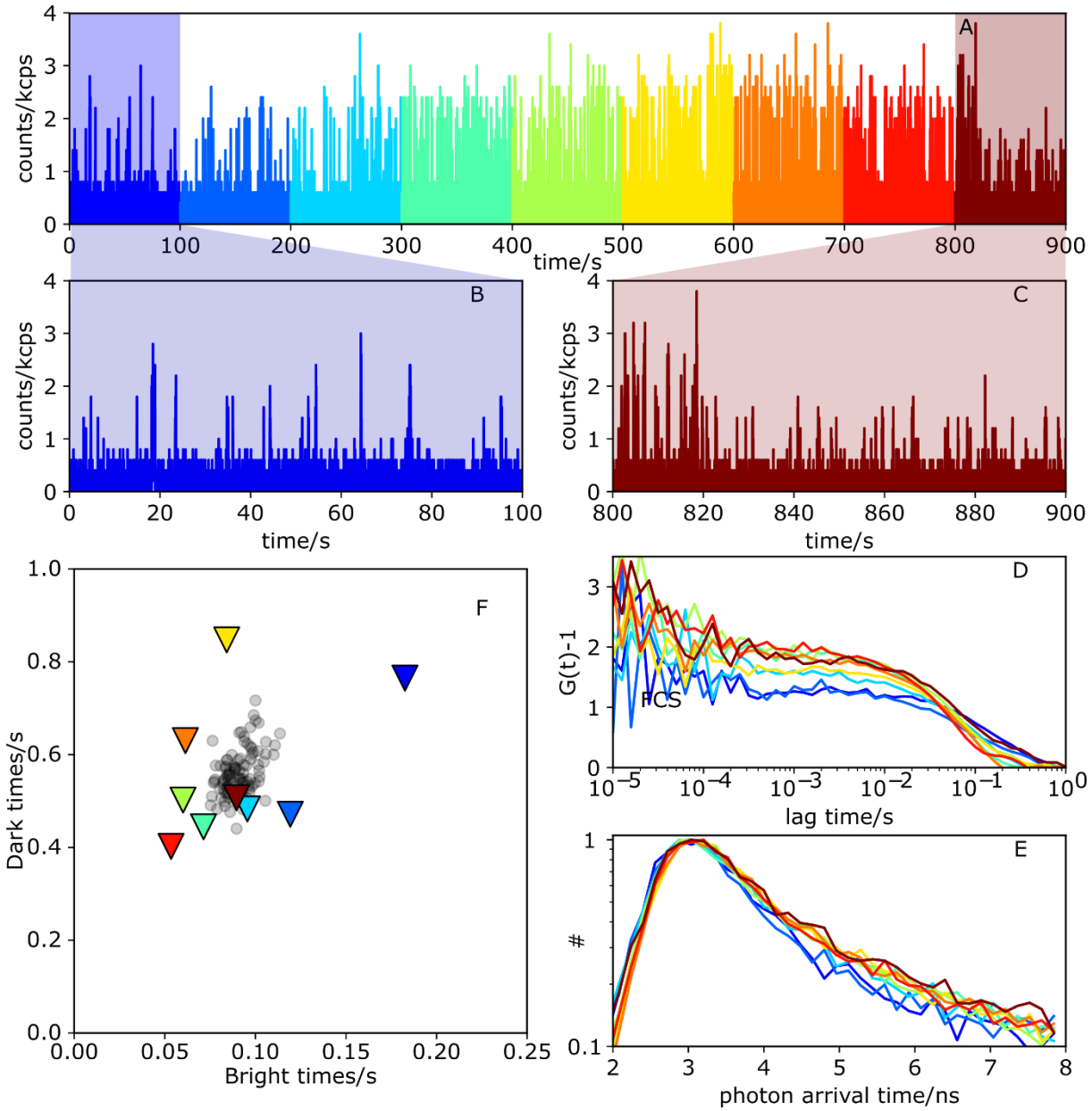

Figure S37: Dynamic heterogeneity from a change point-free segmental analysis. See Fig. S13 for details.

1.10. Dynamic Heterogeneity in Cu-azurin-ATTO655

This section shows similar results to section 1.9 of change-point and segmental analysis of all Cu-Az-ATTO655 molecules for which time traces were long enough to be taken into account (arbitrarily numbered 1-15). The figures are presented for each molecule in the form of those in section 1.9. Some of the molecules below were prepared in the presence of 0.1 mM sodium ascorbate ($C_6H_7O_6^-Na^+$), however this did not have any discernable influence on the observed data. As ATTO655 is redox sensitive, blinking due to interaction between dye and electron mediator can in principle occur.[15] However, at the measurement potential of 150 mV this effect is negligible (for reference, the deliberately blinking time trace shown in Fig. S7 was recorded at -50 mV).

As described in the main text, ATTO655 was attached at a different position (K122 vs. C42 for ATTO647N) in order to test if the label environment has an effect on the redox processes.

One further important difference between ATTO647N-labeled and ATTO655-labeled Az is that, since ATTO655 can accept an electron, it can provide an additional pathway for ET to and from Cu, in addition to the inherent Cu-to-Fe transfer. Indeed, the significant influence from such a process may be apparent from the absolute values of the bright times of ATTO655, which are roughly an order of magnitude shorter than those of ATTO647. A similar, but much less pronounced effect is observed for the dark times.

1.10.1. Molecule 1

Molecule 1 presents large variations, by a factor of 3-5, of bright and dark times in the first 200 s of the time trace. Although variations occur in the same time interval for bright and dark times, we note that the bright times come back to shorter values between 40 and 100 s, so that both correlated and uncorrelated changes are present between bright and dark times. The variations are clearly appearing in the time histograms (Fig. S38B, D), the scatter plots (Fig. S38H, I) and the time correlation function (Fig. S38J). The segmental analysis (Fig. S39) confirms these variations in the intensity correlation functions and the lifetime histograms.

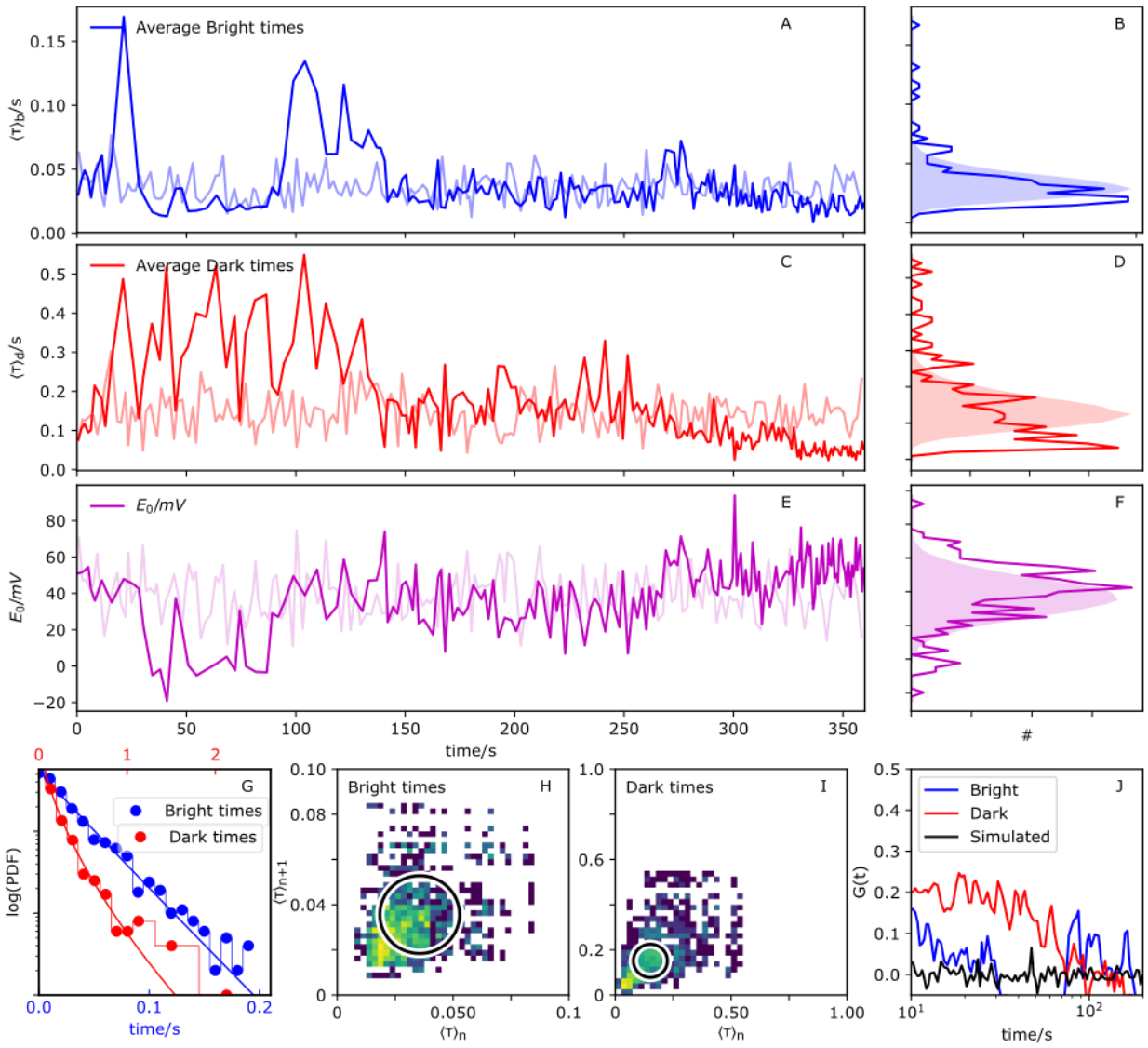

Figure S38: Dynamic heterogeneity from a change point analysis. See Fig. S12 for details.

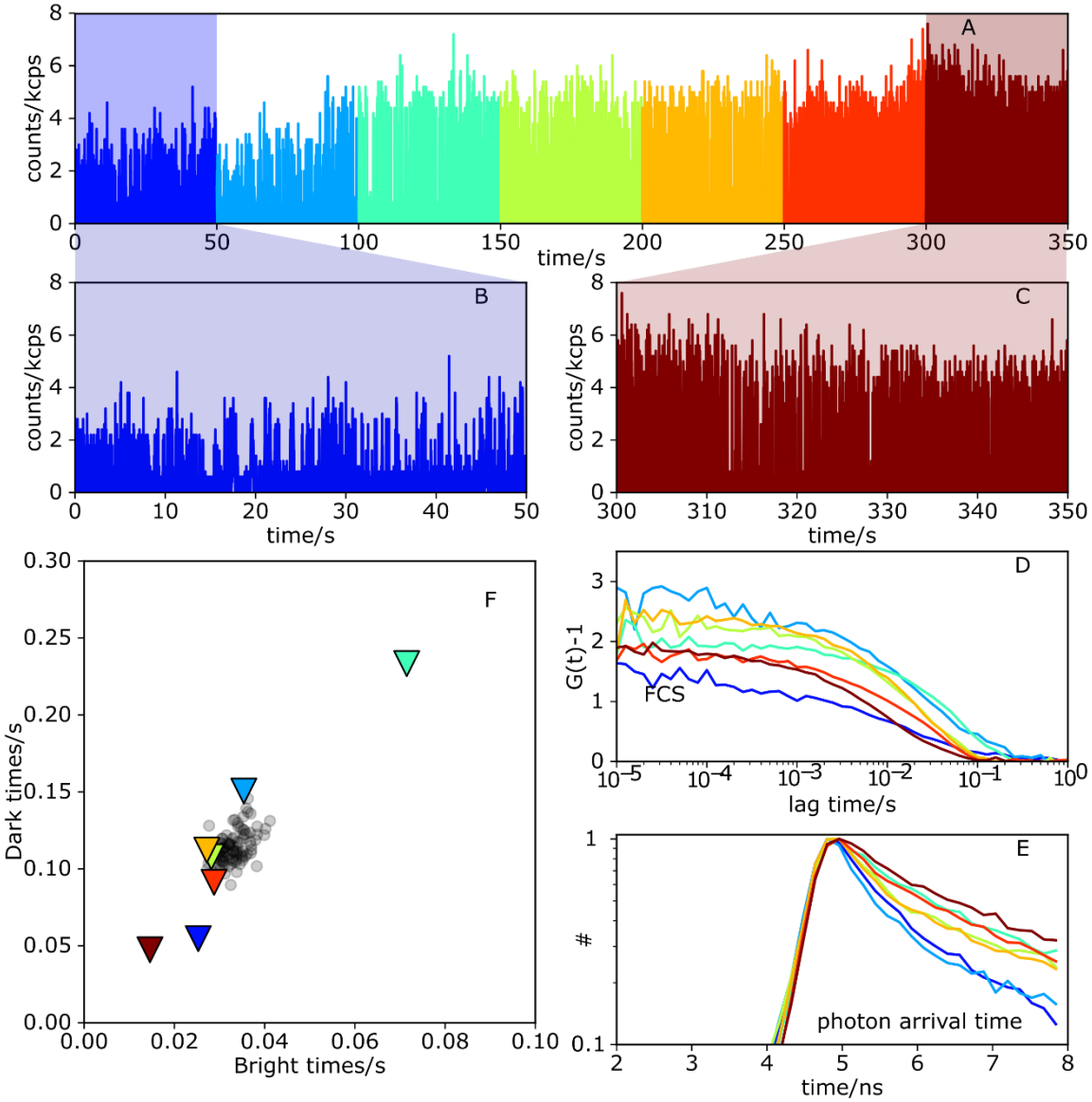

Figure S39: Dynamic heterogeneity from a change point-free segmental analysis. See Fig. S13 for details.

1.10.2. Molecule 2

The bright times of molecule 2 show a significant deviation to longer times at the beginning of the trace, and the dark times at the end of it. The variations are small (a factor of less than 2), but show up clearly in the scatter plots of Fig. S40H, I, and to a lesser extent in the histograms of Fig. S40B, D. The segmental analysis of Fig. S41 also does show some changes of the correlation function, but they barely exceed the statistical noise of the data.

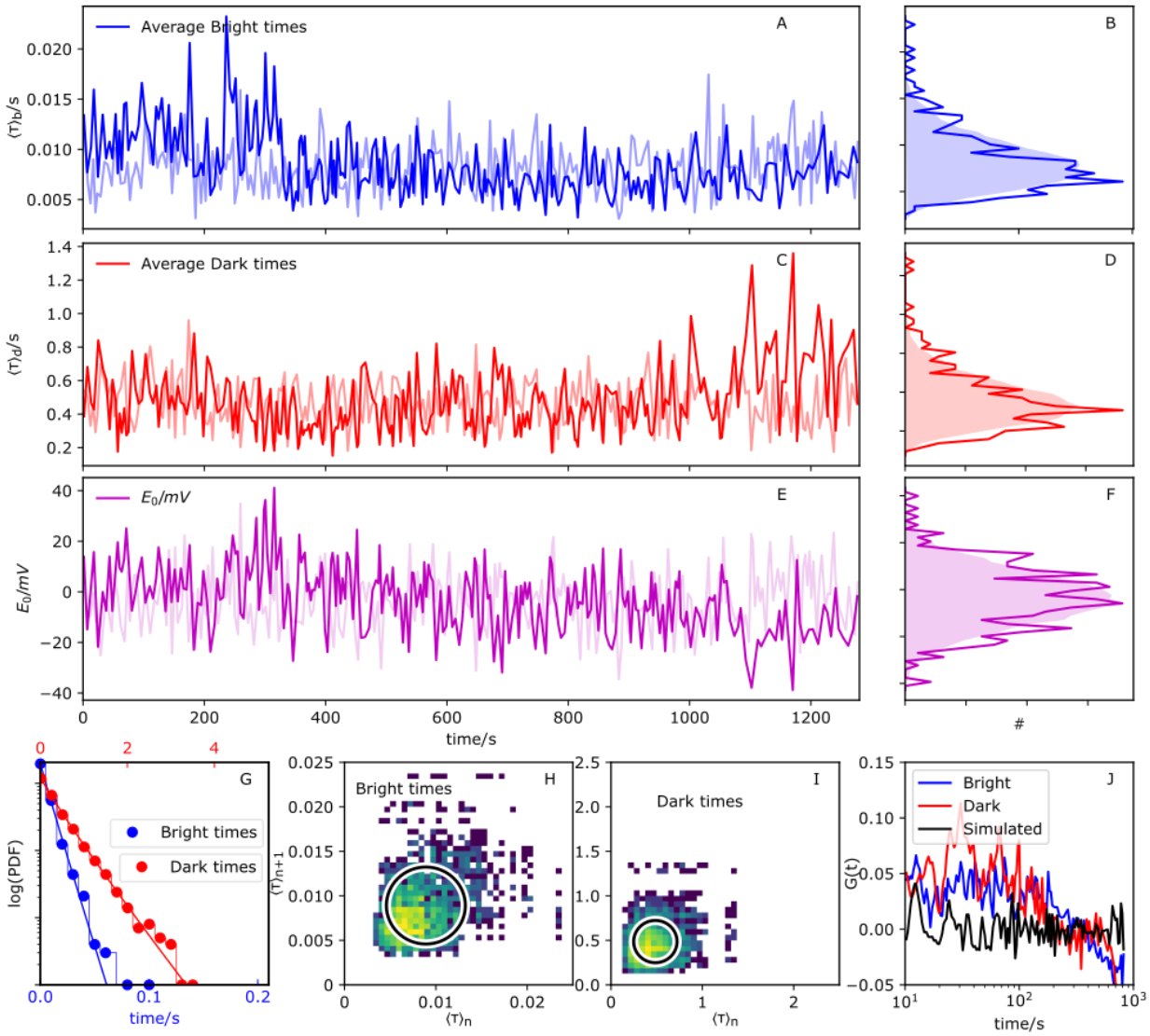

Figure S40: Dynamic heterogeneity from a change point analysis. See Fig. S12 for details.

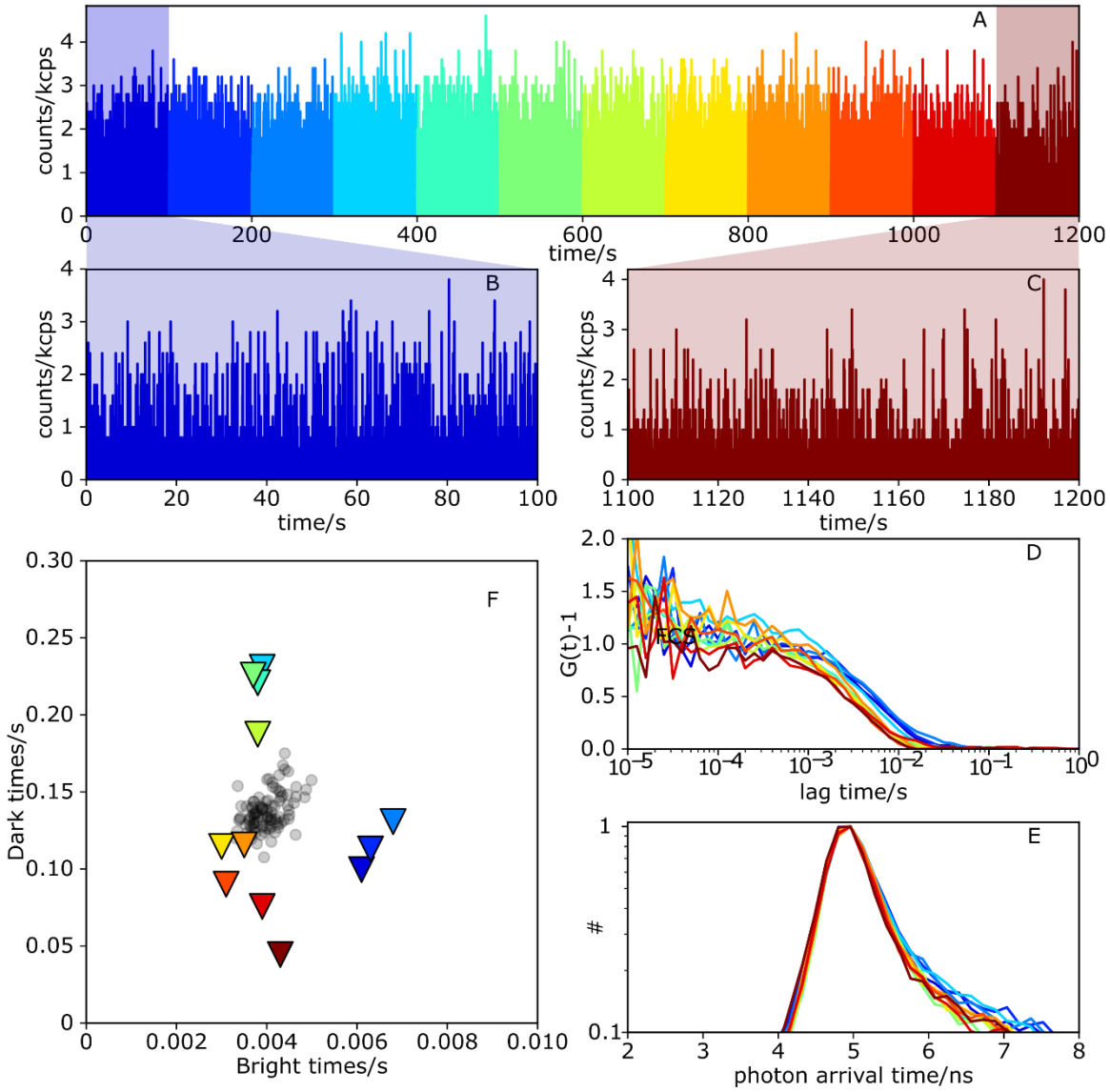

Figure S41: Dynamic heterogeneity from a change point-free segmental analysis. See Fig. S13 for details.

1.10.3. Molecule 3

Molecule 3 displays weak heterogeneity, with a shortening of bright times and a correlated lengthening of dark times after 400 s, combining in a significant change of mid-point potential in this time interval (see Fig. S41E). The small deviations are not very apparent in the scatter plot of consecutive times (Fig. S41H, I). The changes of the correlation function also just exceed statistical noise in the segmental analysis of Fig. S42, except at the end of the trace (brown color).

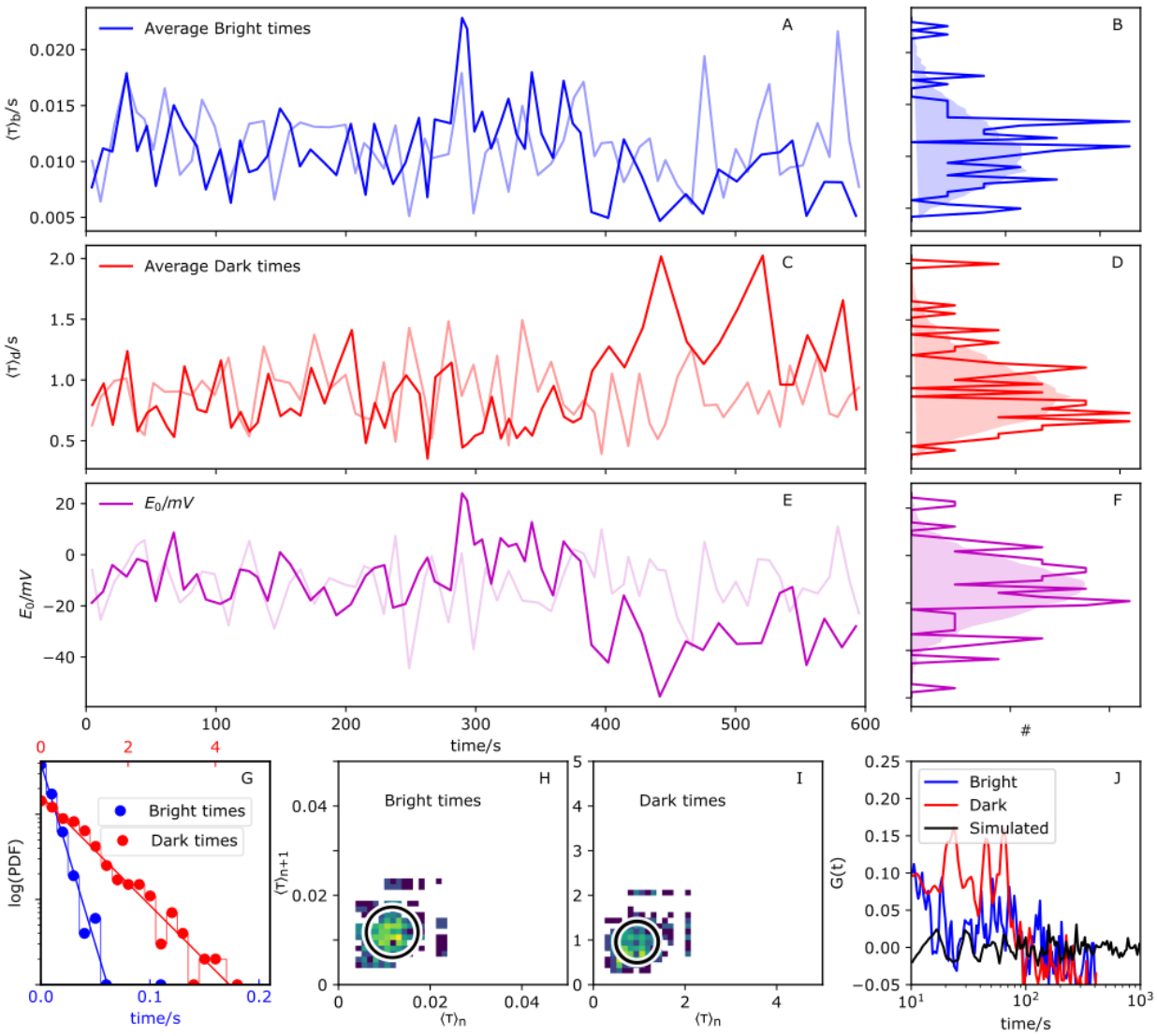

Figure S42: Dynamic heterogeneity from a change point analysis. See Fig. S12 for details.

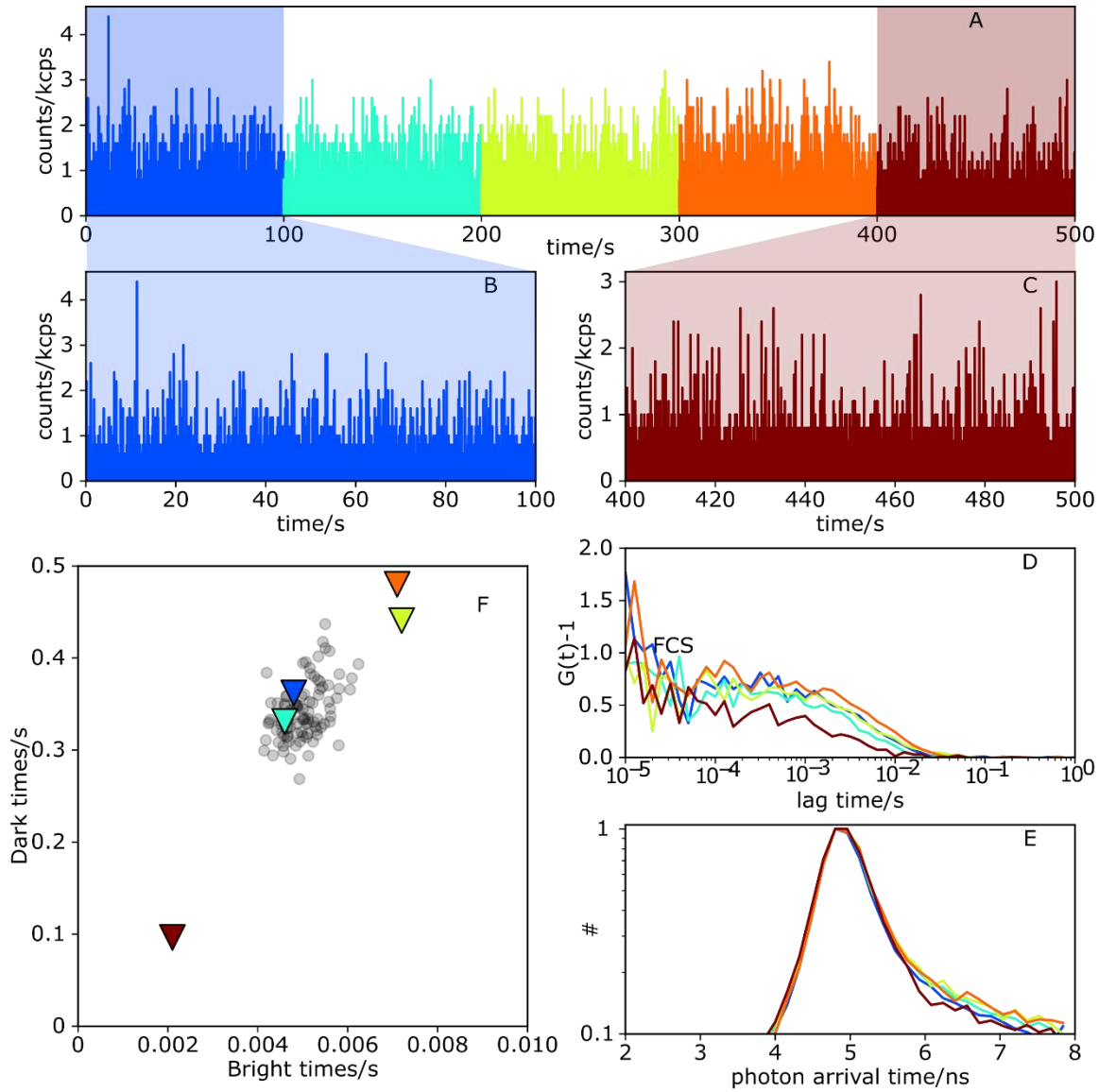

Figure S43: Dynamic heterogeneity from a change point-free segmental analysis. See Fig. S13 for details.

1.10.4. Molecule 4

Molecule 4 shows a single dramatic event of extremely lengthened bright time at 100 s (Fig. S44A). The rest of the trace is very much compatible with a purely random trace, without heterogeneity. The segmental correlation functions (Fig. S45D) confirm the behavior, with the anomaly of the first interval where the lengthening event happens (dark blue trace).

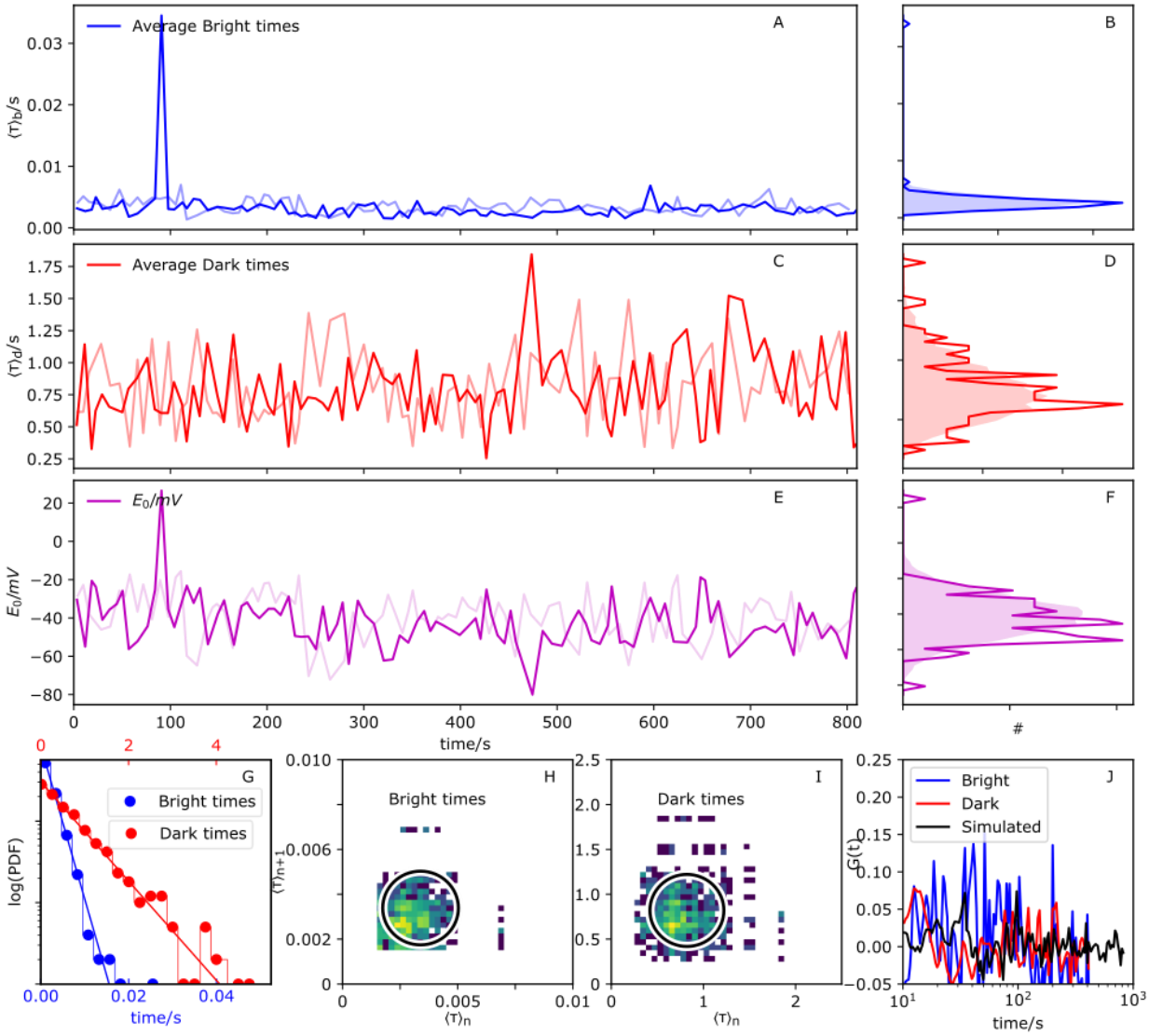

Figure S44: Dynamic heterogeneity from a change point analysis. See Fig. S12 for details.

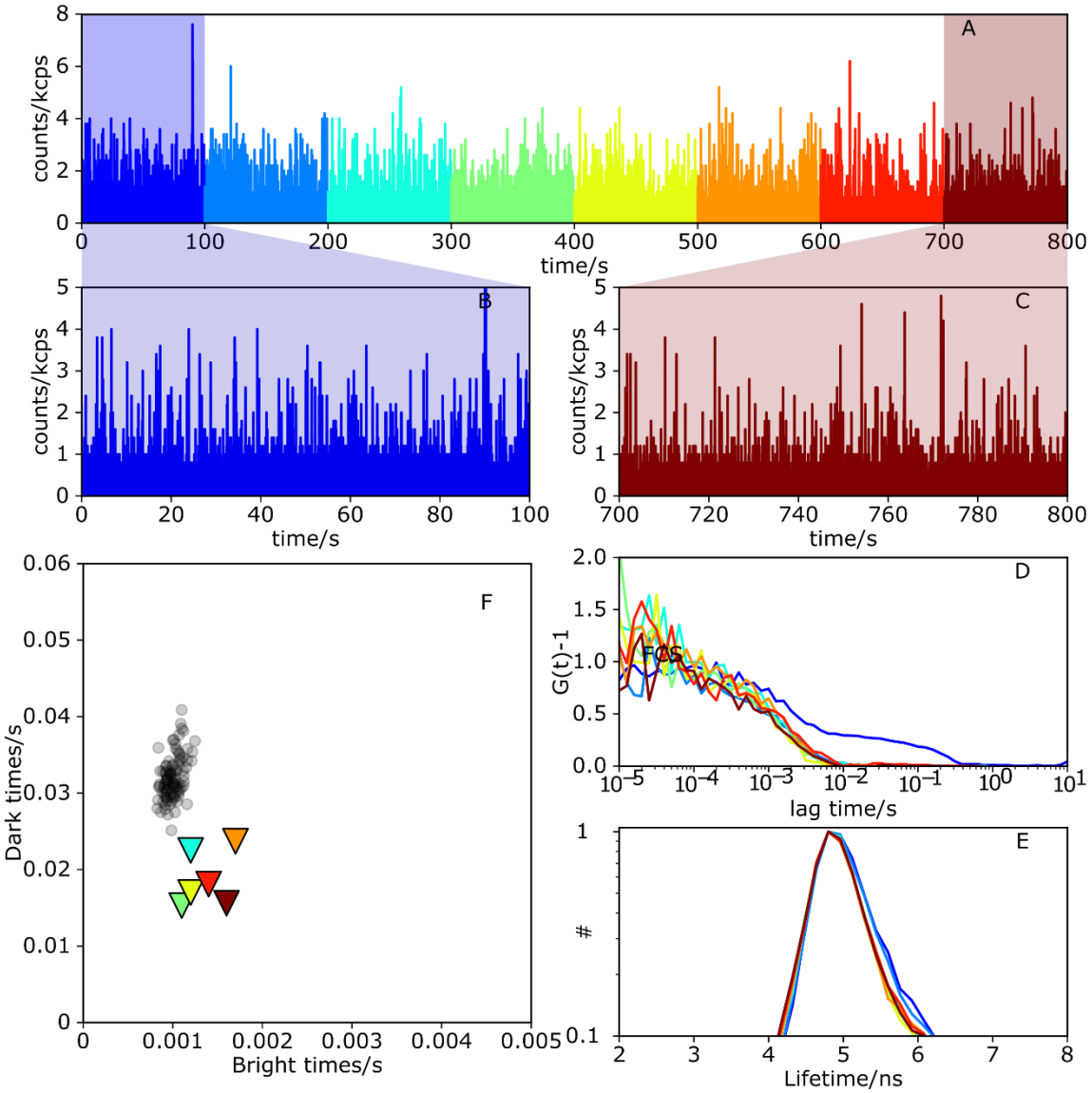

Figure S45: Dynamic heterogeneity from a change point-free segmental analysis. See Fig. S13 for details. The large deviation from the average in (F) is due to the short event in the first segment (0-100 s, dark blue), not shown in the plot.

1.10.5. Molecule 5

Molecule 2 shows weak, if any at all, deviation from purely random traces. A possible sign of heterogeneity is the deviation of the correlation function contrast of the first interval (light blue) in Fig. S47D.

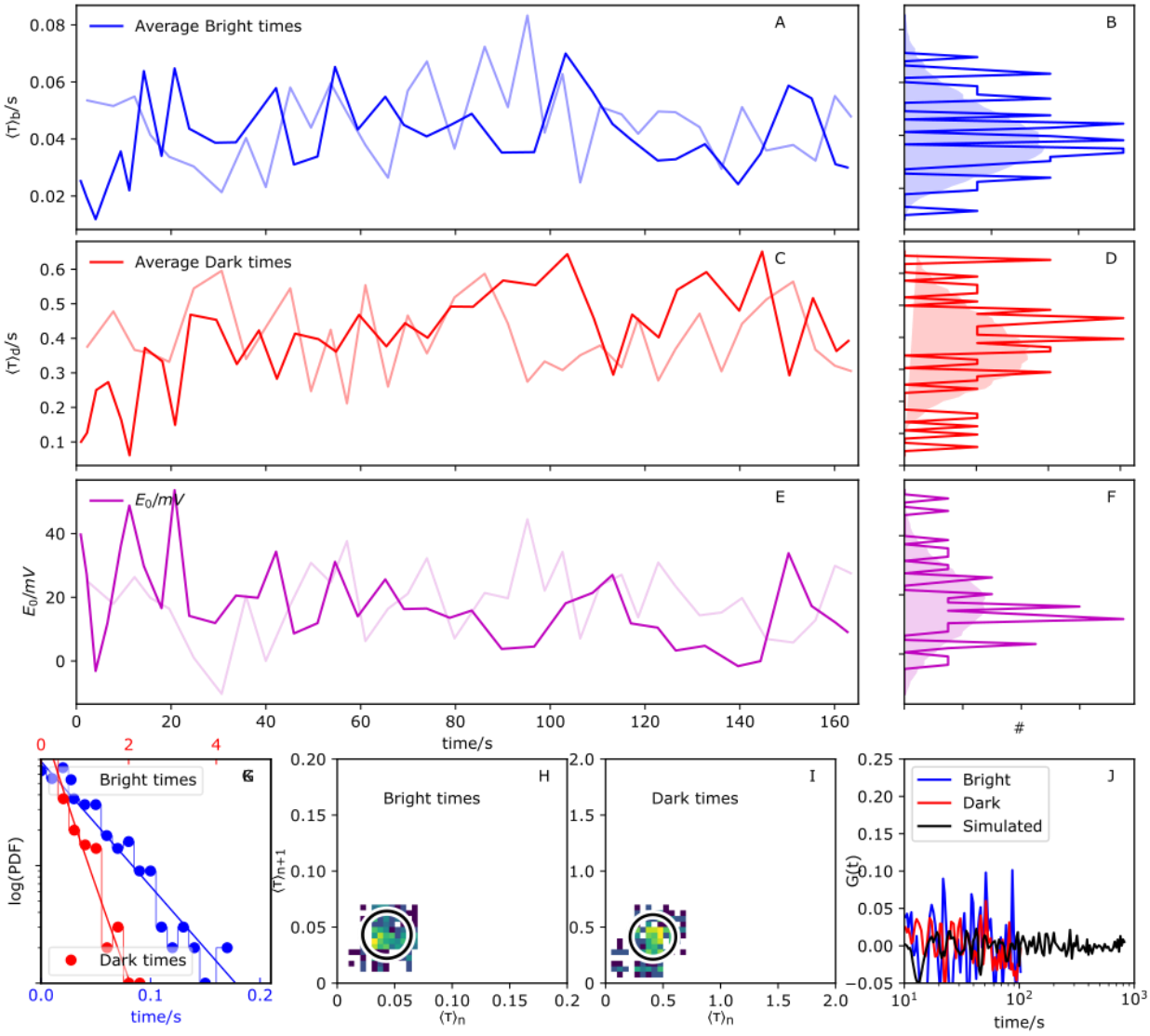

Figure S46: Dynamic heterogeneity from a change point analysis. See Fig. S12 for details.

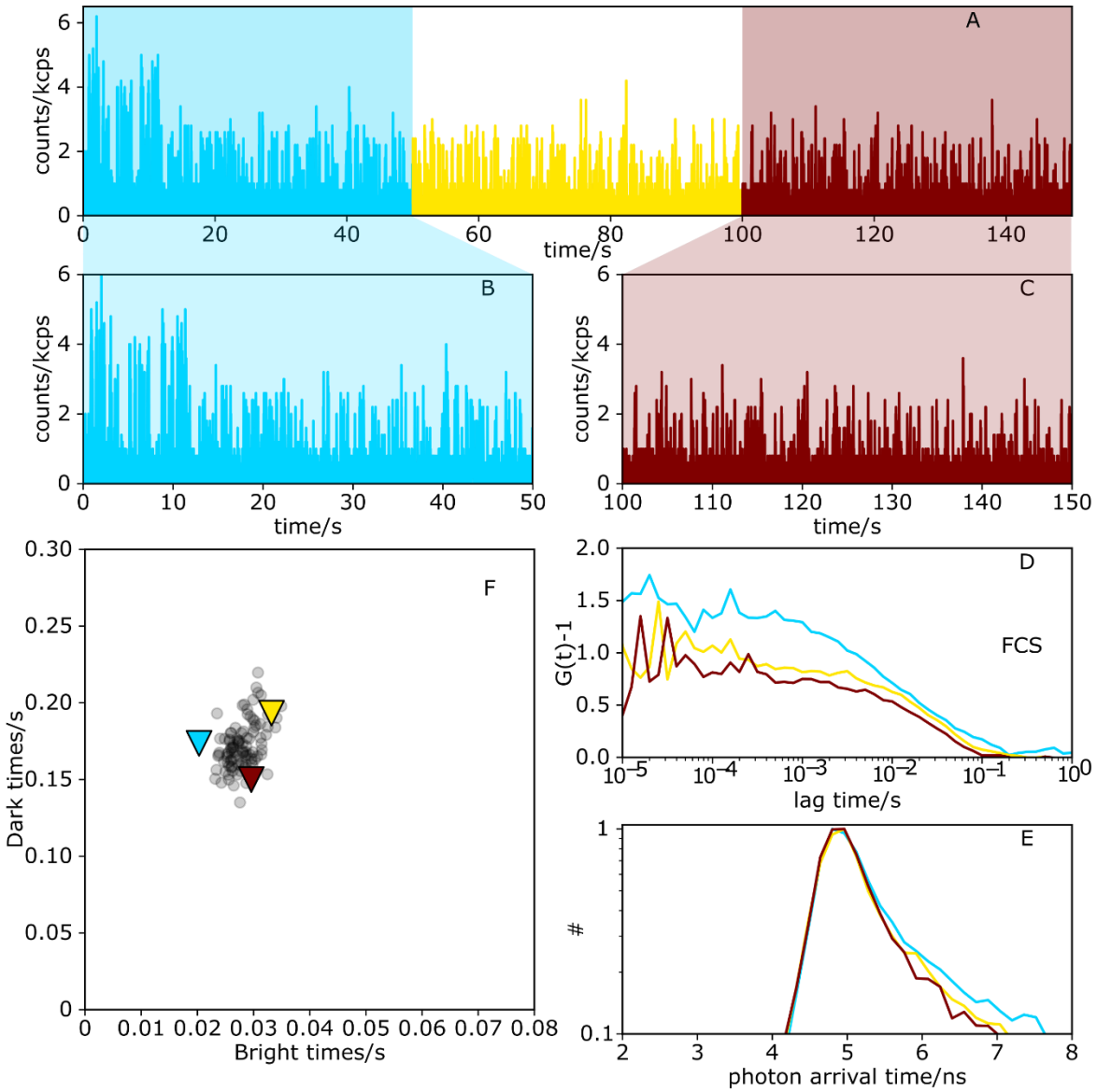

Figure S47: Dynamic heterogeneity from a change point-free segmental analysis. See Fig. S13 for details.

1.10.6. Molecule 6

Deviations from random traces are weak for this molecule, except for a few short events with longer bright times around 600 and 700 s. Those events also appear in the scatter plots of Fig. S48H. Weaker deviations might also be present in the trace of dark times and appear in the scatter plot of Fig. S48I. These deviations are clearer in the segmental analysis of Fig. S49D.

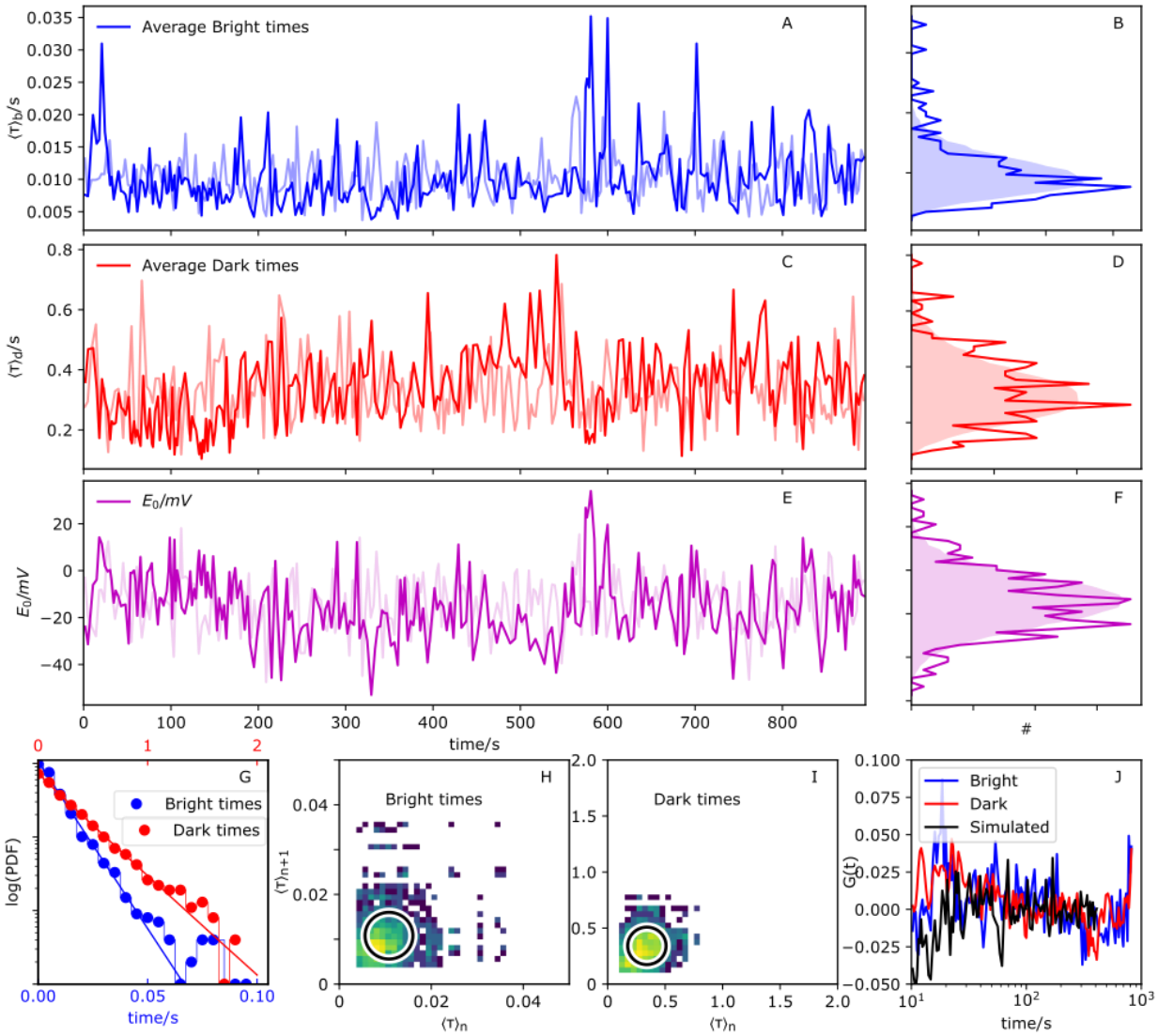

Figure S48: Dynamic heterogeneity from a change point analysis. See Fig. S12 for details.

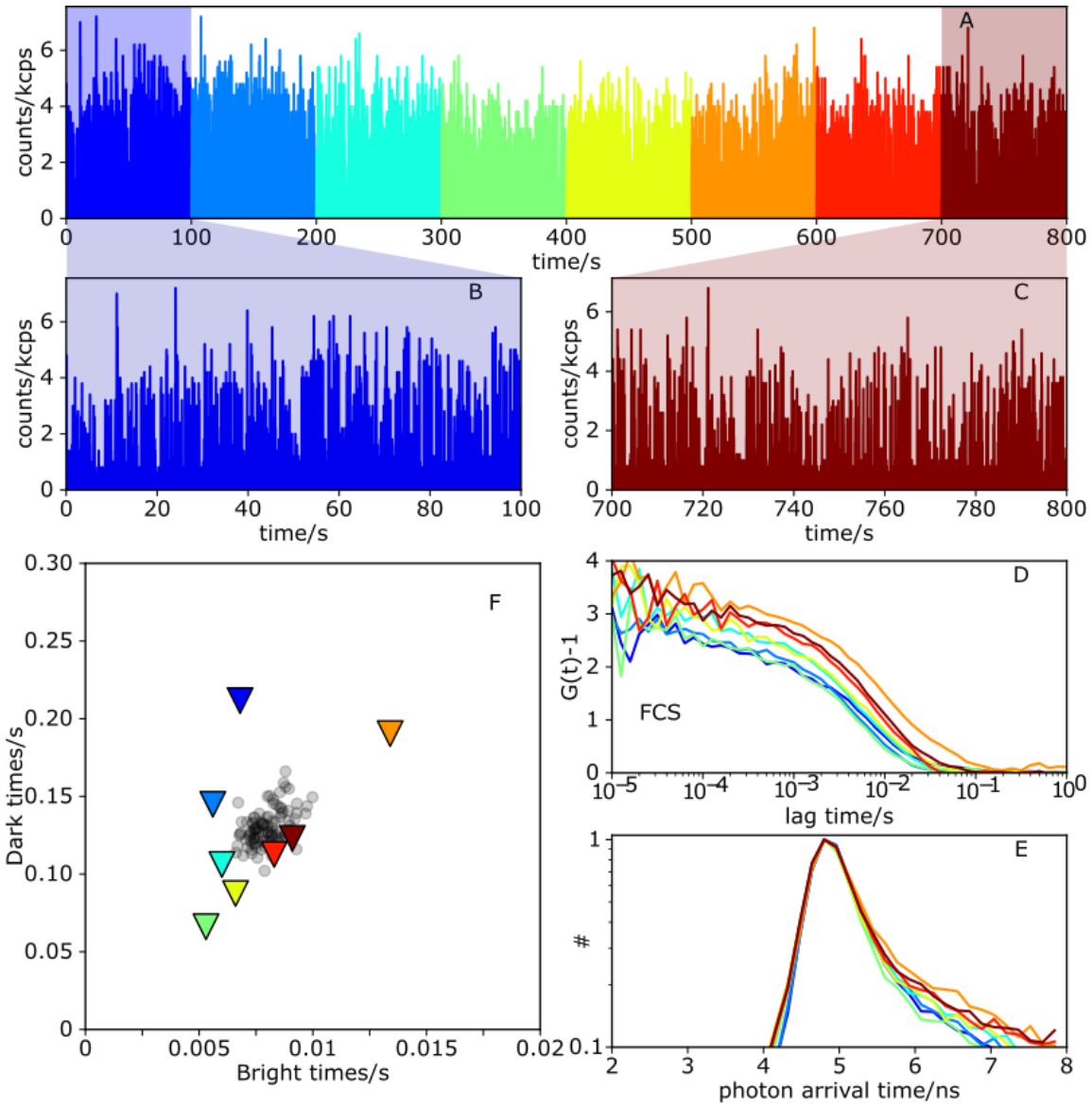

Figure S49: Dynamic heterogeneity from a change point-free segmental analysis. See Fig. S13 for details.

1.10.7. Molecule 7

The bright times of molecule 7 present a multistep decrease, starting at 15 ms in the first few seconds of the trace, then remaining around 8 ms until 140 s, then decreasing again to about 4 ms between 140 and 320 s, and perhaps decreasing further after 320 s (the statistics there are poor because of lengthening dark times). Dark times, on the other hand, show a significant lengthening after 300 s. These deviations are very apparent in the histograms and in the correlation plots of Fig. S50H, I, as well as in the correlation of Fig. S50J. The segmental analysis of Fig. S51 confirms the dramatic change of the correlation function, both in contrast and decay time, between the beginning and the end of the trace.

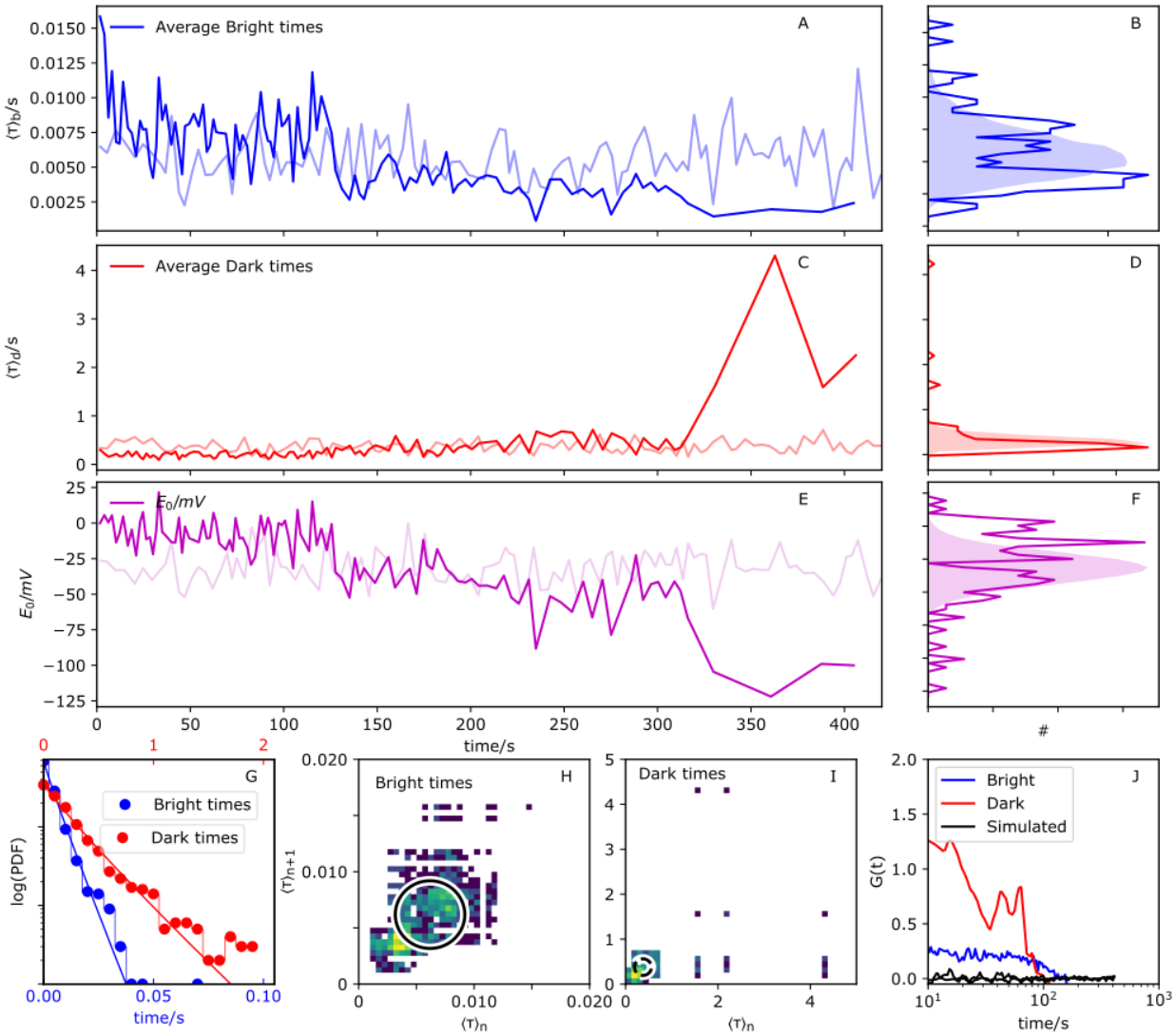

Figure S50: Dynamic heterogeneity from a change point analysis. See Fig. S12 for details.

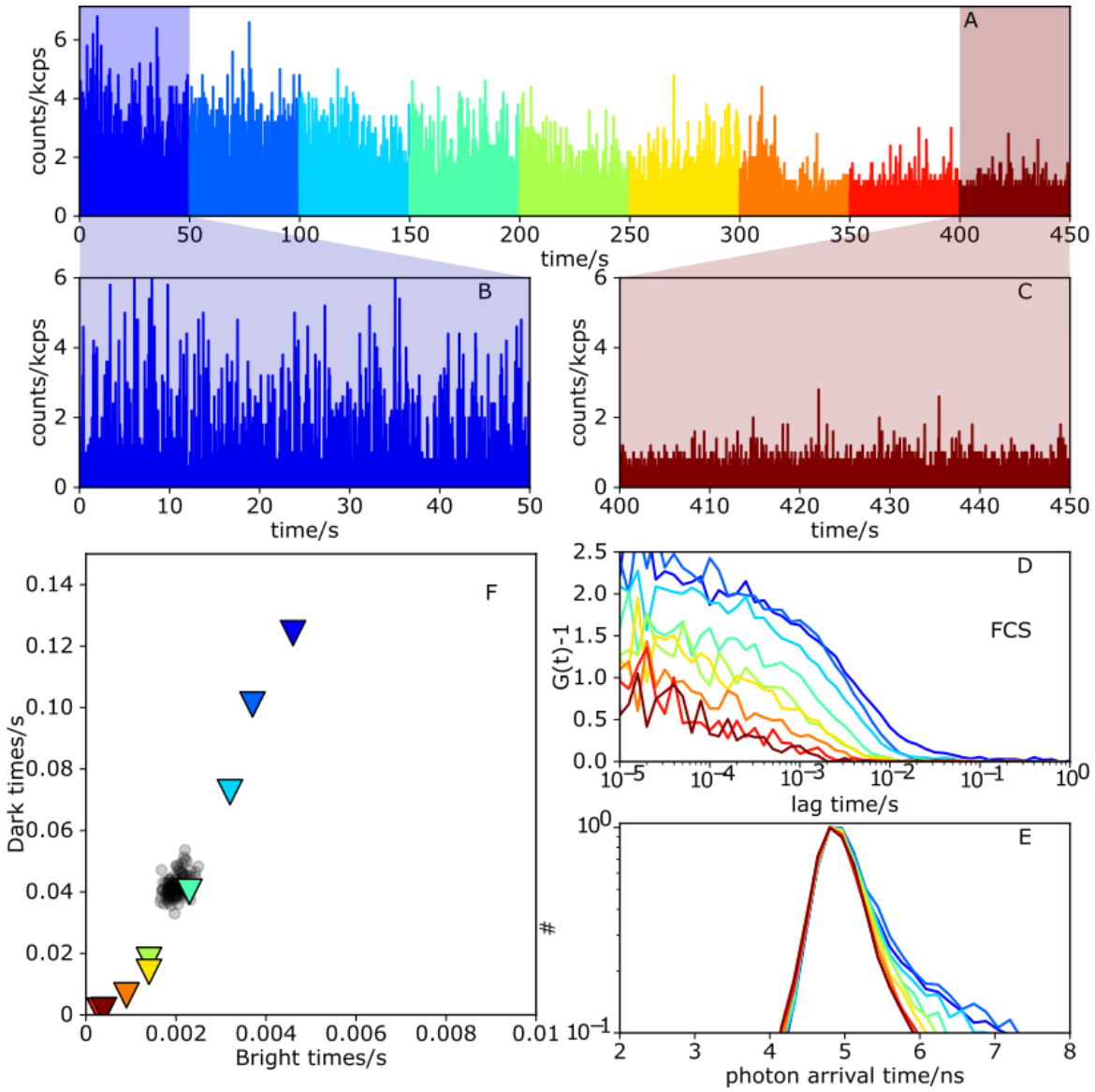

Figure S51: Dynamic heterogeneity from a change point-free segmental analysis. See Fig. S13 for details.

1.10.8. Molecule 8

The fluorescence trace of molecule 8 starts with a very long dark time (27 s, see Fig. S52A), which shifts the averages by the same amount. It is unclear which mechanism gave rise to this long dark time, during which the dye was in the quenched state (but was not bleached). After this initial event, the rest of the traces is very regular and doesn't display any significant sign of heterogeneity.

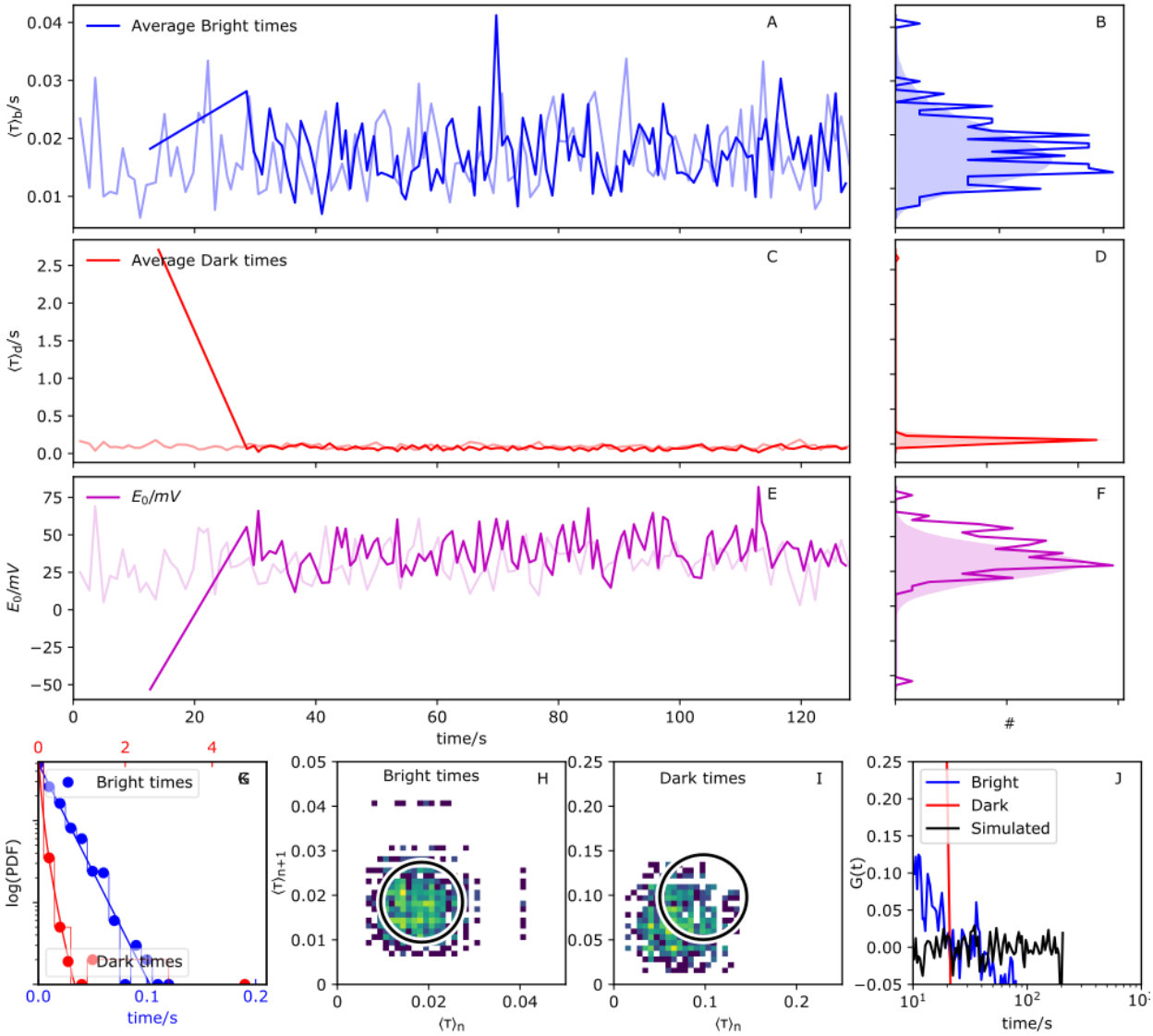

Figure S52: Dynamic heterogeneity from a change point analysis. See Fig. S12 for details.

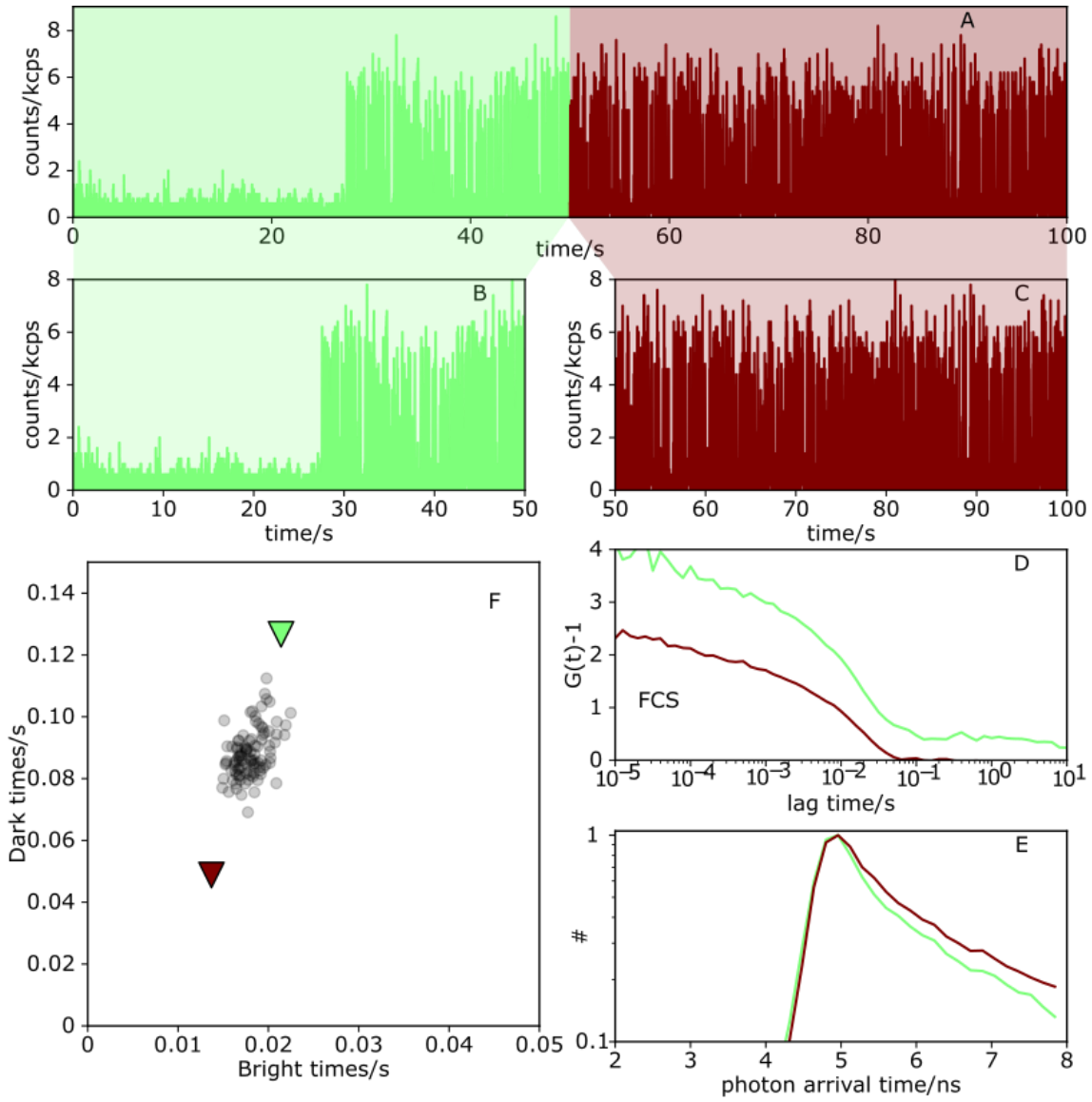

Figure S53: Dynamic heterogeneity from a change point-free segmental analysis. See Fig. S13 for details.

1.10.9. Molecule 9

Molecule 9 shows uneventful traces, mostly compatible with constant rates and the absence of any heterogeneity. A possible indication of weak rate fluctuations can be seen in the scatter plots of Fig. S54H, I. The correlation functions of the segmental analysis are remarkably reproducible (Fig. S55D).

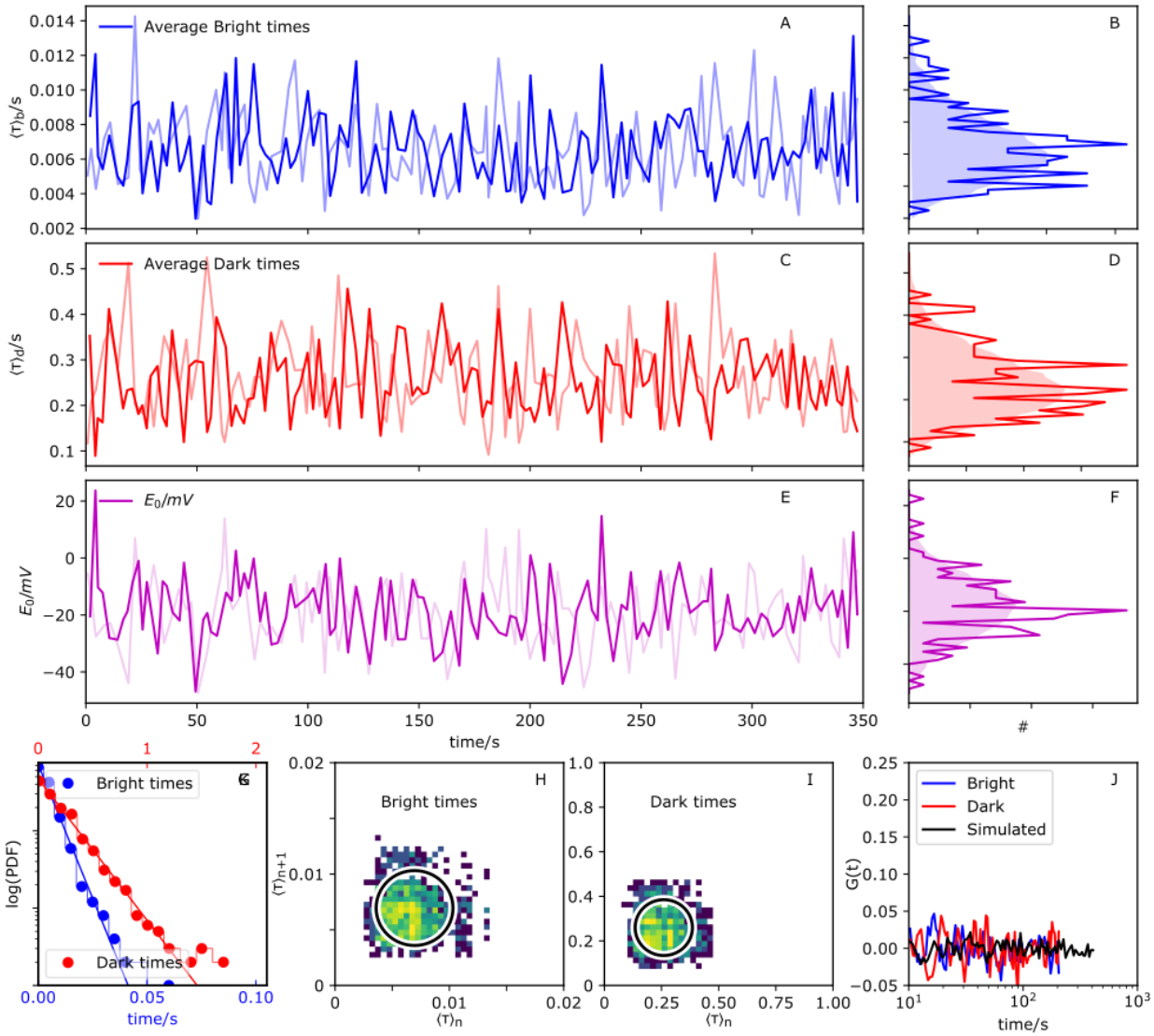

Figure S54: Dynamic heterogeneity from a change point analysis. See Fig. S12 for details.

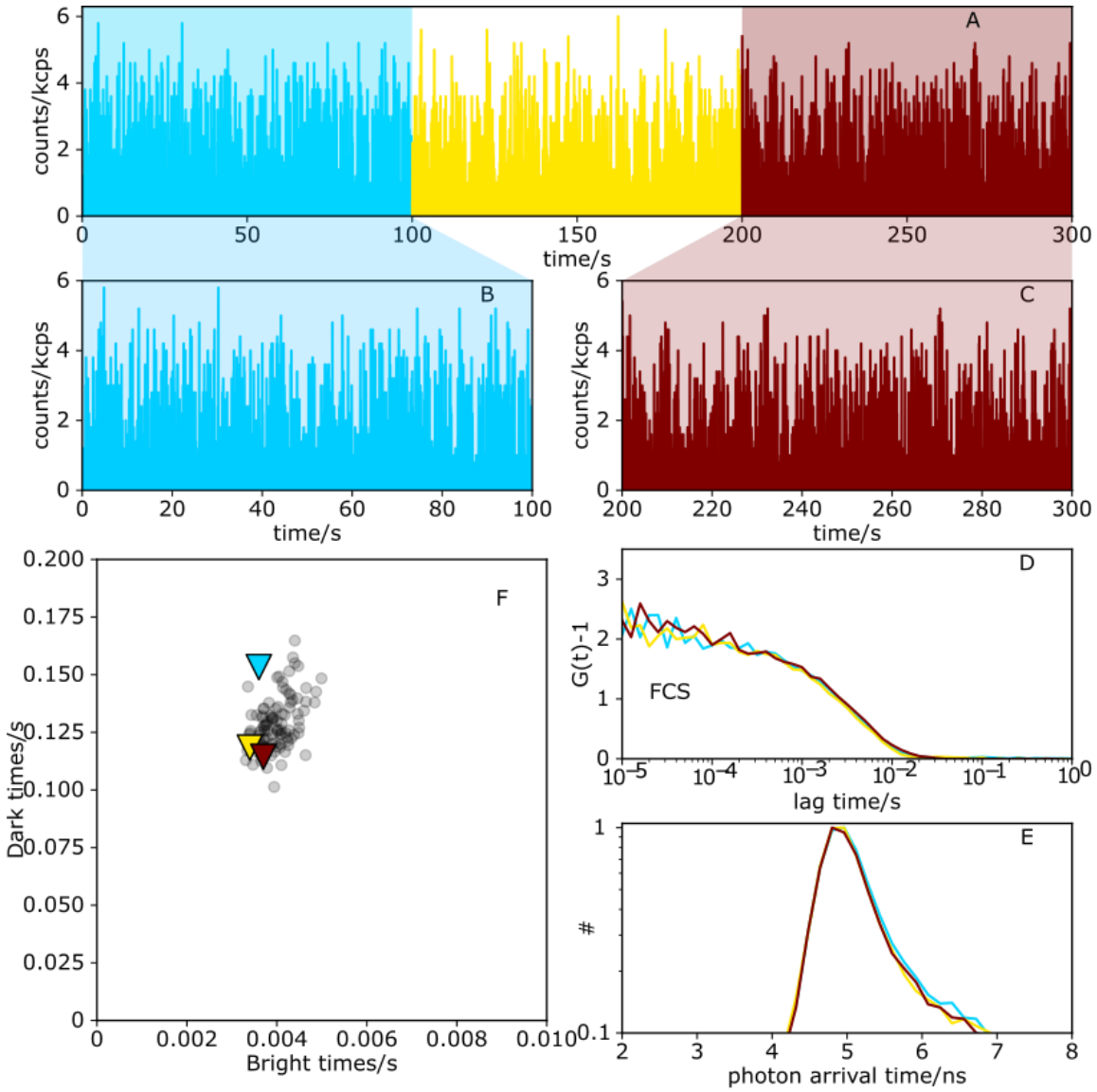

Figure S55: Dynamic heterogeneity from a change point-free segmental analysis. See Fig. S13 for details.

1.10.10. Molecule 10

Molecule 10 is very similar to molecule 9, mostly compatible with constant rates and the absence of any heterogeneity, with again possible indications of weak rate fluctuations in the scatter plots of Fig. S56H, I. The correlation functions of the segmental analysis show only minor changes (Fig. S57D).

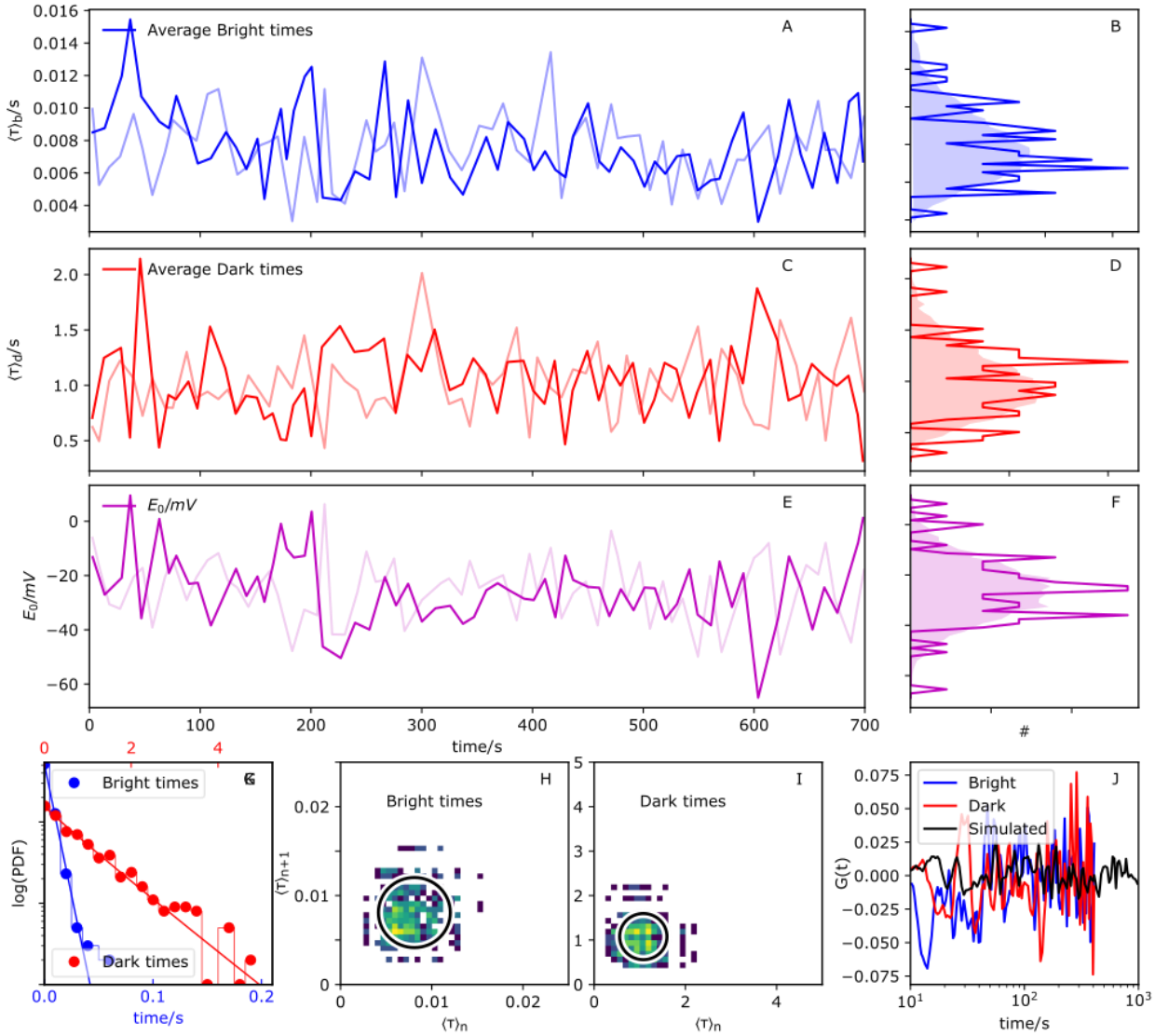

Figure S56: Dynamic heterogeneity from a change point analysis. See Fig. S12 for details.

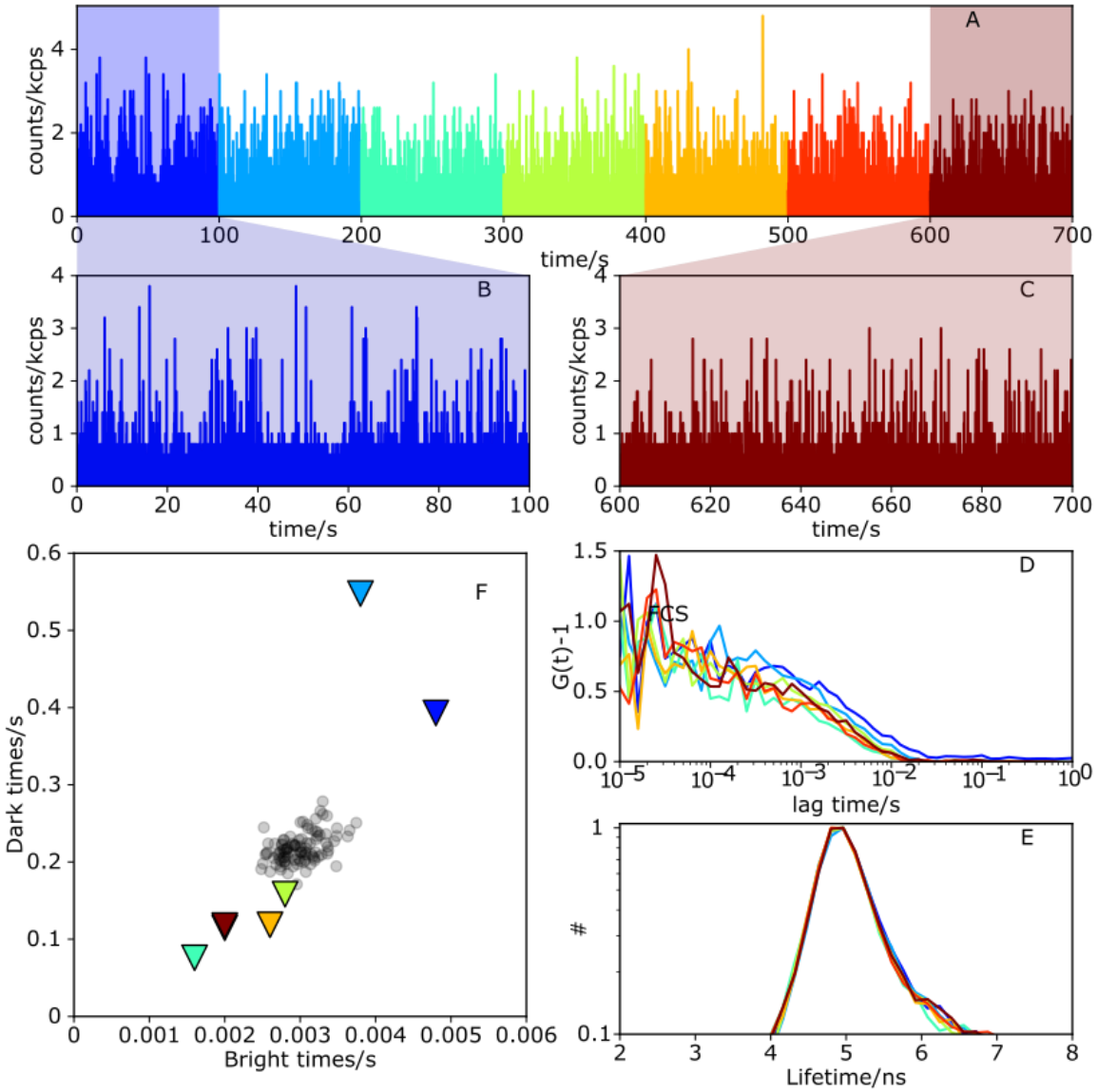

Figure S57: Dynamic heterogeneity from a change point-free segmental analysis. See Fig. S13 for details.

1.10.11. Molecule 11

Another case of uneventful traces as molecules 9 and 10. Maybe slightly shorter bright times and longer dark times from 0 s until 150 s, leading to a deviation of the mid-point potential (Fig. S58E). The trace is compatible with constant rates and weak or absent heterogeneity. A possible indication of weak rate fluctuations can be seen in the scatter plot of Fig. S58I. The correlation functions of the segmental analysis are largely reproducible (Fig. S59D).

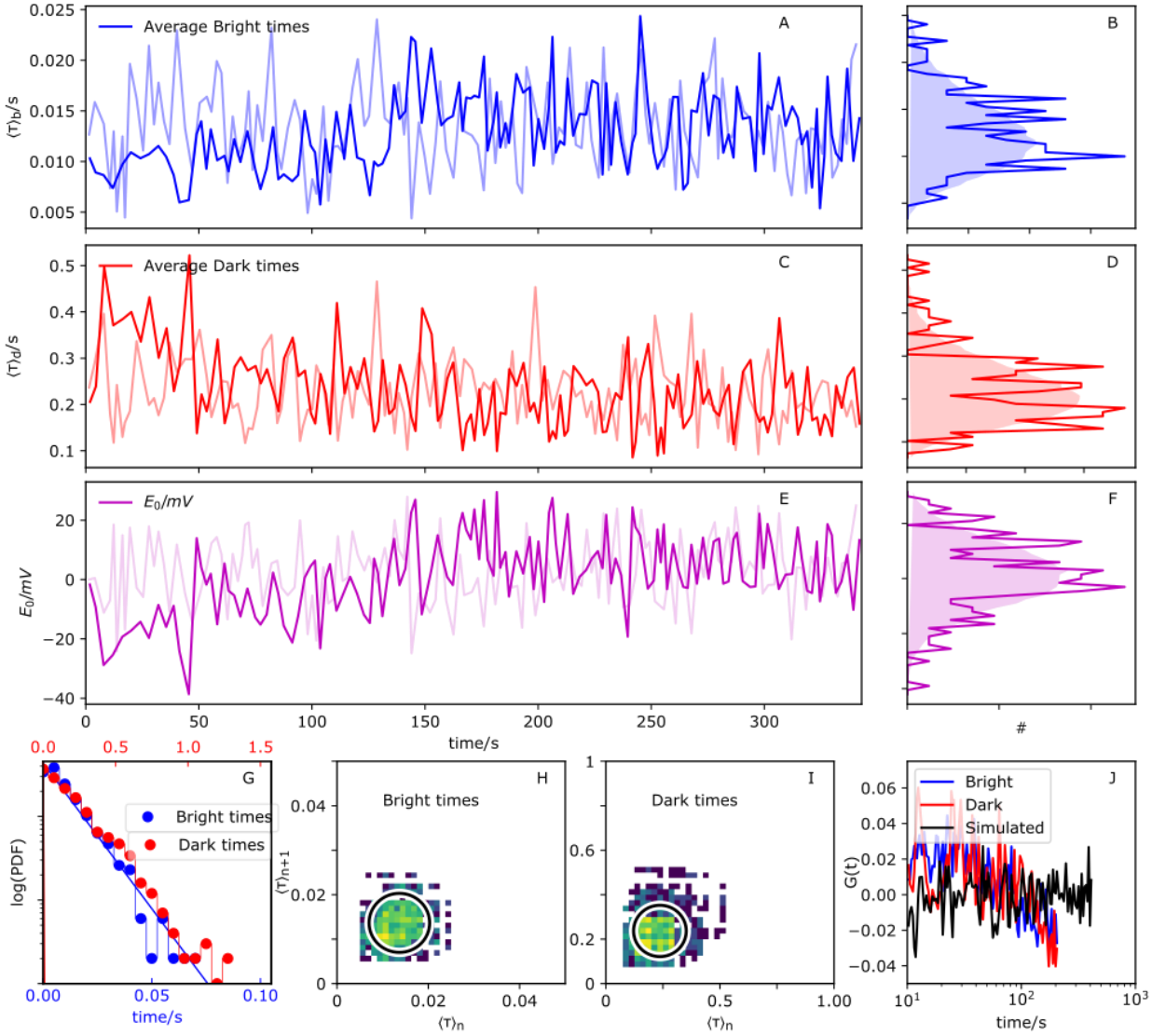

Figure S58: Dynamic heterogeneity from a change point analysis. See Fig. S12 for details.

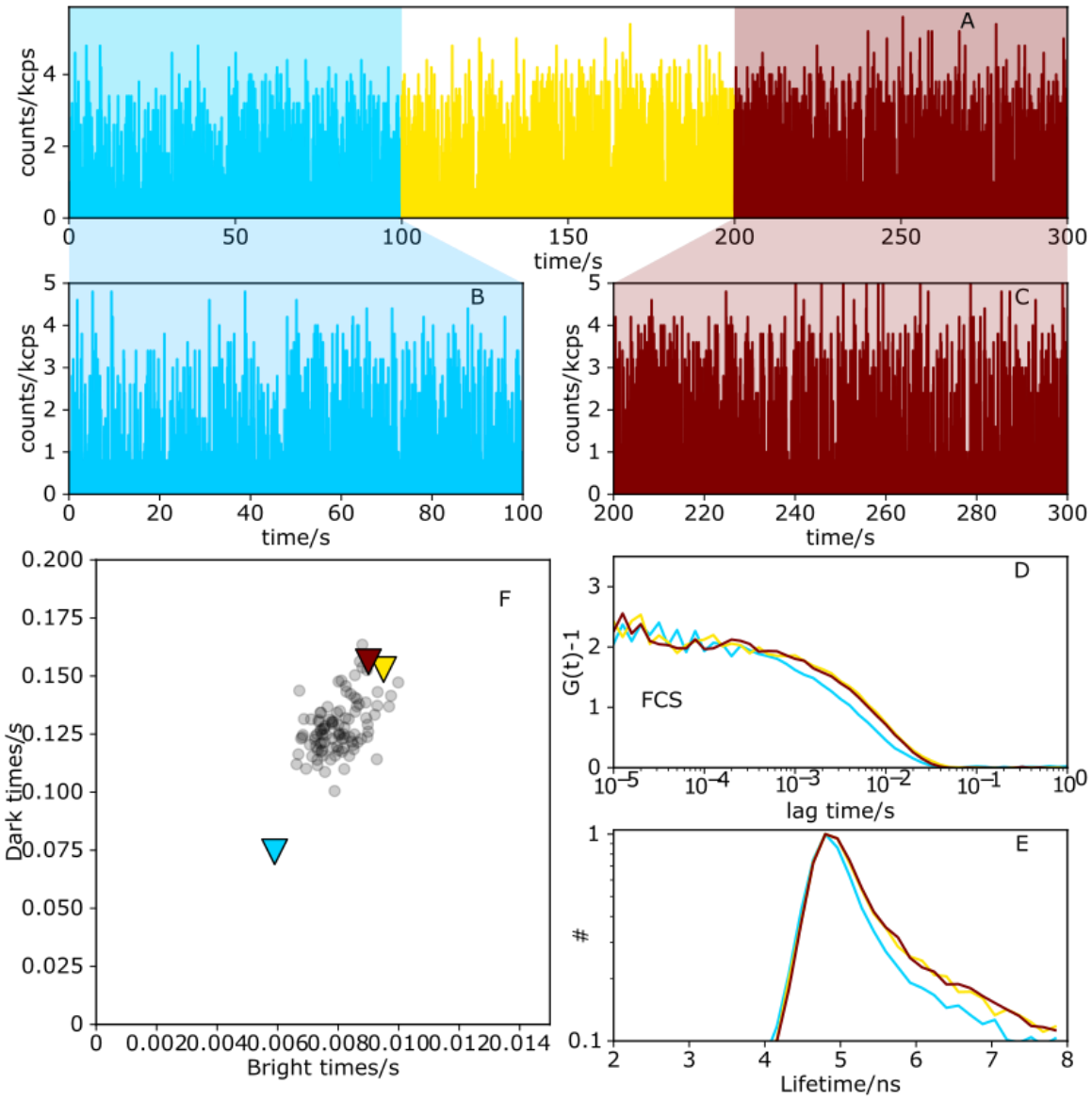

Figure S59: Dynamic heterogeneity from a change point-free segmental analysis. See Fig. S13 for details.

1.10.12. Molecule 12

Molecule 12 shows again shows quiet blinking traces, except at times longer than 1100 s, which show significantly shorter bright times and somewhat longer dark times. These two events might be correlated. Although these short events do not appear in the histograms of Fig. S60B, D, they may be traced in the scatter plots of Fig. S60H, I, and in the correlation function of the segmental analysis (brown trace in Fig. S61D).

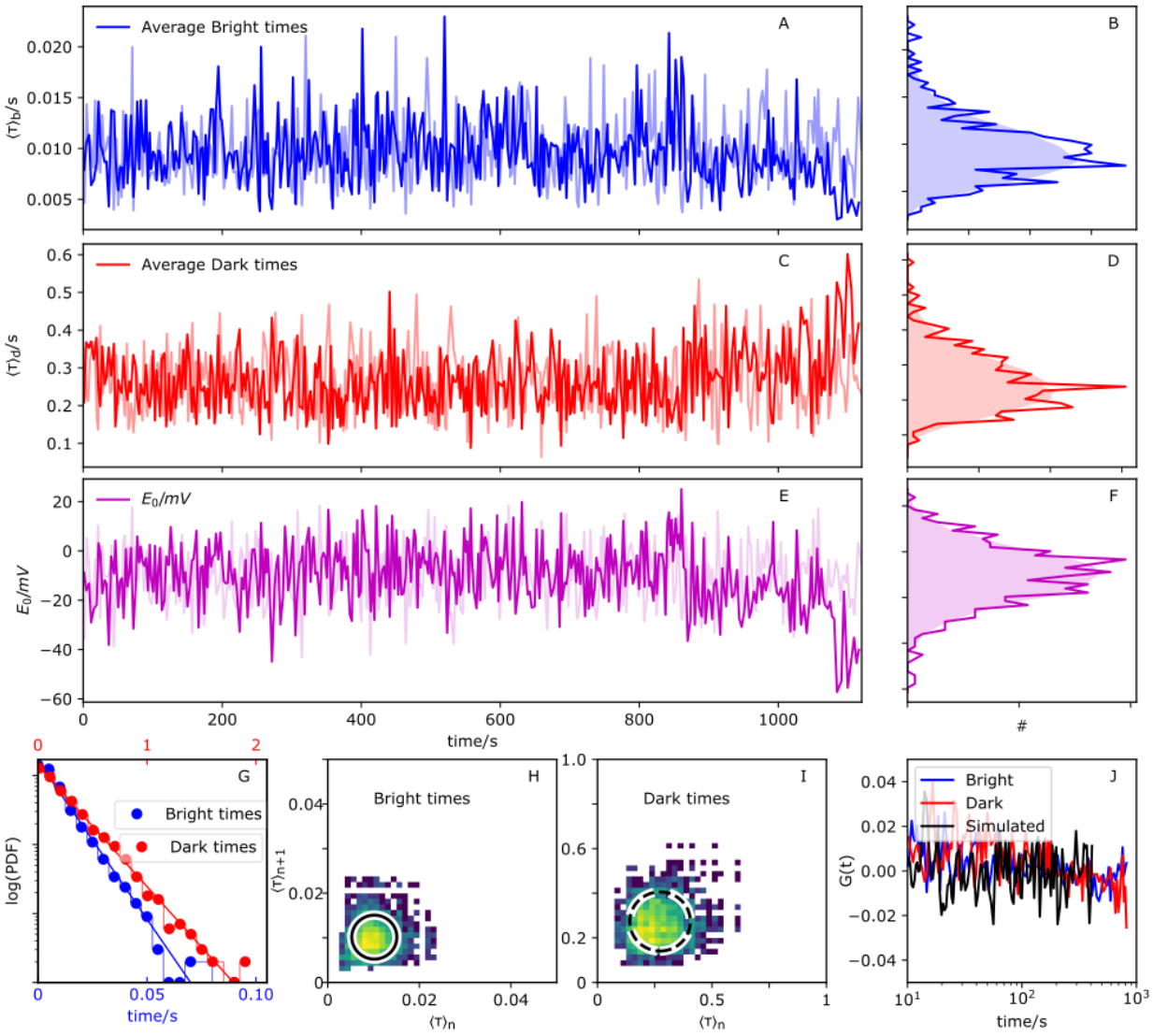

Figure S60: Dynamic heterogeneity from a change point analysis. See Fig. S12 for details.

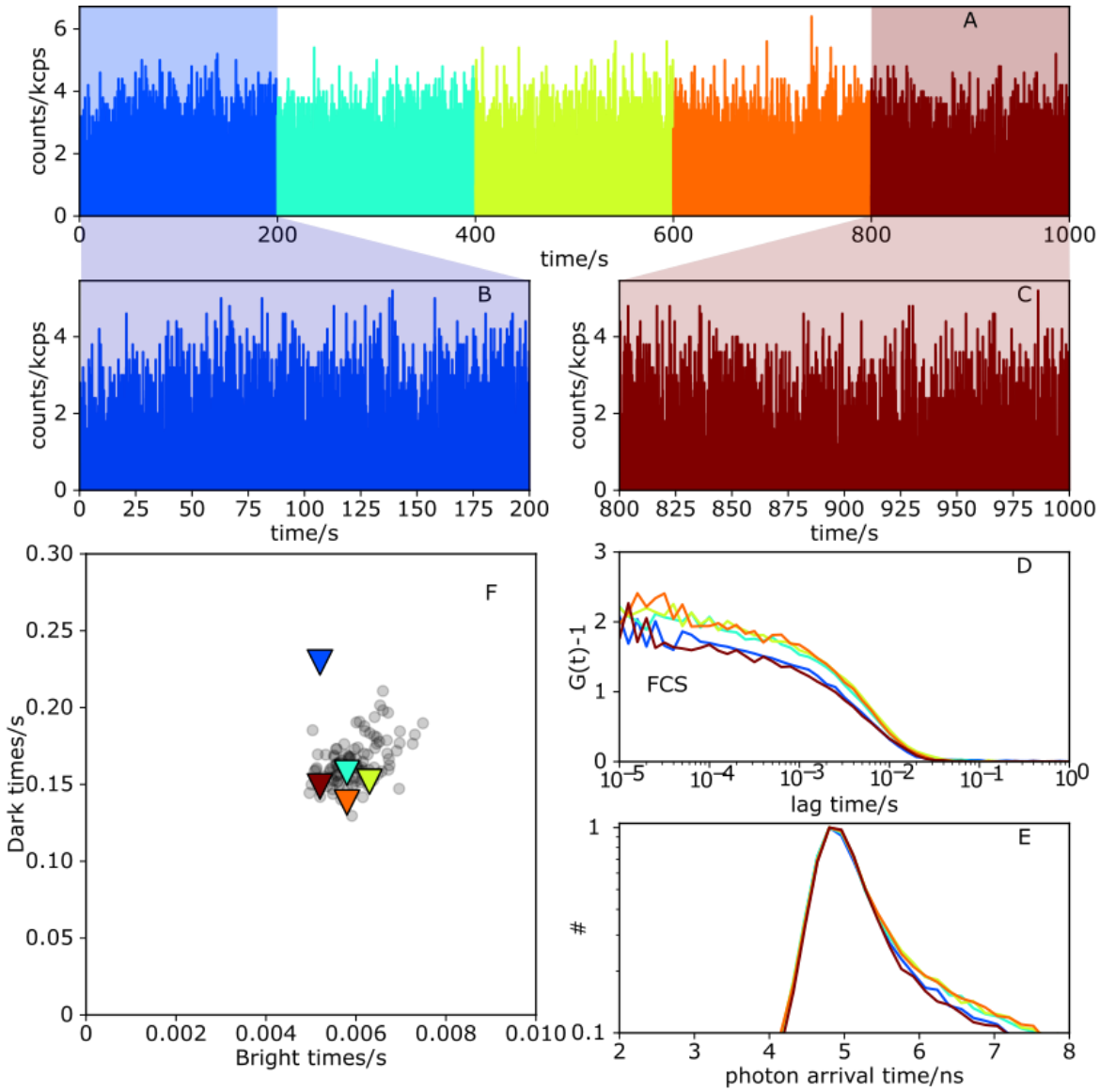

Figure S61: Dynamic heterogeneity from a change point-free segmental analysis. See Fig. S13 for details.

1.10.13. Molecule 13

Molecule 13 is a clear case of a strong reduction in bright times at 600 s, correlated with a weaker increase of dark times at the same point of the trace. These two events combine to give a large change of 40 mV in the trace of mid-point potential (Fig. S62E). The two regimes lead to conspicuous deviations in the histograms of times and in the scatter plots. The scatter plot of bright times (Fig. S62H) clearly shows two sets of points corresponding to the two regimes of the trace. The segmental correlation functions also show a distinct change in time and contrast between the beginning and the end of the trace (3 first blue curves versus the later ones in Fig. S63D).

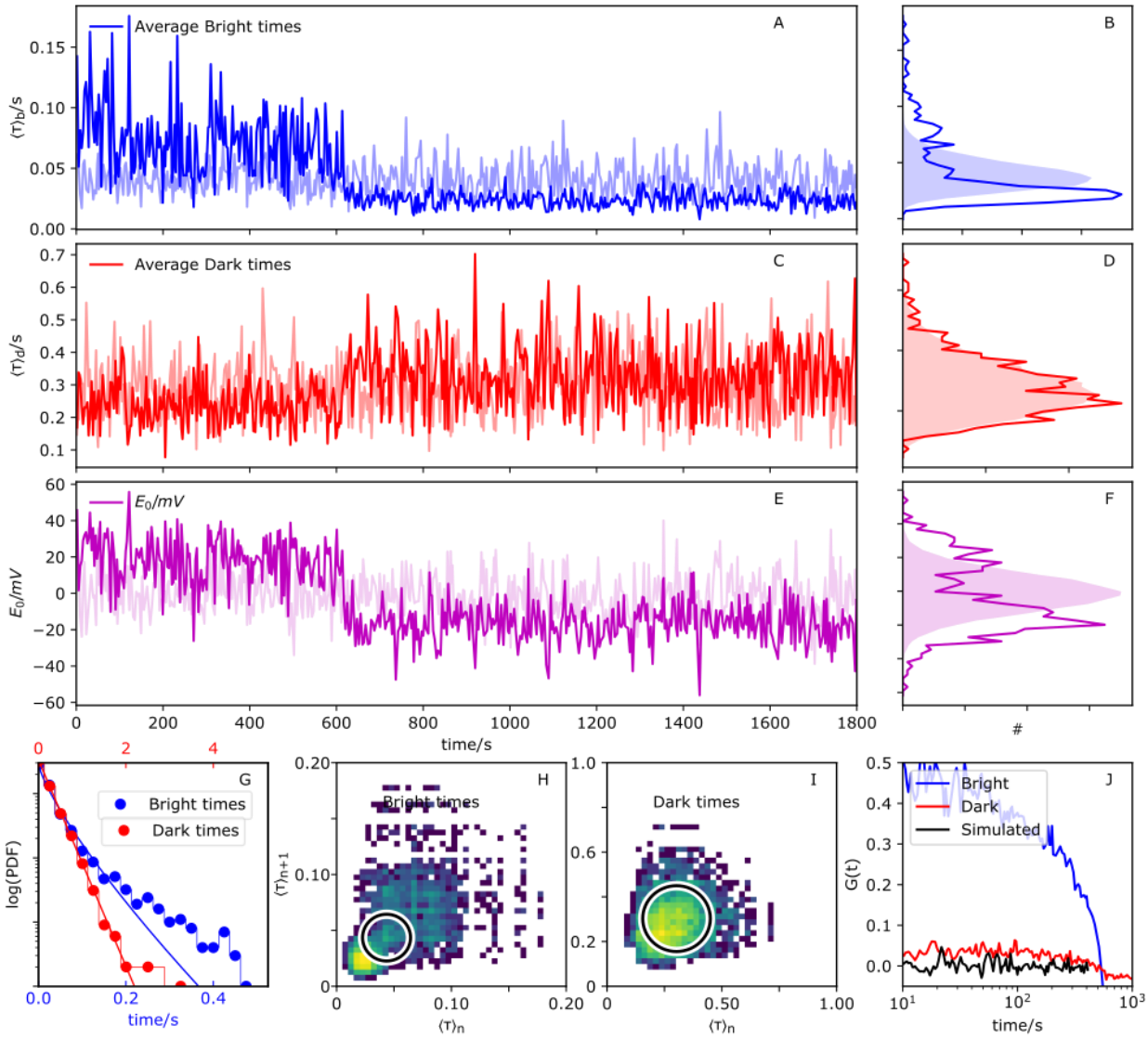

Figure S62: Dynamic heterogeneity from a change point analysis. See Fig. S12 for details.

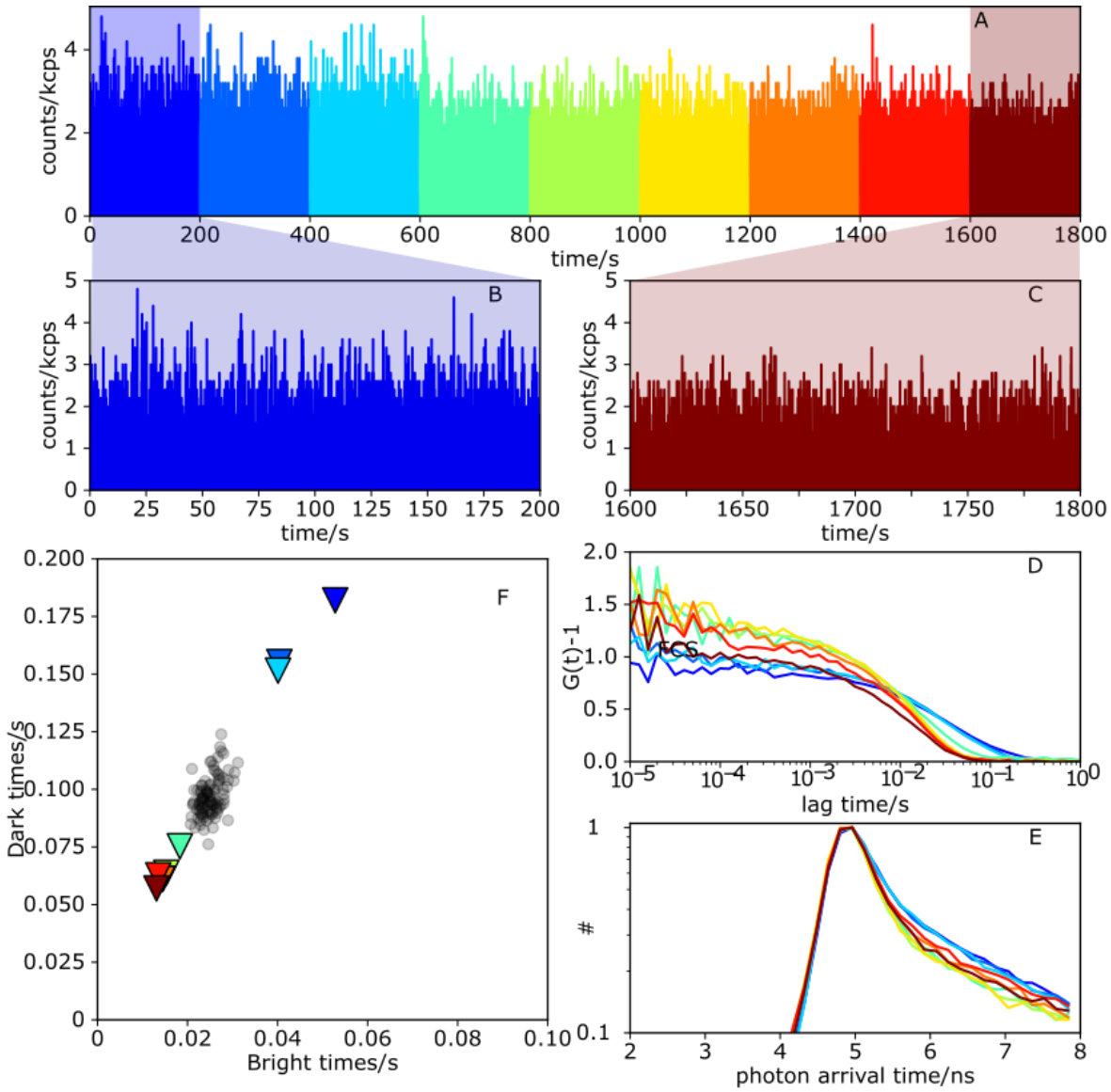

Figure S63: Dynamic heterogeneity from a change point-free segmental analysis. See Fig. S13 for details.

1.10.14. Molecule 14

Another case of a transition between two regimes, as for molecule 13. This time correlated changes appear at the end of the trace, after 400 s. Bright times become much shorter whereas dark times become longer. Note again the histogram deviations and the two clusters of points both in the scatter plot of bright times (Fig. S64H) and dark times (Fig. S64I). Here also, the segmental correlation functions show a distinct change in time and contrast between the beginning and the end of the trace (4 first curves versus the last two ones in Fig. S65D).

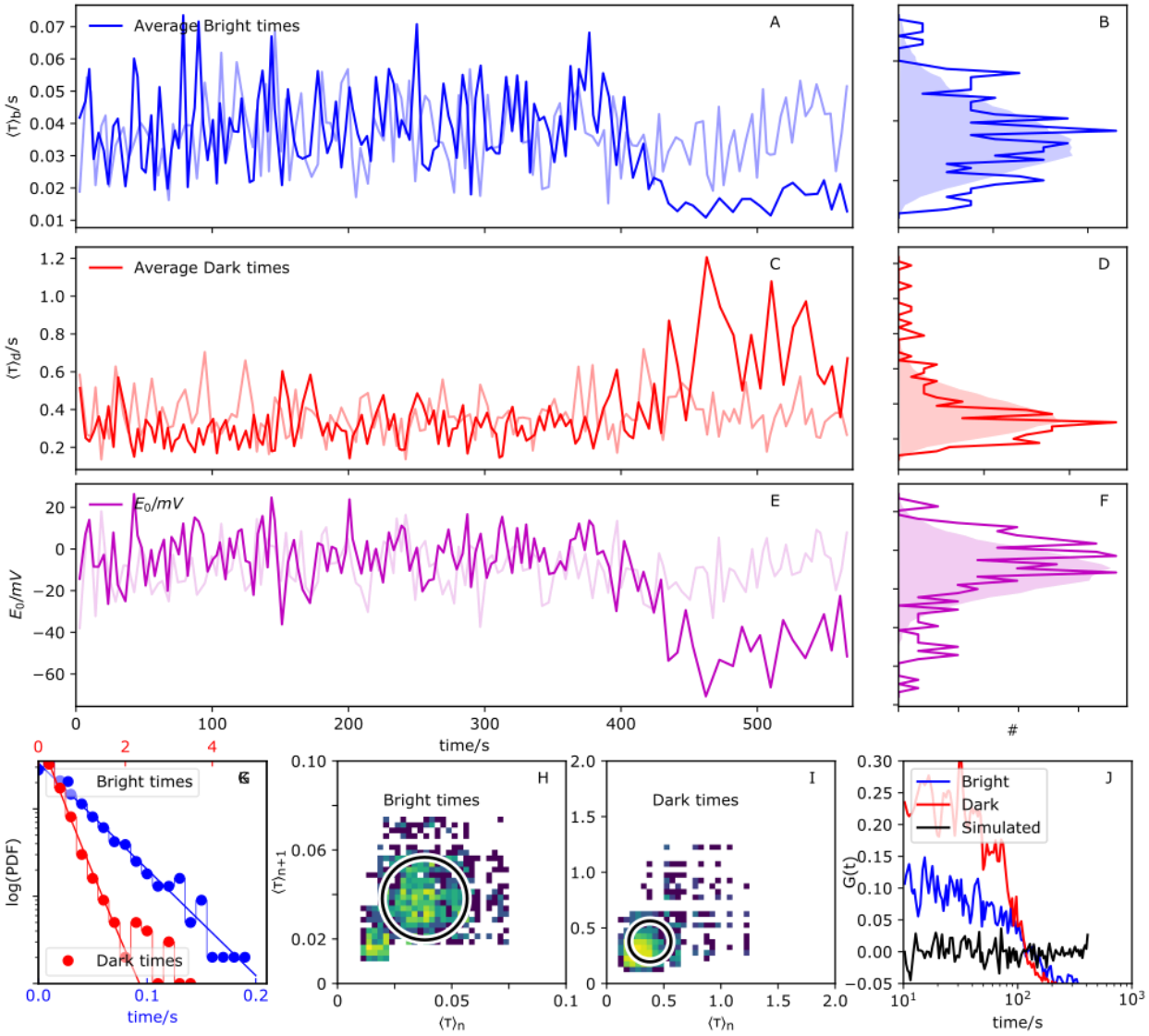

Figure S64: Dynamic heterogeneity from a change point analysis. See Fig. S12 for details.

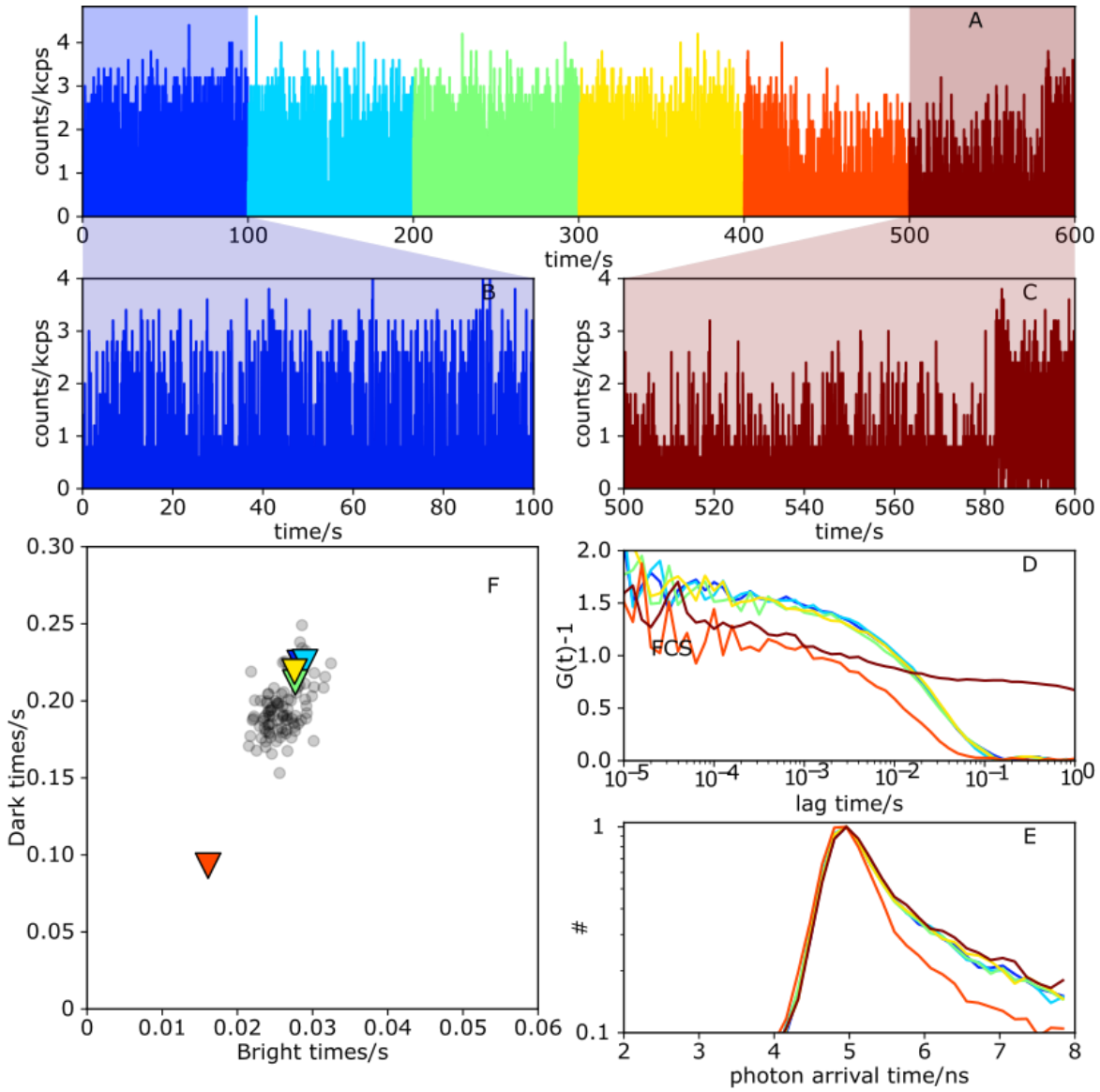

Figure S65: Dynamic heterogeneity from a change point-free segmental analysis. See Fig. S13 for details.

1.10.15. Molecule 15

Molecule 15 shows a transition from long bright times (500 ms) in the first 100 s of the trace to much shorter bright times (about 25 ms) for the whole rest of the trace. A correlated episode of lengthened dark times (2.5 s) compared to the rest of the trace (about 200 ms) may be observed, so that the mid-point potential doesn't show any significant change during this episode (Fig. S66E). The first (dark blue) trace of the segmental correlation functions shows a distinct change in shape and contrast (Fig. S67D).

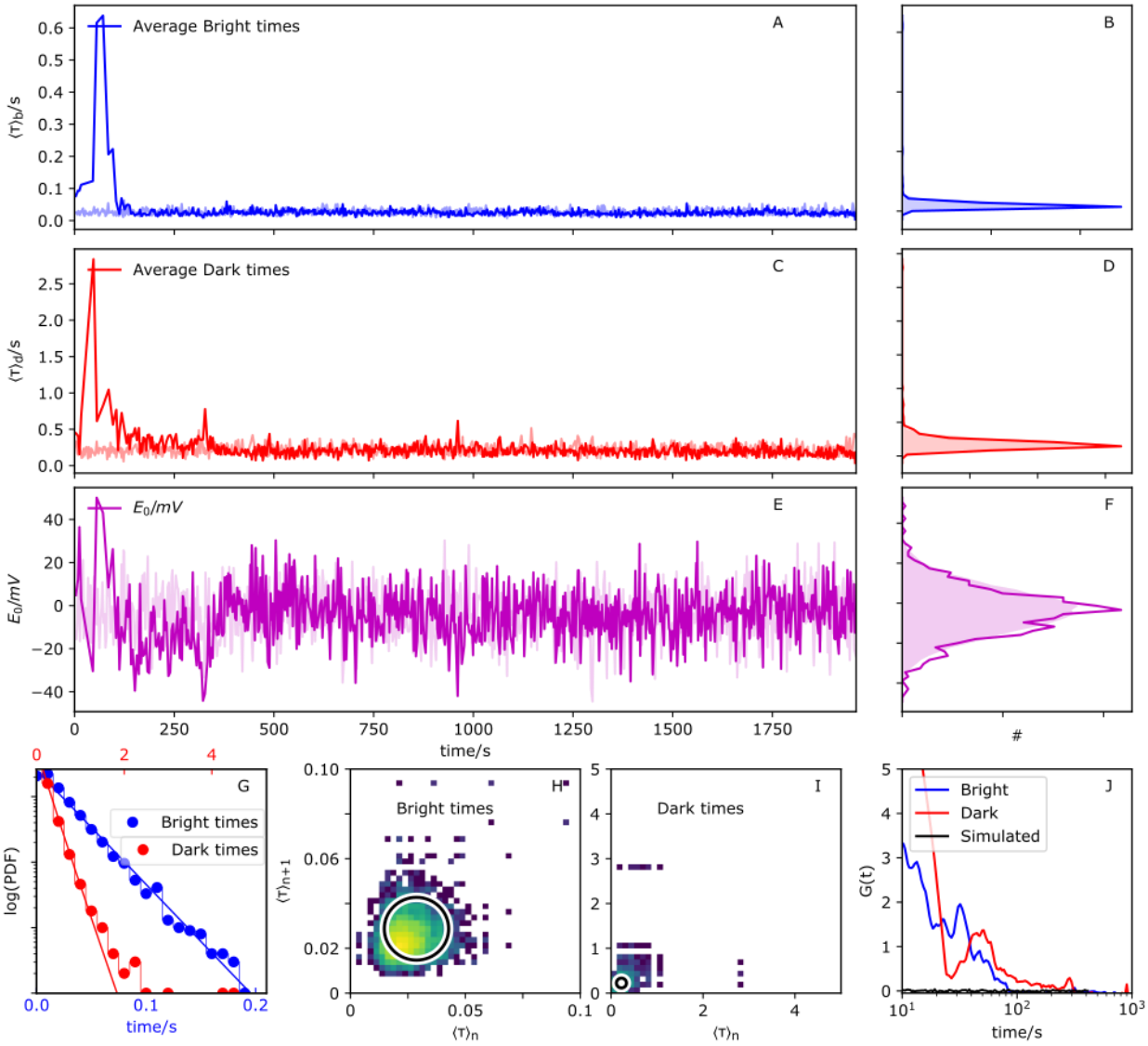

Figure S66: Dynamic heterogeneity from a change point analysis. See Fig. S12 for details.

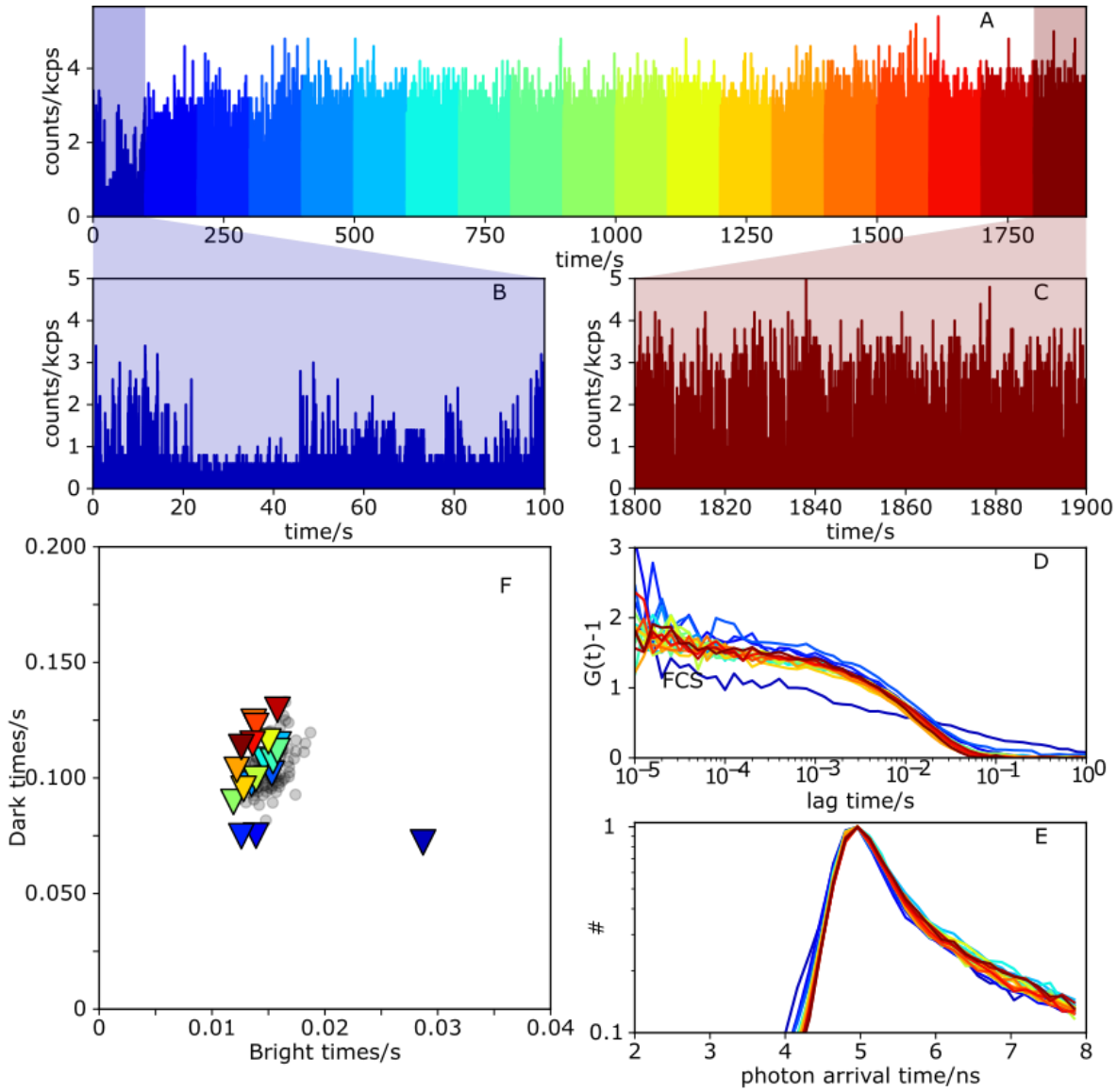

Figure S67: Dynamic heterogeneity from a change point-free segmental analysis. See Fig. S13 for details.

1.11. Change event categorization

In order to give a qualitative overview of the observed changes in dark and bright times, we identified in each trace events where the respective times change abruptly (as stated in the description of each data set S12-S67). Each event was then categorized according to whether the dark/bright times increased, decreased or stayed unchanged (Fig. S68). Thus, each event is assigned two coordinates (bright time change/dark time change), where each coordinate can indicate either an increase (+), decrease (-) or no change (0). Traces without discernable events were counted as one event with coordinates (0/0), i.e. no change. Tables T1 (ATTO647N) and T2 (ATTO655) list the assigned events, while Figs. 5 and S69 show the resulting histograms for ATTO647N-labeled (Fig. 5A,B) and ATTO655-labeled (S69A,B) Az as well as the combined data (S69D,E). Clearly, the dark time and bright time changes are uncorrelated.

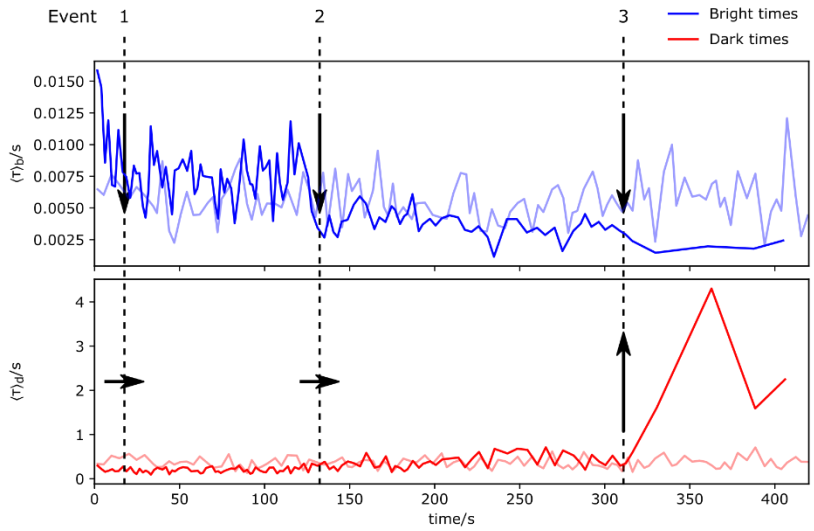

Figure S68: Qualitative picture of the observed sudden changes in bright and dark time. In each trace, the events where the dark or bright times change were identified (dotted lines). Each event was then classified according to the change in dark/bright time (black arrows), in this example (-/0), (-/0) and (-/+) for events 1-3. Traces without any change event were categorized as (0,0). Data taken from ATTO655, molecule 7 (Fig. S50). For a full list of events categorizations, see Table S69,S70.

Table T1. List of qualitatively assigned change events in all ATTO647-labeled Az molecules. See text and Fig. S68 on details how the assignment was performed. Multiple events in a single timetrace are listed in the order they occurred, separated by / (i.e. 1st/2nd/3rd/…). + indicates an increase, - a decrease and 0 no change in the corresponding time. Traces with no changes were assigned 0 in both dark and bright times.

Molecule # Az ATTO647N	Bright time change	Dark time change
1	0 / + / - / -	+ / - / 0 / 0
2	0	0
3	0	+
4	+ / -	+ / -
5	- / 0 / 0	- / + / -
6	-	0
7	0	+
8	0	+
9	0	0
10	0	0
11	0	-
12	0	0
13	0 / +	- / +

Table T2. List of qualitatively assigned change events in all ATTO647-labeled Az molecules. See text and Fig. S68 on details how the assignment was performed. Multiple events in a single timetrace are listed in the order they occurred, separated by / (i.e. 1st/2nd/3rd/…). + indicates an increase, - a decrease and 0 no change in the corresponding time. Traces with no changes were assigned 0 in both dark and bright times.

Molecule # Az ATTO655	Bright time change	Dark time change
1	+ / - / + / - / -	+ / 0 / 0 / - / -
2	- / 0	0 / +
3	-	+
4	+ / -	0 / 0
5	0	0
6	0	0
7	- / - / -	0 / 0 / +
8	0	0
9	0	0
10	0	0
11	0	0
12	-	+
13	-	+
14	-	+
15	-	-

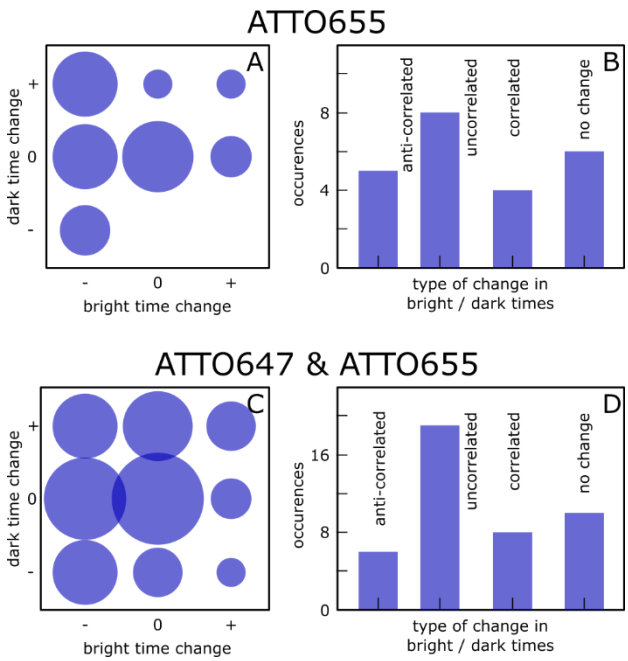

Figure S69: Qualitative picture of the observed sudden changes in bright and dark time. A) Overview of observed change events in ATTO655-labeled Az, categorized as shown in Fig. S68. The area of the disks indicates the total number of events exhibiting the corresponding behavior, ranging from 0 (0,-/+,-) to 6 (0,0). B) Histogram derived from (A), showing the number of events where changes of bright and dark times were anti-correlated, correlated, uncorrelated, or where no change occurred. C) Same as (A), but with the combined data from ATTO655- and ATTO647-labeled Az. D) histogram derived from (C).

1.12. Ensemble intensity vs. intensity derived from bright/dark times

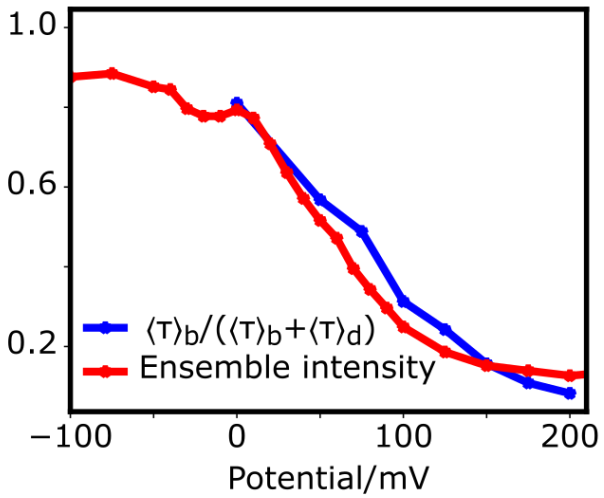

Figure S70: Intensity as a function of the applied potential, measured in an ensemble (red) compared to derived from the average bright and dark times of all measured individual molecules. Clearly, the average of individual molecules approaches the ensemble measurement

1.13. Azurin Surface Potential

To estimate the likelihood of the vicinity of His117 being the binding site, we calculated the Azurin surface potential for the Cu(I) and Cu(II) forms under our experimental conditions. To this end, the protonation states of solvent-exposed residues as well as the hydrogen bond and water network was calculated in PDB2PQR[16] / PROPKA[17] using the PARSE force field. The surface potential was then calculated using the Adaptive Poisson-Boltzmann Solver ABPS[18]. The results are presented in Fig. S73. As can clearly be seen (Fig. S73B), the surface-exposed patch at His117 itself is weakly (< 1 kT/e) negatively charged in the Cu(I) form and neutral for Cu(III). However, there is a strongly positively (> 7 kT/e) charged exposed patch closeby, on the reverse side of the helix containing His117, which is protonated under our experimental conditions. The reverse side of the protein shows large surface-exposed areas carrying significant negative charge (Fig. S73C). It is therefore likely that hexacyanoferrate docks to this positively charged spot and transfers the electron via His117 to and from the Cu.

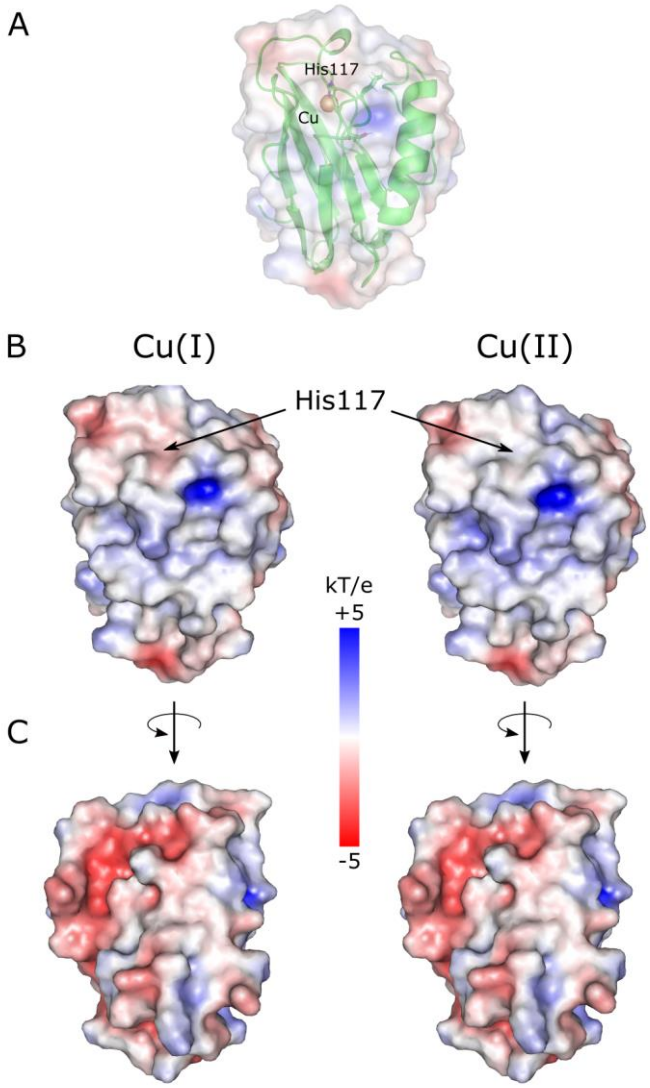

Figure S71: Calculated surface potential of Azurin Cu(I) and Cu(II) forms. A) View along the axis of the helix containing the His117 binding site (top), with the protein structure (green) and Cu(I) on (orange). B) Surface potential showing negatively (red) and positively (blue) charged areas oft he protein in Cu(I) (left) and Cu(II) (right) forms. The view is identical to that in A. C) Reverse side of Az showing a for the most part negatively charged surface.

2. References

[1] E. Vijgenboom, J. E. Busch, G. W. Canters, *Microbiology* **1997**, *143*, 2853-2863.

[2] U. Kolczak, C. Dennison, A. Messerschmidt, G. W. Canters, in: *Handbook of Metalloproteins, Wiley* **2006**, 1170–1194.

[3] H. Nar, A. Messerschmidt, R. Huber, M. van de Kamp, G. W. Canters, *J. Mol. Biol.* **1991**, *221*, 765-775.

[4] A. P. Kalverda, M. Ubbink, G. Gilardi, S. S. Wijmenga, A. Crawford, L. J. C. Jeuken, G. W. Canters, *Biochemistry* **1999**, *38*, 12690-12697.

[5] D. M. Korzhnev, B. G. Karlsson, V. Y. Orekhov, M. Billeter, *Protein Sci.* **2003**, *12*, 56-65.

[6] A.V. Zhuravleva, D. M. Korzhnev, E. Kupce, A.S. Arseniev, M. Billeter, V. Y. Orekhov, *J. Mol. Biol.* **2004**, *342*, 1599-1611.

[7] H. A. O. Hill, B. E. Smith, *J. Inorg. Biochem*. **1979**, *11*, 79-93.

[8] L. J. C. Jeuken, L. J. Wisson, F. A. Armstrong, *Inorg. Chim. Acta* **2002**, *331*, 216-223.

[9] H. A. O. Hill, J. C. Leer, B. E. Smith, C. B. Storm, R. P. Ambler, *Biochem. Bioph. Res. Co.* **1976**, *70,* 331-338.

[10] R. T. Ullmann, G. M. Ullmann, *J. Phys. Chem. B* **2011**, *115*, 10346-10359.

[11] M. van de Kamp, G. W. Canters, C. R. Andrew, J. Sanders-Loehr, C. J. Bender, J. Peisach, *Eur. J. Biochem.* **1993**, *218*, 229–238.

[12] C. S. St.Clair, W. R. Ellis, H. B. Gray, *Inorg. Chim. Acta* **1992**, *191*, 149-155.

[13] E. T. Adman, L. H. Jensen, *Isr. J. Chem.* **1981**, *21*, 8–12.

[14] T. G. Terentyeva, H. Engelkamp, A. E. Rowan, T. Komatsuzaki, J. Hofkens, C.-B. Li, K. Blank, *ACS Nano* **2012**, *6*, 346–354.

[15] A. Andreoni, S. Sen, P. L. Hagedoorn, W. J. Buma, T. J. Aartsma, G. W. Canters, *Chem. Eur. J.* **2018**, *24*, 646-654.

[16] T. J. Dolinsky, P. Czodrowski, H. Li, J. E. Nielsen, J. H. Jensen, G. Klebe, N. A. Baker, *Nucleic Acids Res.*, **2007,** *35*, W522-5.

[17] C. R. Sondergaard,M. H. M. Olsson, M. Rostkowski, J. H. Jensen, *J. Chem. Theo. Comp.*, **2011**, *7*, 2284-2295.

[18] E. Jurrus, D. Engel, K. Star, K. Monson, J. Brandi, L. E. Felberg, D. H. Brookes, L. Wilson, J. Chen, K. Liles, M. Chun, P. Li, D. W. Gohara, T. Dolinsky, R. Konecny, D. R. Koes, J. E. Nielsen, T. Head-Gordon, W. Geng, R. Krasny, G. W. Wei, M. J. Holst, J. A. McCammon, N. A. Baker, *Protein Science*, **2018**, *27*, 112-128.